

Institute of Experimental and Clinical Pharmacology and Toxicology  
Center for Experimental Medicine  
University Medical Center Hamburg-Eppendorf

**Investigation of molecular mechanisms regulating the  
expression of cMyBP-C mutants in  
familial hypertrophic cardiomyopathy**

**Dissertation**

submitted to the

Department of Chemistry

Faculty of Mathematics, Informatics and Natural Sciences

University of Hamburg

for the degree

Doctor of Natural Sciences

by

**Saskia Schlossarek**

Hamburg 2008

1. Referee: Prof. Dr. Michael Korth
2. Referee: Prof. Dr. Thomas Eschenhagen

Day of the disputation: 07.03.2008

## Table of contents

<b>1</b>	<b>Introduction</b>	<b>1</b>
1.1	The heart structure and function	1
1.2	The cardiac myosin-binding protein-C	4
1.3	Familial hypertrophic cardiomyopathy	7
1.4	Mutations and proposed pathophysiological hypotheses of FHC	9
1.5	Potential molecular mechanisms involved in the regulation of cMyBP-C mutants	10
1.5.1	The nonsense-mediated mRNA decay	10
1.5.2	The ubiquitin-proteasome system	13
1.6	Mouse models with <i>MYBPC3</i> mutations	15
1.7	Aim of the thesis	18
<b>2</b>	<b>Material and Methods</b>	<b>20</b>
2.1	Material	20
2.1.1	Chemicals	20
2.1.2	Chemicals with risk (R-) and safety (S-) phrases	23
2.1.3	Antibodies	24
2.1.4	Bacterial strain	25
2.1.5	Kits	25
2.1.6	Oligonucleotides	25
2.1.7	Consumable material	26
2.1.8	Laboratory equipment	27
2.1.9	Animal models	28
2.1.9.1	The M7t mouse model	28
2.1.9.2	The cMyBP-C knock-in mouse model	33
2.1.9.3	The cMyBP-C knock-out mouse model	34
2.1.9.4	The Ub <sup>G76V</sup> -GFP mouse model	35
2.1.9.5	The GFPdgn mouse model	36
2.2	Methods	37
2.2.1	Genotyping	37
2.2.1.1	Genotyping by Southern Blot	37
2.2.1.2	Genotyping by PCR	37

2.2.2	Organ extraction	39
2.2.3	RNA analysis	39
2.2.3.1	RNA isolation	39
2.2.3.2	RNA concentration determination	39
2.2.3.3	Reverse transcription (RT)	40
2.2.3.4	Classical RT-PCR	40
2.2.3.5	Quantitative RT-PCR	41
2.2.4	Protein analysis	46
2.2.4.1	Protein extraction	46
2.2.4.2	Determination of the protein concentration	46
2.2.4.3	Western blot analysis	47
2.2.4.4	Measurement of the 20S proteasome activities	48
2.2.5	Cell isolation	51
2.2.5.1	Neonatal mouse cardiomyocytes	51
2.2.5.2	Adult mouse ventricular myocytes	51
2.2.5.3	Mouse fibroblasts	52
2.2.6	Treatments	53
2.2.6.1	Treatment of NMCM	53
2.2.6.2	Treatment of AMVM	53
2.2.6.3	Treatment of fibroblasts	53
2.2.6.4	Treatment of mice	54
2.2.7	Transfection	54
2.2.8	Immunofluorescence analysis	55
2.2.9	Echocardiography	55
2.2.10	Statistical analysis	56
<b>3</b>	<b>Results</b>	<b>57</b>
3.1	Generation and characterization of targeted cMyBP-C mouse models	57
3.1.1	Generation and characterization of the M7t mouse model	58
3.1.1.1	Generation of the M7t mouse model	58
3.1.1.2	Genotyping	58
3.1.1.3	Molecular characterization at the mRNA level	59
3.1.1.4	Molecular characterization at the protein level	62
3.1.1.5	Functional characterization	64

3.1.2	Generation and characterization of the cMyBP-C knock-in mouse model	67
3.1.2.1	Generation of the cMyBP-C knock-in mouse model	67
3.1.2.2	Genotyping	67
3.1.2.3	Molecular characterization at the mRNA level	68
3.1.2.4	Molecular characterization at the protein level	70
3.1.2.5	Functional characterization	72
3.1.3	Summary	74
3.2	Analysis of the UPS involvement <i>ex vivo</i>	75
3.2.1	Inhibition of the UPS in M7t-TG mice	75
3.2.2	Inhibition of the UPS in KI mice	78
3.2.3	Summary	81
3.3	Investigation of the UPS function <i>in vivo</i>	82
3.3.1	Investigation of ubiquitination and degradation in myocardial tissue of M7t-TG and KI mice	82
3.3.1.1	Investigation of ubiquitination and degradation in the M7t-TG mice	82
3.3.1.2	Investigation of ubiquitination and degradation in the KI and KO mice	84
3.3.2	Investigation of the UPS reporter mouse models	92
3.3.2.1	Investigation of the Ub <sup>G76V</sup> -GFP mouse model	92
3.3.2.2	Investigation of the GFPdgn mouse model	96
3.3.3	Investigation of the UPS function in the KI and KO mice crossed with Ub <sup>G76V</sup> -GFP mice	99
3.3.3.1	Investigation of the UPS function in the KI mice crossed with Ub <sup>G76V</sup> -GFP mice	100
3.3.3.2	Investigation of the UPS function in the KO mice crossed with Ub <sup>G76V</sup> -GFP mice	102
3.3.4	Summary	104
3.4	Investigation of the nonsense-mediated mRNA decay	105
3.4.1	Investigation of the nonsense-mediated mRNA decay in the KI and Het mice	105
3.4.2	Summary	110
<b>4</b>	<b>Discussion</b>	<b>111</b>
<b>5</b>	<b>Summary</b>	<b>128</b>
<b>6</b>	<b>References</b>	<b>135</b>

<b>7</b>	<b>Appendix</b>	<b>147</b>
7.1	Abbreviations	147
7.2	Standard amino acid abbreviations	152
7.3	Risk and safety phrases	152
7.4	Curriculum Vitae	158
7.5	Publications and congress participations	159
7.5.1	Publications	159
7.5.2	Congress participations	159
7.6	Declaration	163
7.7	Acknowledgement	164

# 1 Introduction

## 1.1 The heart structure and function

The heart is a pear-shaped muscular organ responsible for pumping blood through the blood vessels to the organs, tissues and cells of the body by repeated, rhythmic contractions. It is usually situated in the middle of the thorax and consists of four chambers (the two upper atria and the two lower ventricles) with one-way flaps called valves. A wall of muscle called the septum separates the left and right sides of the heart (Fig. 1.1).

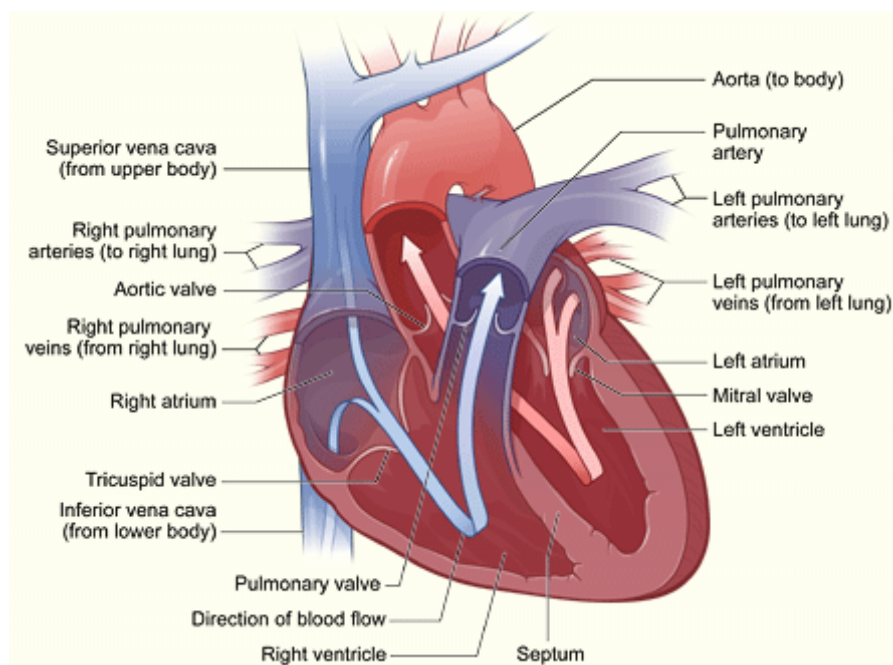


**Figure 1.1: The structure of the heart.** The illustration shows a heart cross-section and its internal structures. The blue arrow shows the direction in which low-oxygen blood flows from the body to the lungs. The red arrow shows the direction in which oxygen-rich blood flows from the lungs to the rest of the body (picture taken from the National Heart, Lung and Blood Institute website).

The function of the heart is to receive deoxygenated venous blood from the body in the right atrium and to pump it via the right ventricle into the lungs, where carbon dioxide can be dropped off and oxygen picked up. Oxygenated blood from the lungs flows into the left atrium, and from here the blood moves to the left ventricle, which pumps it out to the body (Opie, 2004a). The huge pumping force of the heart is generated by the cardiac muscle, an involuntary striated muscle tissue, which is found

only within this organ. In the cardiac muscle, 20% of the cells are cardiomyocytes that constitute 80% of the mass, and each cardiomyocyte is made up of many myofibrils, which in turn consist of myofilaments. There are three types of myofilaments: titin, the thin and the thick filaments. The classification of the latter ones is based on their relatively lighter or darker appearance, when viewed through the light microscope (Opie, 2004b). The thin filaments contain actin, which forms two intertwining helical chains,  $\alpha$ -tropomyosin, which forms a parallel coiled dimer binding to seven actin monomers and troponin T, and the troponin complex, which is composed of the troponins T, C and I and which occurs at regular intervals along the  $\alpha$ -tropomyosin (Redwood et al., 1999; Opie and Solaro, 2004; Fig. 1.3). The thick filaments consist of myosin and are held in place by the third filament titin. Myosin itself is a hexamer consisting of two heavy chains together with two regulatory light chains and two essential light chains (Redwood et al., 1999). The thin and thick filaments have a specific and constant length of a few micrometers and are organized into repeated subunits along the length of the myofibril, which gives the cardiac muscle its striated pattern. The subunits are called sarcomeres (Fig. 1.2).

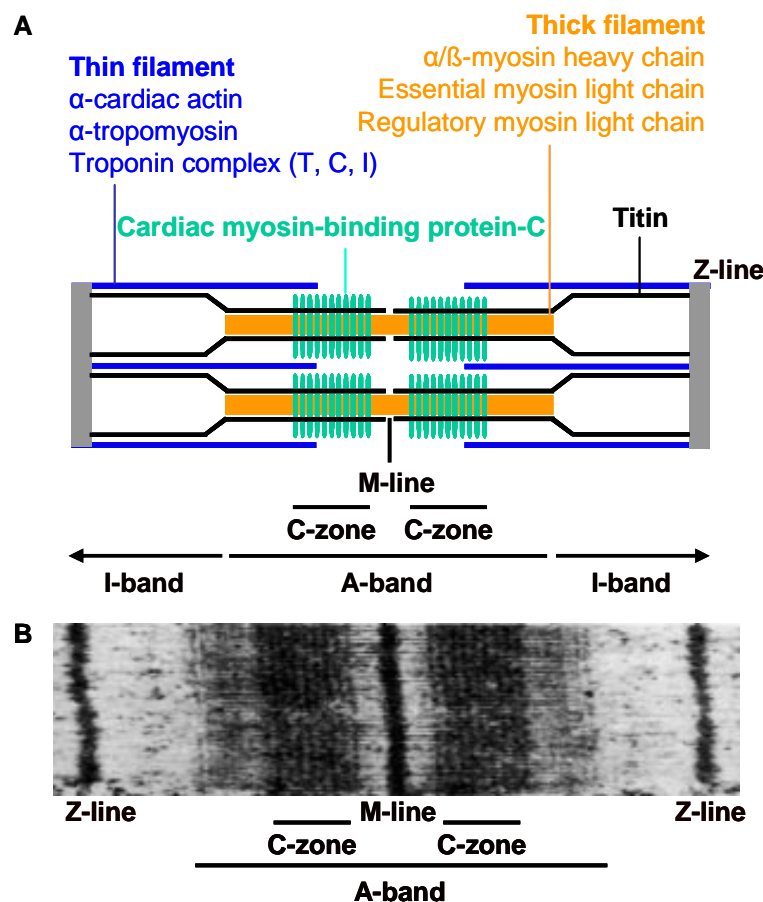


**Figure 1.2: The structure of the sarcomere.** **A**, Schematic structure of the sarcomere (adapted from Bonne et al., 1998). **B**, Electron microscopic picture of the sarcomere (adapted from Craig and Offer, 1976).



Each sarcomere is delimited by two very dark colored bands called Z-lines. Surrounding the Z-line is the region of the I-band and in contiguity to them the A-band. Within the A-band, the thin M-line and the C-zones are located (Fig. 1.2). Actin filaments are the major component of the I-band and extend into the A-band. Myosin filaments extend throughout the A-band. The third filament titin tethers the myosin filaments to the Z-line, thereby stabilizing the thick filaments (Opie and Solaro, 2004). In the C-zones of the A-band, another sarcomeric protein is located - the cardiac myosin-binding protein-C, which will be discussed in detail in the next chapter.

The sarcomere is the fundamental contractile unit: The interaction between the two chief contractile proteins, actin and myosin, is responsible for the muscle contraction. Contraction is initiated when cytosolic calcium rises after release of calcium from the sarcoplasmic reticulum (calcium-induced calcium release). In a resting muscle,  $\alpha$ -tropomyosin overlays the myosin-binding sites on actin and is locked down in this position by troponin T (T stands for tropomyosin binding) and troponin I (I stands for inhibitory). The binding of intracellular calcium by troponin C (C stands for calcium) induces a conformational change in the troponin complex, and this unlocks  $\alpha$ -tropomyosin from actin, allowing the interaction between actin and myosin. Myosin hydrolyzes then adenosine triphosphate (ATP) and undergoes a series of conformational changes so that it is displaced along the thin filament. Thin and thick filaments slide past each other (sliding filament theory), driving sarcomere shortening and muscle contraction (Fig. 1.3). As calcium is sequestered by the sarcoplasmic reticulum, troponin I and T lock  $\alpha$ -tropomyosin in the blocking position, and the thin filaments slide back to the resting state (Seidman and Seidman, 2001; Opie and Solaro, 2004).

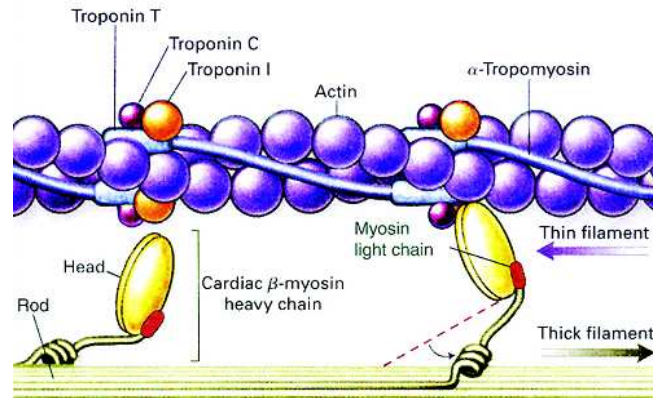


**Figure 1.3: Muscle contraction by sliding of the myofilaments.** Contraction begins with calcium binding to the thin filaments that subsequently leads to an actin-myosin binding. ATP is then hydrolyzed by myosin, and the thick filaments are displaced along the thin filaments. As calcium is sequestered by the sarcoplasmic reticulum, actin-myosin interactions are prevented (adapted from Kamisago et al., 2000).

## 1.2 The cardiac myosin-binding protein-C

Myosin-binding protein-C (MyBP-C) is a large multidomain protein of 140-150 kDa and is located in doublets in the C-zone of the A-band, where it forms a series of seven to nine transverse stripes in each half A-band (Fig. 1.2). It belongs to the intracellular immunoglobulin (Ig) superfamily and has a conserved domain pattern consisting of immunoglobulin set (IgC2-like) and fibronectin (FN3) domains (Weber et al., 1993; Gautel et al., 1995). MyBP-C exists in three isoforms: the slow-skeletal, the fast-skeletal and the cardiac isoform.

The *MYBPC3* gene encoding the cardiac isoform (cMyBP-C) in humans was localized by fluorescence *in situ* hybridization on chromosome 11p11.2 (Gautel et al., 1995). In 1997, the organization and sequence of *MYBPC3* was determined: *MYBPC3* comprises >21000 bp and contains 35 exons (Carrier et al., 1997; Fig. 1.4). The cMyBP-C protein is specifically expressed in the heart during development and adult life in humans and mice (Fougerousse et al., 1998; Gautel et al., 1998) and contains eleven modules labeled C0 to C10 from the N- to the C-terminus (Fig. 1.4).

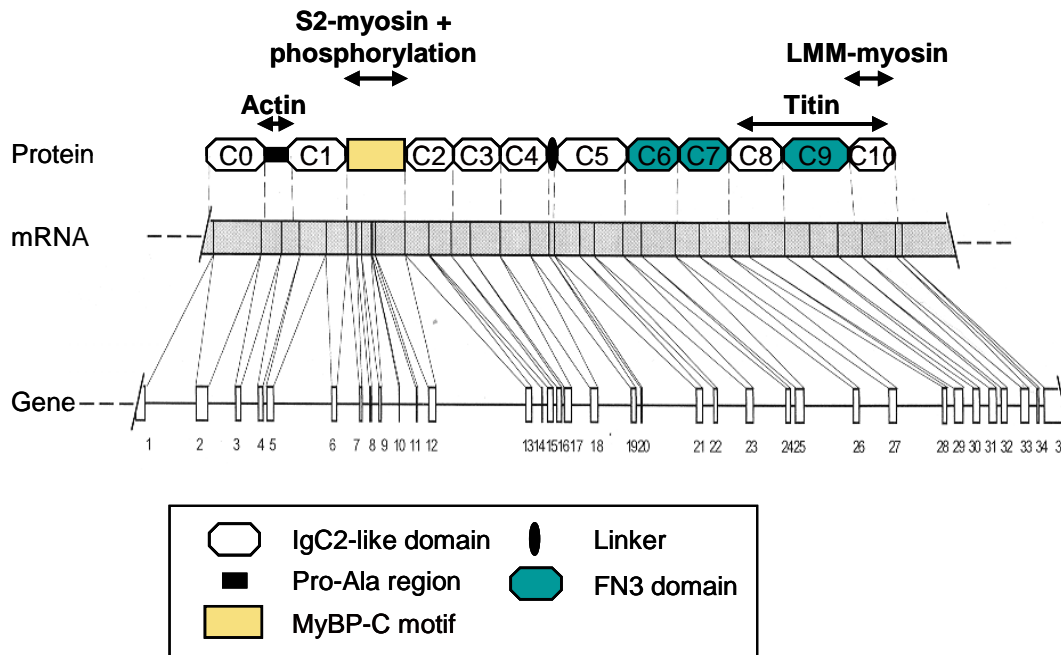


**Figure 1.4: Schematic organization of the human *MYBPC3* gene and alignment of exons with structural domains of the protein.** On the top, the structural domains of the cMyBP-C protein, composed of 8 immunoglobulin (IgC2-like) and 3 fibronectin (FN3) domains and a specific MyBP-C motif, are shown. The localization of the domains involved in binding to other sarcomeric proteins is indicated. In the middle, the mRNA with the limits of exons is depicted. On the bottom, the schematic organization of the *MYBPC3* gene with locations of exons shown by boxes and introns by horizontal lines is illustrated. The exons are numbered from the 5'-end of the gene. The exons coding for structural domains are signed by interrupted lines (adapted from Carrier et al., 1997).

The cMyBP-C protein has both structural and regulatory roles. Via the C10 domain it binds the light meromyosin, whereas the myosin subfragment 2 is bound through the MyBP-C motif, which is a 105-residue stretch linking the C1 and C2 domains (Starr and Offer, 1978; Okagaki et al., 1993; Alyonycheva et al., 1997). By binding to myosin, cMyBP-C is thought to modulate myosin assembly and stabilize the thick filaments (Koretz, 1979; Seiler et al., 1996; Sébillon et al., 2001). In addition, it binds titin via the C8-C10 domains (Freiburg and Gautel, 1996) and actin in the Pro-Ala rich sequence, which is located between the C0 and C1 domains (Kulikovskaya et al., 2003; Herron et al., 2006). The structural basis for the incorporation of cMyBP-C into the thick filament is not fully elucidated, but one possibility is that cMyBP-C molecules trimerize to form a collar around the thick filament (Moolman-Smook et al., 2002; Fig. 1.5).

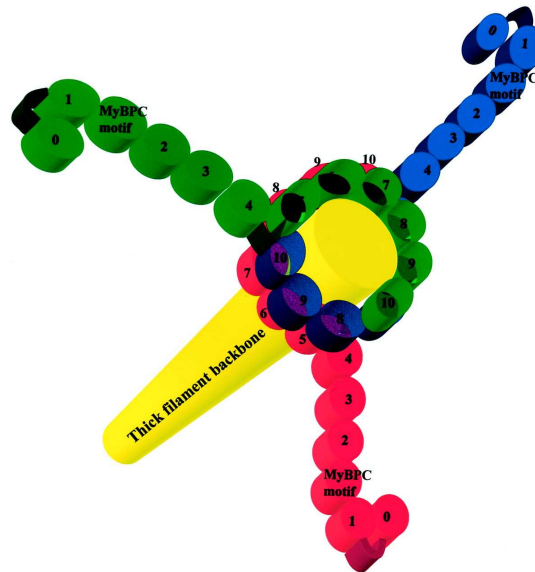


**Figure 1.5: Proposed trimeric collar model of cMyBP-C around the thick filament backbone.** Three cMyBP-C molecules are supposed to trimerize to form a collar around the thick filament, with overlaps of domains C5-C7 of one cMyBP-C molecule with domains C8-C10 of the ensuing molecule with staggered parallel orientation of the proteins. Domains C5-C10 of each cMyBP-C molecule form part of the two molecule-thick collar, while the N-terminal domains C0-C4 are extended into the interfilamental space, where the cMyBP-C motif binds to the myosin subfragment 2 (adapted from Moolman-Smook et al., 2002).

The cMyBP-C protein has three known phosphorylation sites (Ser-273, Ser-282 and Ser-302), which are located in the MyBP-C motif. These phosphorylation sites are mainly regulated in response to  $\beta$ -adrenergic stimulation by a cAMP-dependant protein kinase (PKA) (Hartzell and Titus, 1982; Garvey et al., 1988). The dephosphorylated form of cMyBP-C binds to the myosin subfragment 2, whereas after phosphorylation the Pro-Ala rich sequence between the C0 and C1 domains binds to actin (Gruen et al., 1999; Kunst et al., 2000; Kulikovskaya et al., 2003). The phosphorylation of cMyBP-C increases the force of contraction, and it has been shown that the phosphorylation of cMyBP-C is cardioprotective (Sadayappan et al., 2005; Sadayappan et al., 2006). Recent studies revealed a decreased amount of the phosphorylated form in human failing heart (El-Armouche et al., 2007) and in human atrial fibrillation (El-Armouche et al., 2006). The role of cMyBP-C in cardiac contraction has been enigmatic for long, but recent data by our group suggest that cMyBP-C is essential for normal (complete) diastolic relaxation by inhibiting actin-myosin interactions at low intracellular calcium concentrations (Pohlmann et al., 2007).

### 1.3 Familial hypertrophic cardiomyopathy

To date, cardiovascular diseases are the most common cause of death, of which cardiomyopathies play a decisive role. Cardiomyopathies are defined as diseases of the myocardium with cardiac dysfunction (Richardson et al., 1996) and are classified into four main distinct forms according to the type of anatomical and functional impairment: dilated, hypertrophic, restrictive and arrhythmogenic right ventricular cardiomyopathy. Hypertrophic cardiomyopathy (HCM) is characterized by an asymmetrical left ventricular hypertrophy (LVH), which predominantly involves the interventricular septum and occurs in the absence of another cardiac or systemic disease (e.g. hypertension or aortic stenosis) that could induce hypertrophy (Richardson et al., 1996; Fig. 1.6). LVH is generally associated with a normal systolic function, whereas diastolic function is impaired (Maron et al., 1987). The histopathological features of HCM are myocyte hypertrophy with myocardial disarray and interstitial fibrosis (Richardson et al., 1996; Fig. 1.6).

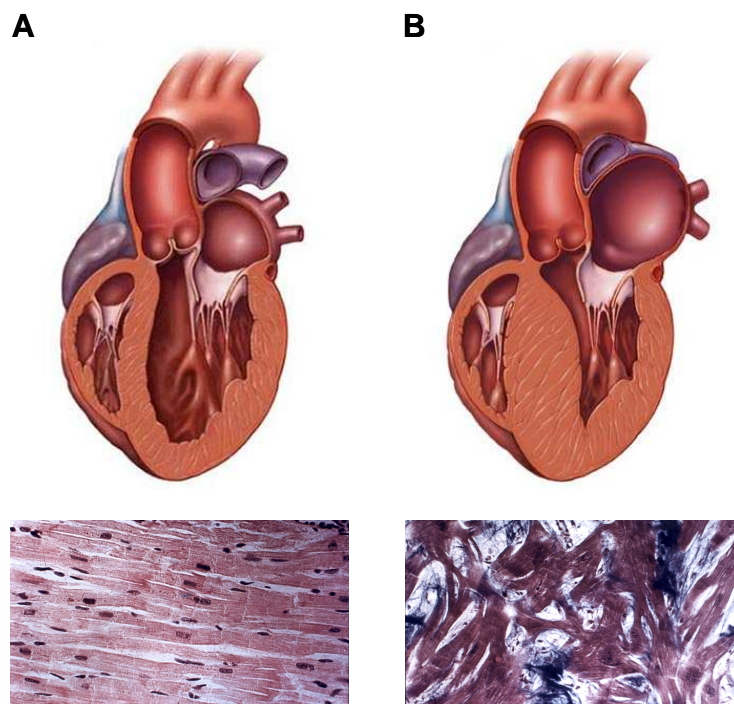


**Figure 1.6: Characteristics of hypertrophic cardiomyopathy.** **A**, On the top, a schematic longitudinal cardiac section of a healthy heart is shown. Below, transversal sections of a healthy heart stained with Sirius Red are represented. **B**, On the top, a schematic longitudinal cardiac section of a hypertrophied heart is shown. The walls of the left ventricle are increased. Below in the transversal sections, the cardiomyocytes lost their parallel arrangement, and by Sirius Red staining interstitial fibrosis (in blue) was found (adapted from the Mayo clinic website (upper part) and from Geisterfer-Lowrance et al., 1990 (lower part)).

The prevalence of the disease is approximately 1:500 in young adults and therefore much more common than previously recognized (Maron et al., 1995). The phenotypical pattern is highly heterogeneous: Many patients have no symptoms during their whole life, but on the other hand in some cases, HCM may lead to severe symptoms such as vertigo, chest pain, syncope or dyspnea, to severe heart failure, to malignant arrhythmia or to sudden death. In fact, HCM remains the most prevalent cause of sudden death in young athletes during exercise (Maron, 2002). Up to now, no specific therapy is available for this disease, only symptomatic treatments for aspects of the syndrome are possible (Roberts and Sigwart, 2001a; Roberts and Sigwart, 2001b).

In the majority of cases (~ 63%) HCM is familial (FHC; Richard et al., 2003) and is transmitted as an autosomal-dominant trait (Maron et al., 1984). Molecular genetic studies have demonstrated that the typical forms of FHC involve more than 450 different mutations in 13 different genes encoding sarcomeric proteins (Alcalai et al., 2007; Table 1.1). The most common genes (together ~ 80%) responsible for FHC are *MYH7*, which encodes the  $\beta$ -myosin heavy chain, and *MYBPC3*, which encodes cMyBP-C.

<b>FHC gene</b>	<b>Symbol</b>	<b>Mutations</b>
Beta-myosin heavy chain	<i>MYH7</i>	212
Myosin-binding protein-C	<i>MYBPC3</i>	165
Troponin T	<i>TNNT2</i>	33
Troponin I	<i>TNNI3</i>	27
Alpha-tropomyosin	<i>TPM1</i>	12
Regulatory myosin light chain	<i>MYL2</i>	10
Actin	<i>ACTC1</i>	7
Essential myosin light chain	<i>MYL3</i>	5
Titin	<i>TTN</i>	2
Muscle LIM protein	<i>CSRP3</i>	3
Telethonin	<i>TCAP</i>	2
Troponin C	<i>TNNC1</i>	1
Alpha-myosin heavy chain	<i>MYH6</i>	1

**Table 1.1: Sarcomeric genes and mutations involved in FHC.** Table was adapted from Richard et al. (2006) and Alcalai et al. (2007).

Most of the FHC-patients are heterozygous for the mutation, but in 3-5% of the cases two different mutations can be present in the same individual, most often in *MYH7* and *MYBPC3* leading to compound heterozygous patients (i.e. two heteroallelic mutations in the same gene), double heterozygous patients (i.e. two heterozygous mutations in two different genes) or homozygous patients (i.e. same mutation on the two alleles of the same gene; Richard et al., 1999; Richard et al., 2003; Ingles et al., 2005). Compared to *MYH7* mutations, mutations in *MYBPC3* are usually associated with a delayed onset, a lower penetrance, a milder degree of hypertrophy and a better survival (Charron et al., 1998; Niimura et al., 1998; Yu et al., 1998). However, there are also other publications, which show that the clinical phenotype of patients with *MYH7* and *MYBPC3* mutations is comparable (Erdmann et al., 2001). Patients with double mutations, as mentioned above, generally exhibit a more severe form of FHC associated with ventricular arrhythmias than patients with single gene defects; this is especially true for homozygous patients (Richard et al., 1999; Richard et al., 2003). In addition, molecular studies have shown that 20-30% of adult patients do not develop a cardiac hypertrophy, although they carry a mutation at the heterozygous state (Richard et al., 2006). Finally, even within families, there is a great variability of phenotypes suggesting the presence of modifying factors such as lifestyle, environment and polymorphisms in other genes, so-called modifier genes, which could modulate the phenotype (Suzuki et al., 2002).

## **1.4 Mutations and proposed pathophysiological hypotheses of FHC**

In *MYH7*, about 200 mutations were identified, which are almost exclusively (96%) missense (Richard et al., 2006). In missense mutations, a single base nucleotide is replaced by another nucleotide leading to a different amino acid. The resulting mutant protein has been shown to be stable (Cuda et al., 1993; Bottinelli et al., 1998) and incorporated into the sarcomere (Flavigny et al., 1999) and is supposed to interfere with the wild-type protein, acting as a poison peptide through a dominant negative effect. The incorporation results in an abnormal function and/or assembly of the sarcomeric filaments (Sweeney et al., 1994). This hypothesis is supported by *in vitro*

studies, engineered animal models and *in vivo* studies from explanted hearts from FHC-patients (Bonne et al., 1998; Marian and Roberts, 2001). In *MYBPC3*, about 165 mutations were found, from which the majority (70%) are frameshift or nonsense mutations (Richard et al., 2006; Alcalai et al., 2007). These mutations mainly result in the appearance of a premature termination codon in the transcribed mRNA, which in turn should produce C-terminal truncated cMyBP-Cs. The molecular mechanisms by which nonsense mutations lead to FHC remain elusive. Truncated proteins were consistently undetectable by Western blot in myocardial tissue from patients carrying a frameshift mutation (Rottbauer et al., 1997; Moolman et al., 2000), and overexpression of truncated human cMyBP-C mutants in rat cardiomyocytes (Flavigny et al., 1999) or in transgenic mice (Yang et al., 1999) showed markedly less expression than the wild-type protein. These data suggest that mutant mRNAs and/or proteins are unstable and that nonsense mutations can act as “null alleles” potentially leading to haploinsufficiency: The production of an insufficient amount of normal cMyBP-C would produce an imbalance in the stoichiometry of the thick filament components and this would be sufficient to alter the sarcomeric structure and function.

There are two known molecular mechanisms, which act as a quality control of the cell and which could be responsible for the instability of cMyBP-C mutants leading to haploinsufficiency: 1. the nonsense-mediated mRNA decay (NMD), which degrades mutant transcripts and 2. the ubiquitin-proteasome system (UPS), which degrades mutant proteins.

## **1.5 Potential molecular mechanisms involved in the regulation of cMyBP-C mutants**

### **1.5.1 The nonsense-mediated mRNA decay**

An estimated  $\frac{1}{3}$  of inherited genetic disorders and many forms of cancer are caused by frameshift or nonsense mutations, which result in the appearance of premature termination codons (PTC). PTCs can arise in transcripts also naturally as a



consequence of errors in transcription, faulty or alternative splicing or programmed rearrangements (Culbertson, 1999; Frischmeyer and Dietz, 1999; Maquat, 2004; Lejeune and Maquat, 2005). The majority of mRNAs that harbor such a PTC are recognized and efficiently targeted for degradation by the cell via NMD. This evolutionarily conserved pathway exists in all eukaryotes examined to date (Culbertson, 1999) and is thought to protect the organism from the deleterious dominant-negative or gain-of-function effects of truncated proteins, which would result if PTC-containing transcripts were allowed to be translated. A general rule is that NMD occurs when a PTC is located more than 50-55 nucleotides (nt) upstream of the last exon-exon junction within the mRNA, whereas mRNAs with PTCs downstream of this boundary are usually stable (Nagy and Maquat, 1998). But how does NMD distinguish between premature and normal stop codons? The prevailing opinion is that a second signal downstream of the stop codon dictates whether a stop codon is premature or not. In mammalian cells, the second signal is somehow delivered by an intron downstream of the stop codon (Carter et al., 1996). Therefore normal stop codons, which are almost always found in the last exon (Nagy and Maquat, 1998), intronless transcripts (Maquat and Li, 2001) or transfected cDNAs containing a PTC are not subject to NMD. A second signal in mammals is the so-called exon junction complex (EJC), which is deposited 20-24 nt upstream of every exon junction during mRNA splicing and which remains bound even when it enters the cytoplasm to be read by the ribosomes. The EJC contains at least ten proteins, from which several are involved in NMD.

The exact mechanism of NMD is still not fully elucidated, but in Fig. 1.7 a possible procedure is depicted. Briefly, normal transcripts escape NMD, because all of the EJCs are removed by the ribosome during translation. On the contrary, an aberrant transcript containing a stop codon in a premature position will have at least one EJC downstream of the PTC. This remaining EJC is identified as a problem by NMD factors and the mRNA is degraded.

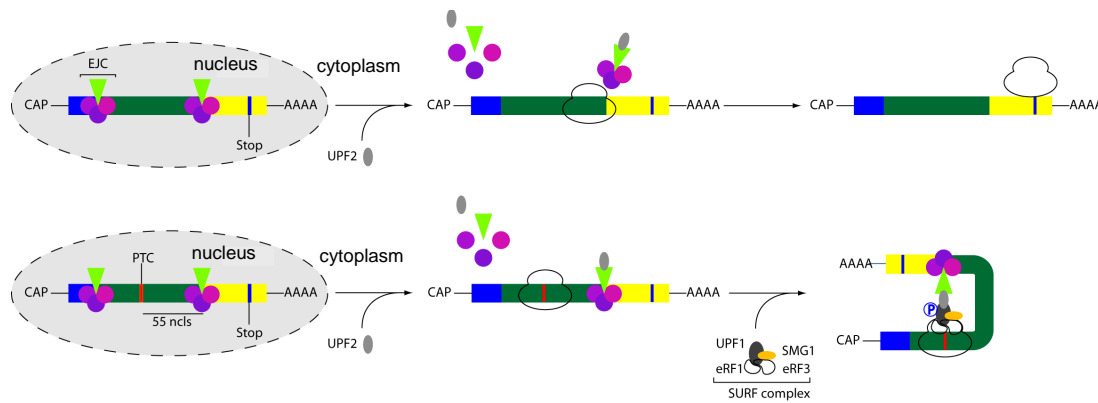


**Figure 1.7: The nonsense-mediated mRNA decay (NMD).** Following splicing in the nucleus, the exon junction complex (EJC), which contains the up-frameshift (UPF) 3 protein (a core protein of the NMD pathway and represented as a green triangle), is associated with the transcript, and the resulting mRNA is exported to the cytoplasm. In the cytoplasm, a second NMD core protein, UPF2, binds to UPF3. In normal mRNAs (upper part), the EJCs are displaced by the ribosome during translation. The translation stops when the ribosome reaches the normal stop codon. In contrast, in mRNAs that contain a PTC (lower part), the ribosome is blocked at the PTC, and the EJC downstream of the PTC remains associated with the mRNA, because it cannot be displaced by the ribosome. This results in binding of the SURF complex (comprising the suppressor with morphogenetic effect on genitalia-1 (SMG-1) protein, UPF1 and the eukaryotic release factors (eRF) 1 and 3) to the ribosome. UPF1 also binds UPF2, thereby linking the EJC to the PTC. Phosphorylation of UPF1 by SMG-1 leads to dissociation of eRF1 and eRF3 and binding of the SMG-7 adaptor protein. Subsequent steps lead to mRNA decay by various pathways, e.g. by decapping or deadenylation (adapted from Garneau et al., 2007).

If a PTC-containing transcript would undergo multiple rounds of translation before being targeted by NMD, large amounts of potentially harmful truncated proteins would be produced. Therefore, mRNAs must be scanned for PTCs and degraded soon after entering the cytoplasm, when they are still associated with the nucleus (Frischmeyer and Dietz, 1999). Thus, NMD likely acts during the pioneer round of translation and due to this, it can be prevented by translation inhibitors like cycloheximide and emetine. Cycloheximide acts as an elongation inhibitor during protein synthesis by competition with the binding of ATP to the 60S ribosomal subunit (Carter et al., 1995), whereas emetine binds to a site on the 40S ribosomal subunit thereby preventing the EF-2-dependent translocation of ribosomes (Vasquez 1979).

### 1.5.2 The ubiquitin-proteasome system

Like the NMD for aberrant mRNAs, the UPS is a quality control of the cell for aberrant proteins. In mammalian cells, 80-90% of the intracellular proteins are degraded via this pathway, whereas the majority of membrane proteins are degraded by the lysosomes (Zolk et al., 2006). One major function of the UPS, which is present in both the nucleus and cytosol, is to prevent the accumulation of damaged, misfolded and mutant proteins, but it has been shown that this system is also involved in intracellular signaling, transcriptional control or regulation of cell death (Zolk et al., 2006). The degradation pathway by the UPS involves two discrete and successive steps: 1. tagging of the substrate by covalent linkage of multiple ubiquitin molecules and 2. degradation of this marked protein by the 26S proteasome complex with release of free and reusable ubiquitin (Fig. 1.8). Conjugation of ubiquitin to the protein occurs via a 3-step process: 1. the ubiquitin-activating enzyme (E1) activates ubiquitin in an ATP-dependent reaction, 2. one out of several ubiquitin-conjugating enzymes (E2) transfers the activated ubiquitin moiety from E1 to the substrate that is specifically bound to one of the ubiquitin ligase enzymes (E3) and 3. the E3 enzyme catalyzes the covalent linkage of ubiquitin to the substrate. Polyubiquitin chains are assembled by adding activated ubiquitin moieties to internal lysine residues on the previous ubiquitin. These polyubiquitin chains are then recognized by the 26S proteasome complex, which degrades the polyubiquitinated proteins to small peptides. During this last process the polyubiquitin chain is hydrolyzed into single ubiquitin moieties, which can be used in a new round of protein degradation.

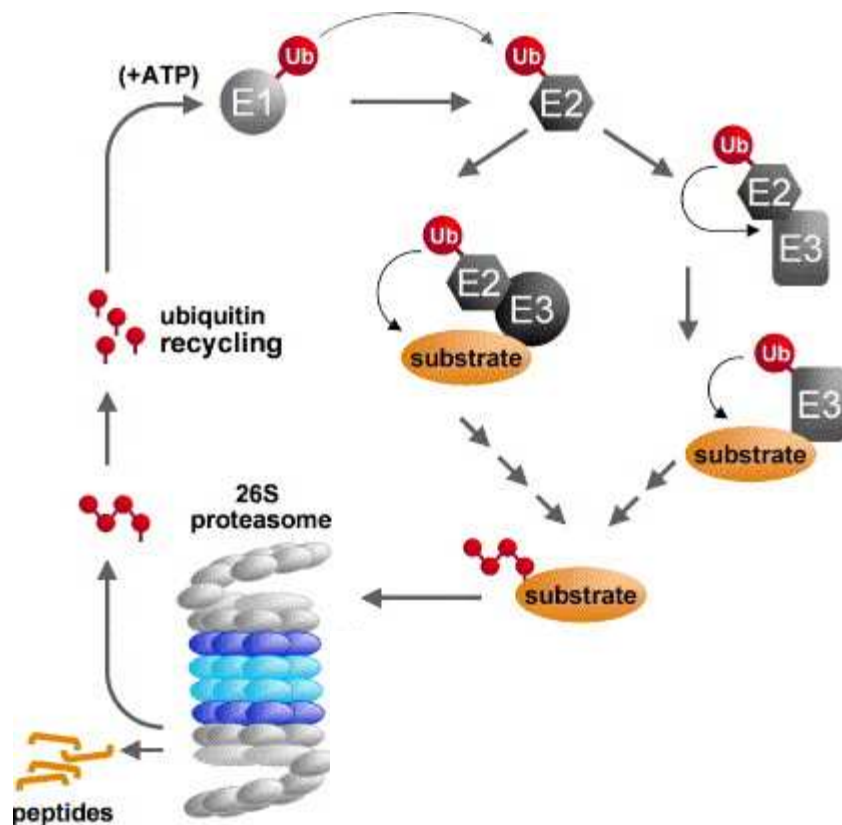


**Figure 1.8: The ubiquitin-proteasome system.** The covalent linkage of ubiquitin (Ub) to protein substrates usually occurs in three steps: an initial activation step catalyzed by E1, an intermediate step, in which ubiquitin is covalently linked to an E2 enzyme, and a final step, in which ubiquitin is attached to the substrate mediated by an E3 enzyme. During the last step ubiquitin is either directly conjugated from E2, whereby E3 acts as a bridge factor or the E3 ligase forms an ubiquitin-thiol-ester intermediate before ubiquitin is transferred to the substrate. Polyubiquitinated protein substrates are degraded by the 26S proteasome to small peptides, and released ubiquitin can be recycled and reused (adapted from Zolk et al., 2006).

The 26S proteasome is a large (2000 kDa) multicatalytic protease and is composed of a 19S regulatory particle and a 20S core that contains the catalytic activity (for review, see (Ciechanover, 2005; Fig. 1.9). The 19S is composed of seventeen distinct subunits, whereof nine are located in a base and eight in a lid subcomplex. The 19S is involved in the recognition, binding, deubiquitination and unfolding of polyubiquitinated proteins, and regulates the opening of the 20S core to channel the unfolded proteins into the 20S. The unfolding and channelling require metabolic energy and therefore the 19S contains six different ATPase subunits, which are located in the base subcomplex. Each extremity of the 20S core can be capped by a 19S. The 20S core has a barrel-shaped structure and is composed of four stacked rings, two outer  $\alpha$ -rings and two inner  $\beta$ -rings. Each  $\alpha$ - and  $\beta$ -ring contains seven distinct subunits.

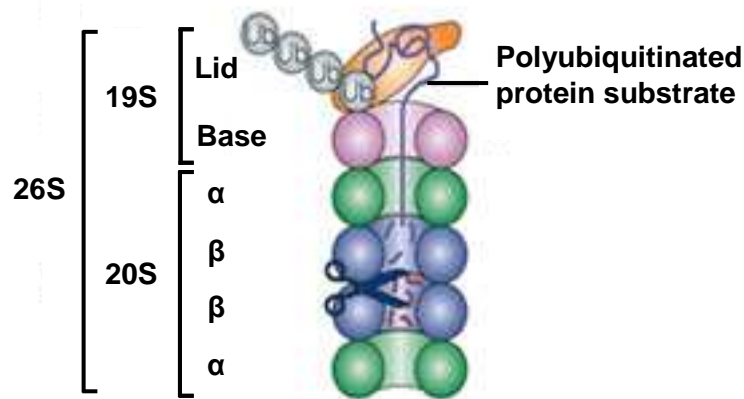


**Figure 1.9: The 26S proteasome.** The 26S proteasome is composed of the 19S and the 20S subcomplex. The 19S regulatory particle has a lid and a base subunit, whereof the base contains all six proteasomal ATPases. The 20S core is made up of four heptameric rings, two outer  $\alpha$ -rings and two inner  $\beta$ -rings. The  $\beta$ -rings are the residences for the three proteolytic activities (adapted from Ciechanover, 2005).

The unfolded protein is degraded in the cavity of the 20S by three major peptidase activities: the chymotrypsin-like, the trypsin-like and the caspase-like activity, which reside in the  $\beta$ 5-,  $\beta$ 2- and  $\beta$ 1-subunit, respectively, on the inner surface of the  $\beta$ -subunit rings. Each peptidase preferentially cleaves after different amino acids: The peptidase of the  $\beta$ 1-subunit cleaves after acidic or small hydrophobic amino acids, the peptidase of the  $\beta$ 2-subunit cuts after basic or small hydrophobic amino acids, while the peptidase of the  $\beta$ 5-subunit hydrolyzes the peptide bond after hydrophobic residues whether bulky or not. All three peptidase activities can be measured using fluorogenic substrates, which are specifically cleaved and release a fluorescent reporter after cleavage, whose fluorescence can be determined. It is also possible to inhibit the three activities with reversible or irreversible proteasome inhibitors to analyse the consequences of this blockage, e.g. the potential accumulation of a target protein.

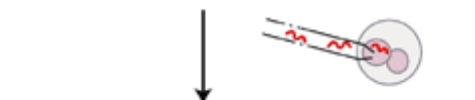
## 1.6 Mouse models with *MYBPC3* mutations

One of the major problems in understanding FHC has been the difficulty in obtaining cardiac specimens from affected patients. Thus, the development of animal models has been started. The advantage of using murine models lies in the ease of genetic

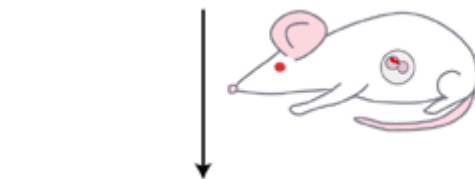
manipulation, short generation time and large number of offspring. To modify the mammalian genome, two distinct but complementary approaches have been developed: the additive and the targeted transgenesis (Fig. 1.10).

### A Additive transgenesis

Transgene DNA is microinjected into the male pronucleus of a fertilised murine oocyte



Injected oocytes are transferred to a 0.5-day pseudopregnant recipient mouse



Offspring are screened for the transgene by DNA analysis

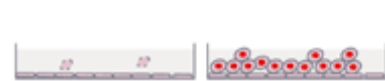


### B Targeted transgenesis

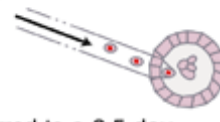
Isogenic transgene DNA is introduced into ES cells (e.g. by electroporation)



Drug selection is used and the surviving colonies are screened for the transgene



Characterised targeted cells are microinjected into 3.5-day mouse blastocysts



Blastocysts are transferred to a 2.5-day pseudopregnant recipient mouse



Chimaeric offspring are identified, and mated to test for germline transmission of the transgene



**Figure 1.10: Additive and targeted transgenesis.** **A**, The additive transgenesis is based on the microinjection of linear DNA sequences into the chromosomes of fertilized eggs. The foreign DNA must be integrated into the genome prior to the doubling of the genetic material that precedes the first cleavage, in order for the animal to be born with a copy of this new information in every cell. Insertion of the transgene is hereby random, and multiple copies of the transgene are added to the endogenous genetic material. **B**, The targeted transgenesis uses homologous recombination to insert modified DNA at a specific gene site leading to an inactivation or mutation and subsequently generation of animals deficient or with a mutation in that gene product. The modified DNA is hereby electroporated in embryonic stem (ES) cells and after subsequent selection and screening procedures, these genetically modified ES cells are microinjected into blastocysts (adapted from Expert Reviews in Molecular Medicine© 2001 Cambridge University Press).

Until now, seven mouse models have been generated which carry a *MYBPC3* mutation. Out of them, three were created by additive transgenesis. The first mouse model expresses a mutant cMyBP-C lacking both the myosin and titin binding

domains (Yang et al., 1998), whereas the second mouse model expresses a mutant cMyBP-C lacking only the myosin binding site (Yang et al., 1999). The third mouse model expresses a mutant cMyBP-C lacking the PKA-dependent phosphorylation site (Yang et al., 2001). In all three mouse models, the mouse  $\alpha$ -myosin heavy chain ( $\alpha$ -MHC) promoter was used to drive cardiac-specific overexpression of the transgene. By targeted transgenesis, four mouse models were generated. Two of them are cMyBP-C knock-out mouse models: One is a functional cMyBP-C knock-out, in which exons 3 to 10 of the endogenous cMyBP-C were replaced by a neomycin resistance gene (Harris et al., 2002). The other one was generated by targeted deletion of exons 1 and 2 of the mouse *MYBPC3* gene, which includes the transcription initiation site, and is therefore a transcriptional knock-out (Carrier et al., 2004). In the third mouse model created by targeted transgenesis, the insertion of a neomycin resistance gene into exon 30 resulted in skipping of this exon leading to a C-terminal truncated cMyBP-C (McConnell et al., 1999; McConnell et al., 2001). Finally, the fourth mouse model expresses a N-terminal truncated cMyBP-C resulting from a replacement of exons 3-6 by a neomycin resistance gene (Witt et al., 2001).

The present cMyBP-C mouse models do not exactly match a human mutation and can therefore not be used to decipher the molecular mechanisms involved in FHC. For instance, the mouse model from McConnell et al. (1999) was created by inserting the neomycin resistance gene into exon 30, whereas the defective *MYBPC3* gene found in family “NN” contains a mutation in the splice donor sequence of intron 30 (Watkins et al., 1995).

## 1.7 Aim of the thesis

The aim of my thesis was to get insights into the molecular mechanisms involved in the regulation of cMyBP-C mutant levels in the context of FHC. It has been recently shown by adenoviral gene transfer of mutant human cDNAs in cardiomyocytes that truncated cMyBP-C proteins are rapidly and quantitatively degraded by the UPS, which was associated with an impairment of the UPS function (Sarikas et al., 2005). Therefore, I investigated whether truncated cMyBP-C mutants are also subject to degradation by the UPS *in vivo* and whether they alter this system. This was examined in two new targeted cMyBP-C mouse models: the transgenic M7t mouse model and the cMyBP-C knock-in mouse model. Both models are based on the same human *MYBPC3* point mutation, but were differently generated. The transgenic M7t mouse model was created by additive transgenesis and represents the appropriate mouse model to verify the data obtained by Sarikas et al. (2005) *in vivo*, because the same mutant cDNA construct was used for the generation of the mouse line as well as for the recombinant adenovirus. In contrast, the cMyBP-C knock-in mouse model was generated by targeted transgenesis, and the heterozygous mice of this model represent the first mice, which mimic exactly a situation found in humans. The point mutation is a G>A transition on the last nucleotide of exon 6 and is associated with a severe phenotype and a poor prognosis in humans (Richard et al., 2003). The molecular consequences of this mutation were not known, except that mutant mRNA deleted of exon 6 has been found in lymphocytes from one patient (“illegitimate transcription”) (Andersen et al., 2004), which suggested an exon skipping as a mechanism to produce a PTC and protein truncation. However, no data were obtained from myocardial tissue.

My work consisted in the development of the transgenic M7t mouse model, in the characterization of its phenotype and in the analysis of the cMyBP-C expression at the mRNA and protein level. Concerning the cMyBP-C knock-in mouse model, which was developed in Paris by Nicolas Vignier and Lucie Carrier, I participated in the analysis of the cMyBP-C expression at mRNA and protein levels. In both mouse models, I investigated *ex vivo* whether the mutant cMyBP-Cs were degraded by the UPS and *in vivo* whether the mutants altered the function of this system. The *in vivo* study included the use of so-called UPS reporter mice, which I initially evaluated to



determine whether they were suitable to monitor the UPS function in the heart. Due to the obtained results in the cMyBP-C knock-in mouse model, I additionally investigated the involvement of NMD in the regulation of the cMyBP-C mutants at mRNA level.

## 2 Material and Methods

### 2.1 Material

#### 2.1.1 Chemicals

Acetone	Merck
Acrylamide/bis solution (29:1)	Bio-Rad
Adenosine 5'-triphosphate (ATP)	Sigma
Agarose	Invitrogen
alpha- <sup>32</sup> P-dCTP	Amersham Biosciences
Ammonium persulfate (APS)	Bio-Rad
Ampicillin trihydrate	Serva
AmpliTaq Gold <sup>®</sup> polymerase	Applied Biosystems
Aqua ad iniectabilia	Baxter GmbH
Bacto <sup>™</sup> Agar	Becton Dickinson
Bacto <sup>™</sup> Tryptone	Becton Dickinson
Bacto <sup>™</sup> Yeast extract	Becton Dickinson
Benzoyl-valyl-glycyl-arginyl-7-amino-4-methylcoumarin (Bz-Val-Gly-Arg-AMC)	Biomol
Benzyloxycarbonyl-leucyl-leucyl-glutamyl-β-naphtylamide (Z-Leu-Leu-Glu-βNA)	Biomol
Boric acid	Merck
Bovine serum albumin (BSA)	Sigma
Bromphenol blue	Merck
2,3-butanedione monoxime (BDM)	Sigma
Calcium chloride hexahydrate (CaCl <sub>2</sub> ·6H <sub>2</sub> O)	Sigma
Calf intestinal alkaline phosphatase (CIP) with corresponding buffer	New England Biolabs
Collagenase type II	Worthington
Complete mini-proteases inhibitor cocktail	Roche Diagnostics

Coomassie Brilliant Blue G-250 reagent	Bio-Rad
Cycloheximide	Sigma
Disodium hydrogen phosphate dihydrate ( $\text{Na}_2\text{HPO}_4 \cdot 2\text{H}_2\text{O}$ )	Merck
DNA polymerase I large fragment (Klenow) with corresponding buffer	New England Biolabs
Deoxyribonucleotide triphosphate (dNTP) mix (dATP, dCTP, dGTP, dTTP)	Applied Biosystems
Depilatory cream elcamed	Asid Bonz
Difco™ trypsin 250	Becton Dickinson
Dimethyl sulfoxide (DMSO)	Sigma
Dithiothreitol (DTT)	Sigma
DNA isolation reagent for genomic DNA	AppliChem
Dulbecco's modified Eagle medium (DMEM) with 4.5 g/L glucose and without pyruvate	Gibco
ECL plus Western blotting detection system	Amersham Biosciences
Emetine	Sigma
Epoxomicin	Calbiochem
Ethidium bromide	Fluka
Ethylenediaminetetraacetic acid (EDTA)	Sigma
ExpressHyb Hybridization solution	Becton Dickinson
Fetal bovine or calf serum (FBS or FCS)	Biochrom
Gene Ruler™ 100 bp DNA ladder	Fermentas
Glucose	Sigma
Glycerol	Merck
Glycine	Roth
Hank`s balanced salt solution (HBSS), calcium/magnesium-free	Gibco
Heparin sodium (Liquemine®)	Roche
Horse serum	Biochrom
Hydrochloric acid (HCl)	Merck
4-(2-hydroxyethyl)piperazine-1-ethanesulfonic acid (HEPES)	Roth
Immunoglobulin G	Sigma
Insulin/transferrin/selenium (ITS)	Gibco
Isoflurane	Abbott
Isotonic 0.9% sodium chloride solution	Baxter GmbH

Laminin	Roche
L-glutamine	Diagnostics
Liberase Blendzyme 3	Gibco
Lipofectamine™ 2000	Roche
Loading dye, 6x	Diagnostics
M199 with Earl`s salt and L-glutamine	Invitrogen
Magnesium acetate tetrahydrate ( $\text{Mg}(\text{CH}_3\text{COO})_2 \cdot 4\text{H}_2\text{O}$ )	Fermentas
Magnesium chloride hexahydrate ( $\text{MgCl}_2 \cdot 6\text{H}_2\text{O}$ )	Gibco
Magnesium sulfate heptahydrate ( $\text{MgSO}_4 \cdot 7\text{H}_2\text{O}$ )	Merck
MassRuler™ DNA ladder	Roth
Methanol	Merck
MG132	Fermentas
MG262	J. T. Baker
Milk powder	Calbiochem
Minimum essential medium (MEM) with Hank`s salt and L-glutamine	Biomol
Mowiol 4-88	Roth
Penicillin-streptomycin	Gibco
Phosphate buffered saline (PBS)	Hoechst
Phosphocreatine	Gibco
Phosphocreatinekinase	Biochrom
Ponceau S	Calbiochem
Potassium chloride (KCl)	Sigma
Potassium hydrogen carbonate ( $\text{KHCO}_3$ )	Serva
Potassium dihydrogen phosphate ( $\text{KH}_2\text{PO}_4$ )	Merck
Power SYBR® Green PCR Master Mix	Merck
Precision Plus Protein Standard™	Applied Biosystems
Restriction enzymes ( <i>Bam</i> HI, <i>Eco</i> RI, <i>Nde</i> I, <i>Nhe</i> I, <i>Sal</i> I, <i>Sfo</i> I, <i>Xho</i> I) with corresponding buffers (containing 1x BSA)	Bio-Rad
Sodium chloride (NaCl)	New England Biolabs
Sodium dodecyl sulfate (SDS)	J. T. Baker
Sodium fluoride (NaF)	Roth
Sodium hydrogen carbonate ( $\text{NaHCO}_3$ )	Merck
	Merck

Sodium hydroxide (NaOH)	Merck
Succinyl-leucyl-leucyl-valyl-tyrosyl-7-amino-4-methylcoumarin (SUC-Leu-Leu-Val-Tyr-AMC)	Calbiochem
SuperSignal <sup>®</sup> West Dura extended duration substrate	Pierce
T4 DNA ligase with corresponding buffer	New England Biolabs
TaqMan <sup>®</sup> Universal PCR Master Mix	Applied Biosystems
Taurine	Merck
Tetramethylethylenediamine (TEMED)	Bio-Rad
ToPro3 <sup>®</sup>	Molecular Probes
Trishydroxymethylaminomethane (Tris) base	Sigma
Tris hydrochloride (Tris-HCl)	Promega
Trisodium citrate dihydrate	Merck
Triton X-100	Sigma
Polyoxyethylene (20) sorbitan monolaurate (Tween <sup>®</sup> 20)	Sigma
Ultrasound transmission gel	Caesar & Loretz

### 2.1.2 Chemicals with risk (R-) and safety (S-) phrases

Acetone	R: 11-36-66-67	S: 9-16-26
Acrylamide/bis solution	R: 23/24/25-45-46-48	S: 36/37/39-45-60
ATP	R: -	S: 22-24/25
APS	R: 8-22-36/37/38-42/43	S: 22-24-26-37
Bromphenol blue	R: -	S: 22-24/25
BDM	R: -	S: 22-24/25
Calcium chloride hexahydrate	R: 36	S: 22-24/25
Coomassie Brilliant Blue G-250 reagent	R: 20/21/22-34-68	S: 26-36/37/39-45
Cycloheximide	R: 28-52/53-61-68	S: 45-53
Disodium hydrogen phosphate dihydrate	R: -	S: 22-24/25
DMSO	R: 36/37/38	S: 23-26-36
DTT	R: 22-36/37/38	S: 26-36

DNA isolation reagent for genomic DNA	R: 20/21/22-32	S: 24/25
ECL plus Western blotting detection system	R: 11-19-36/37-40-66	S: 16-23-36/37
Emetine	R: 28-36/37/38	S: 26-28-36/37-45
Epoxomicin	R: 36/38	S: 26
Ethidium bromide	R: 23-68	S: 36/37-45
EDTA	R: 36-52/53	S: 26-61
Glycine	R: -	S: 22-24/25
Hydrochloric acid	R: 34-37	S: 26-36/37/39-45
Magnesium acetate tetrahydrate	R: -	S: 22-24/25
Methanol	R: 11-23/24/25-39	S: 7-16-36/37-45
MG132	R: 11-36/38	S: 24/25-26-29
PBS	R: -	S: 22-24/25
Ponceau S	R: 36/37/38-51/53	S: 2-25-26-29/56-37-46-57-60-64
Potassium chloride	R: -	S: 22-24/25
SDS	R: 22-36/38	S: 22-24/25
Sodium fluoride	R: 25-32-36/38	S: 22-36-45
Sodium hydroxide	R: 35	S: 26-37/39-45
Taurine	R: 36/37/38	S: 26-36
TEMED	R: 11-20/22-34	S: 16-26-36/37/39-45-60
Tris base	R: 36/37/38	S: 26-36
Tris hydrochloride	R: 36/37/38	S: 26-36
Triton X-100	R: 22-41-51/53	S: 26-36/39-61

### 2.1.3 Antibodies

Anti-cMyBP-C (C0C1-domains), polyclonal	Mathias Gautel, King's College London, London
Anti- $\alpha$ -actinin (clone EA-53), monoclonal	Sigma
Anti-c-myc, monoclonal	Invitrogen

Anti-titin-Z1, polyclonal	Siegfried Labeit, Mannheim University, Mannheim
Anti-ubiquitin (P4D1), monoclonal	Santa Cruz Biotechnology
Anti-GFP (FL), polyclonal	Santa Cruz Biotechnology
Alexa Fluor <sup>®</sup> 488 anti-mouse IgG	Molecular Probes
Alexa Fluor <sup>®</sup> 546 anti-rabbit IgG	Molecular Probes
Anti-rabbit IgG	Sigma
Cy3 conjugate	
Anti-rabbit IgG peroxidase conjugate	Sigma and Dianova
Anti-mouse IgG peroxidase conjugate	Dianova

#### 2.1.4 Bacterial strain

Escherichia coli (DH10B) cells	Invitrogen
--------------------------------	------------

#### 2.1.5 Kits

QIAGEN Plasmid Maxi Kit	Qiagen
QIAquick gel extraction kit	Qiagen
QIAquick PCR purification kit	Qiagen
Rediprime <sup>™</sup> II kit	Amersham Biosciences
Extract-N-Amp <sup>™</sup> Tissue PCR Kit	Sigma
SV Total RNA Isolation Kit	Promega
SuperScript <sup>™</sup> III First-Strand Synthesis System for RT-PCR	Invitrogen

#### 2.1.6 Oligonucleotides

All primers and probes were designed using the Primer Express software or the Primer3 program, which is online available, and purchased from the MWG Biotech AG.

### 2.1.7 Consumable material

Blotting paper (Whatman 3MM)	Schleicher & Schuell
Cell scraper	Sarstedt AG & Co.
Cell strainer	Becton Dickinson
Coverslips (Ø 10 mm)	Glaswarenfabrik Karl Hecht KG
Cuvettes (10 x 4 x 45 mm)	Sarstedt AG & Co.
Culture flasks (T75)	Sarstedt AG & Co.
Culture plates (6-well)	Greiner Bio-One GmbH
Culture plates (12-well)	Nalge Nunc International
Falcon tubes (15 and 50 ml)	Sarstedt AG & Co.
Glassware	Schott Duran
Hypodermic needles (Sterican® Gr.20)	Braun
Insulin syringes (BD Plastipak™ U-40 1 ml)	Becton Dickinson
Lab-Tek™ chambers	Nalge Nunc International
Latex gloves	Paul Hartmann AG
Microscope slides	Paul Marienfeld GmbH
Micro tubes (1.5, 2.0 ml)	Sarstedt AG & Co.
Multiple well plates (96-wells)	Sarstedt AG & Co.
Nitrile gloves	Ansell
Nitrocellulose membrane (Protran® BA 85)	Schleicher & Schuell
Nylon membrane (Hybond N+)	Amersham Biosciences
PCR tubes	Sarstedt AG & Co.
Pipette tips (for 10, 100 and 1000 µl pipettes)	Sarstedt AG & Co.
Phospho Imager plates	Fuji
Serological pipettes (2, 5, 10 and 25 ml)	Sarstedt AG & Co.
Serological pipettes (10 ml, wide tip)	Becton Dickinson
Sterile filter (0.22 µm)	Sarstedt AG & Co.



## 2.1.8 Laboratory equipment

Accu-jet pipetting aid	Brand GmbH
Analytical balance (GENIUS)	Sartorius AG
Benchtop centrifuge	Sarstedt AG & Co.
Blotting system (Mini Trans-Blot <sup>®</sup> cell)	Bio-Rad
Centrifuge (5810 R)	Eppendorf AG
Chemie Genius <sup>2</sup> Bio imaging system with Gene Tools software	Syngene
Electrophoresis system (Sub-Cell GT)	Bio-Rad
Electrophoresis system (Mini PROTEAN <sup>®</sup> 3 electrophoresis cell)	Bio-Rad
Ice machine	Scotsman
Incubators (B 5050 E and Hera cell 240)	Heraeus Instruments
Incubator shaker (C25 classic)	New Brunswick Scientific
Magnetic stirrer (IKAMAG <sup>®</sup> RCT)	Janke & Kunkel GmbH
Microplate reader (Tecan Safire <sup>2</sup> )	Tecan
Microcentrifuge (5415 R)	Eppendorf AG
Microscope (Axiovert 25)	Zeiss
Microscope (Axiovert 200 M) with a 40x-oil objective and with a LSM 5 image system	Zeiss
Microwave	Sharp
Neubauer chamber	Glaswarenfabrik Karl Hecht KG
PCR cycler (GeneAmp <sup>®</sup> PCR system 9700)	Applied Biosystems
PCR sprint thermal cycler	Thermo Hybaid
pH-meter	Knick GmbH
Phospho Imager system (FLA-3000)	Fuji
Pipettes (10, 100, 1000 µl)	Eppendorf AG
Portable balance (Scout <sup>™</sup> Pro)	Ohaus
Power supply	Bio-Rad
Precision balance (Precision Advanced)	Ohaus
Rectal thermometer	Physitemp
Spectrophotometer (Smart Spec <sup>™</sup> 3000)	Bio-Rad

Sterile work bench (Lamin Air HB 2448)	Heraeus Instruments
Surgical instruments	Karl Hammacher GmbH
Taqman ABI Prism 7900HT sequence detection system with ABI 7900HT SDS 2.2 software	Applied Biosystems
Tissue Lyser	Qiagen
Thermomixer comfort	Eppendorf AG
Ultra-pure water system Milli-Q plus	Millipore
Ultrasonograph (Visual Sonics Vevo 770 <sup>®</sup> ) with a 30-MHz central frequency transducer	Visual Sonics
Vortexer (Vibrofix VF1)	Janke & Kunkel GmbH
Water bath	GFL

### 2.1.9 Animal models

The investigations conform to the guide for the care and use of laboratory animals published by the NIH (Publication No. 85-23, revised 1985).

#### 2.1.9.1 The M7t mouse model

The transgenic M7t mouse model was developed in Hamburg by me. It was generated by microinjection of a targeted cDNA construct (Fig. 2.1) in the pronucleus of single-cell mouse embryos. The generation was authorized by the Behörde für Wissenschaft und Gesundheit der Freien und Hansestadt Hamburg (Org 72/04).

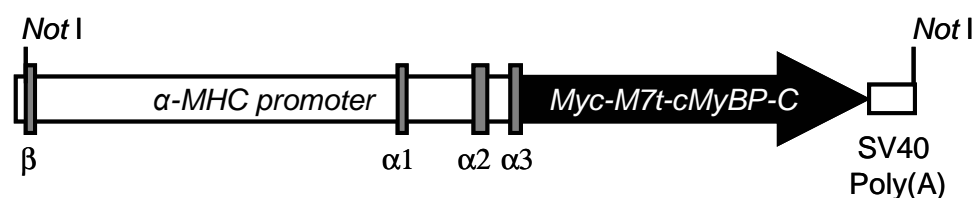


**Figure 2.1: Schematic illustration of the transgenic construct of the M7t mice.** The transgene contains the mouse  $\alpha$ -MHC promoter, the human Myc-M7t-cMyBP-C cDNA and the SV40 polyadenylation signal. Restriction sites used for transgene excision are indicated.

Three different plasmids were used to get the targeted cDNA construct:

1. The pMT-Myc-M7t plasmid, which contains the coding sequence for the human M7t-cMyBP-C cDNA deleted of exon 6 and a c-myc epitope in the 5'-end of the cDNA. This plasmid was developed by Lucie Carrier in Paris to create the recombinant adenovirus expressing the Myc-M7t-cMyBP-C (Sarikas et al., 2005).
2. The pUC18-Mae- $\beta_2$  plasmid, which contains the C-terminal part of the mouse  $\alpha$ -MHC-promoter, which is required for the heart-specific expression of the transgene. This plasmid was kindly given by Stefan Engelhardt (University of Würzburg, Rudolf-Virchow Center, DFG Research Center for Experimental Biomedicine, Würzburg).
3. The pBlue-MHC- $\beta_2$  plasmid, from which the N-terminal part of the mouse  $\alpha$ -MHC-promoter was isolated. This plasmid was also given by Stefan Engelhardt.

At first, all three plasmids, which contain the ampicillin resistance gene, were transformed into chemically competent *Escherichia coli* (DH10B) cells by heat shock. After plating the transformation mixtures on ampicillin-containing Luria-Bertani (LB) agar plates (1.5% agar and 100  $\mu$ g/ml ampicillin in LB-medium (1% tryptone, 0.5% yeast extract, 1% NaCl, pH 7.4)) and subsequent incubation overnight at 37 °C, single bacterial colonies from each transformation were inoculated in ampicillin-containing LB-medium and incubated overnight at 37 °C under agitation. DNAs were then isolated and purified according to the instruction manual of the QIAGEN Plasmid Maxi Kit. DNA concentration of each maxi preparation was determined with a spectrophotometer by measuring the absorbance at a wavelength of 260 nm and assuming that 1 unit of absorbance corresponds to 50  $\mu$ g of DNA. Absorbance was also determined at the wavelength of 280 nm and the ratio  $A_{260}/A_{280}$  was calculated to check for protein contamination.

To obtain the targeted cDNA construct (Fig. 2.1), the following cloning strategy was performed (summarized in Fig. 2.2): The plasmid pMT-Myc-M7t was digested with the restriction enzymes *NheI*, *XhoI* und *NdeI* to isolate the insert Myc-M7t-cMyBP-C, the plasmid pUC-Mae- $\beta_2$  was cut with the restriction enzyme *BamHI* to isolate the C-

terminal (Cter) part of the  $\alpha$ -MHC-promoter (in the following named pUC-Mae), and the plasmid pBlue-MHC- $\beta_2$  was digested with the restriction enzymes *NdeI* und *SalI* to isolate the N-terminal (Nter) part of the  $\alpha$ -MHC- promoter (in the following named pBlue-MHC). All digestions were performed in appropriate buffers (containing 1x BSA) overnight at 37 °C and then separated by electrophoresis on 1% agarose gels (1% agarose and 0.4  $\mu$ g/ml ethidium bromide in TBE buffer (45 mM Tris base, 45 mM boric acid, 1 mM EDTA, pH 8.0). The corresponding fragments were excised from the gels and the contained DNAs were extracted and purified according to the instruction manual of the QIAquick gel extraction kit. The isolated DNA fragments were checked on a 1% agarose gel and DNA concentrations were determined with a MassRuler™ DNA ladder, which was also loaded on the gel. A Klenow-reaction was performed at 25 °C for 15 min with the isolated Myc-M7t-cMyBP-C and the isolated pUC-Mae using the DNA polymerase I large fragment (Klenow, 5 U/ $\mu$ l) in corresponding 1x buffer containing 33  $\mu$ M dNTPs. Klenow reaction was stopped by adding 10 mM EDTA and heating at 75 °C for 20 min. DNAs were then extracted and purified with the QIAquick PCR purification kit, and DNA concentrations were determined with the MassRuler™ DNA ladder on a 1% agarose gel. Following Klenow reaction, pUC-Mae was dephosphorylated using the calf intestinal alkaline phosphatase (CIP, 1 U/ $\mu$ l) in corresponding buffer at 37 °C for 30 min. Reaction was stopped by adding 10 mM EDTA and heating at 65 °C for 15 min. DNA was extracted and purified with the QIAquick PCR purification kit, and DNA concentration was determined as described above. In the next step, Myc-M7t-cMyBP-C (insert) was ligated in pUC-Mae (vector) by using a 1:3 vector to insert ratio and the T4 DNA ligase (400 U/ $\mu$ l) in corresponding 1x buffer. Ligation was performed overnight at 14 °C. The ligation reaction was transformed into chemically competent *Escherichia coli* (DH10B) cells by heat shock and then plated on ampicillin-containing LB agar plates. After incubation overnight at 37 °C, single bacterial colonies were incubated in ampicillin-containing LB-medium overnight at 37 °C under agitation. DNA was isolated and purified according to the instruction manual of the QIAGEN Plasmid Maxi Kit. Positive pUC-M7t-clones (identified by digestion with the restriction enzymes *BamHI* and *XhoI*) were cut with the restriction enzymes *NdeI* and *SalI* in an appropriate buffer (containing 1x BSA) overnight at 37 °C to isolate the part Cter- $\alpha$ -MHC-promoter + Myc-M7t-cMyBP-C. After separation by electrophoresis on a 0.8% agarose gel, the corresponding fragment was excised from

the gel, and the contained DNA was extracted and purified according to the instruction manual of the QIAquick gel extraction kit. This freshly isolated fragment was ligated in the isolated pBlue-MHC as described above. Following transformation, DNA amplification and purification were also performed as described above.

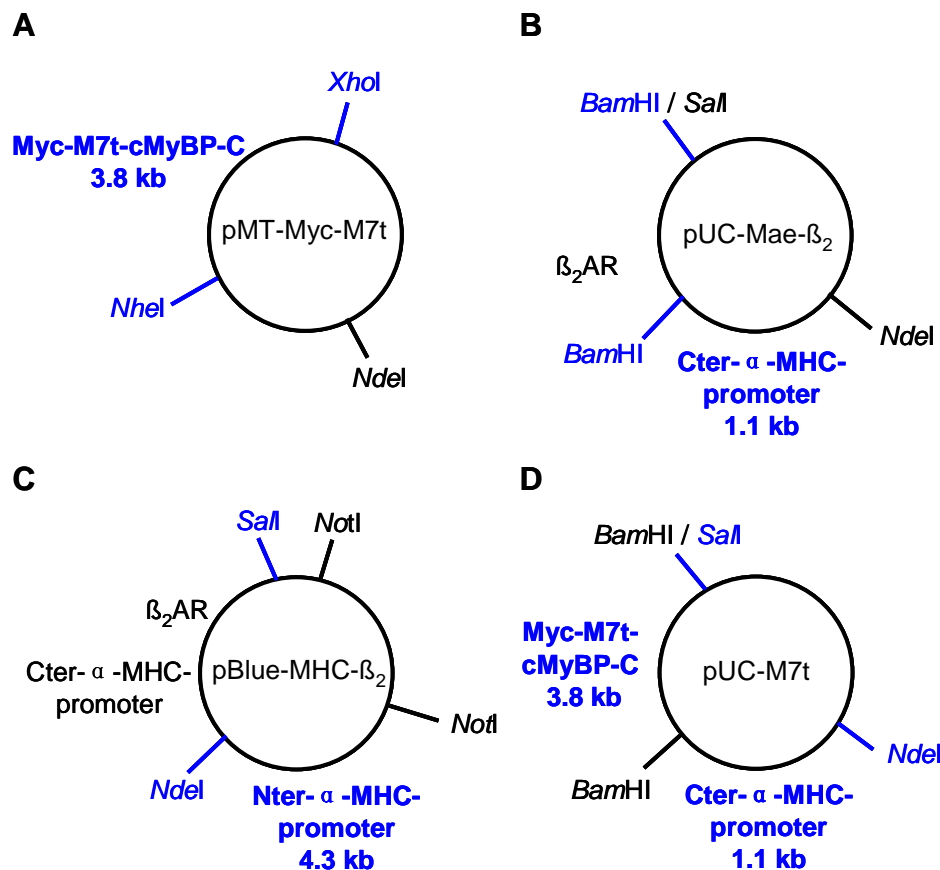


**Figure 2.2: Cloning strategy to create the M7t mouse model.** **A**, The plasmid pMT-Myc-M7t was cut with the restriction enzymes *NheI*, *XhoI* and *NdeI* to isolate the insert Myc-M7t-cMyBP-C. Afterwards, a Klenow-reaction was performed with the isolated Myc-M7t-cMyBP-C. **B**, The plasmid pUC-Mae- $\beta_2$  was cut with the restriction enzyme *BamHI* to isolate the C-terminal part (Cter) of the  $\alpha$ -MHC-promoter (pUC-Mae). Afterwards, a Klenow-reaction was performed with the isolated pUC-Mae followed by a dephosphorylation. **C**, The plasmid pBlue-MHC- $\beta_2$  was cut with the restriction enzymes *NdeI* and *SalI* to isolate the N-terminal (Nter) part of the  $\alpha$ -MHC- promoter (pBlue-MHC). **D**, Myc-M7t-cMyBP-C was ligated in pUC-Mae. Positive pUC-M7t-clones were cut with the restriction enzymes *NdeI* and *SalI* to isolate the part Cter- $\alpha$ -MHC-promoter + Myc-M7t-cMyBP-C. This isolated part was then ligated in the isolated pBlue-MHC to get the final cDNA construct (Fig. 2.3).

The final construct pBlue- $\alpha$ -MHC-prom-Myc-M7t-cMyBP-C (Fig. 2.3) was checked on a 0.8% agarose gel, and DNA concentration was determined with the MassRuler™ DNA ladder.

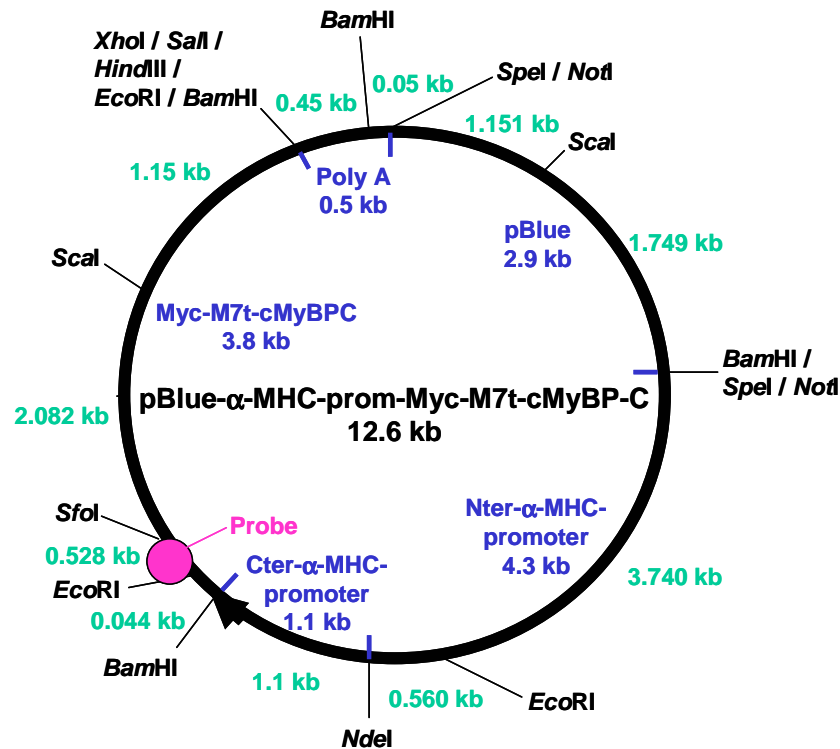


**Figure 2.3: Final construct pBlue- $\alpha$ -MHC-prom-Myc-M7t-cMyBP-C.** This DNA construct was linearized with the restriction enzyme *NotI* to isolate the fragment containing the  $\alpha$ -MHC-promoter and the Myc-M7t-cMyBP-C cDNA for the microinjection. The probe used for the Southern blot (2.2.1.1) is indicated.

To isolate the transgenic construct (Fig. 2.1) for the microinjection, pBlue- $\alpha$ -MHC-prom-Myc-M7t-cMyBP-C (Fig. 2.3) was linearized overnight at 37 °C with the restriction enzyme *NotI*. The corresponding fragment ( $\alpha$ -MHC-promoter + Myc-M7t-cMyBP-C) was excised from a 0.8% agarose gel (without adding ethidium bromide) and purified using the QIAquick gel extraction kit. The purified plasmid was given to Irm Hermans-Borgmeyer (Centre for Molecular Neurobiology Hamburg, Hamburg), who performed the microinjection of the cDNA into the pronucleus of single-cell C57Blx/CBA mouse embryos.

To obtain the probe for the Southern blot (2.2.1.1), the final construct pBlue- $\alpha$ -MHC-prom-Myc-M7t-cMyBP-C (Fig. 2.3) was digested with the restriction enzymes *EcoRI*

and *SfoI* in an appropriate buffer overnight at 37 °C. The corresponding fragment was excised from a 0.8% agarose gel and purified using the QIAquick gel extraction kit. Probe concentration was determined with the MassRuler™ DNA ladder on a 1% agarose gel.

### 2.1.9.2 The cMyBP-C knock-in mouse model

The cMyBP-C knock-in mouse model was developed in Paris by Nicolas Vignier and Lucie Carrier. The G>A transition on the last nucleotide of exon 6 was introduced in mice by gene targeting using the Cre/lox system as depicted in Figure 2.4.

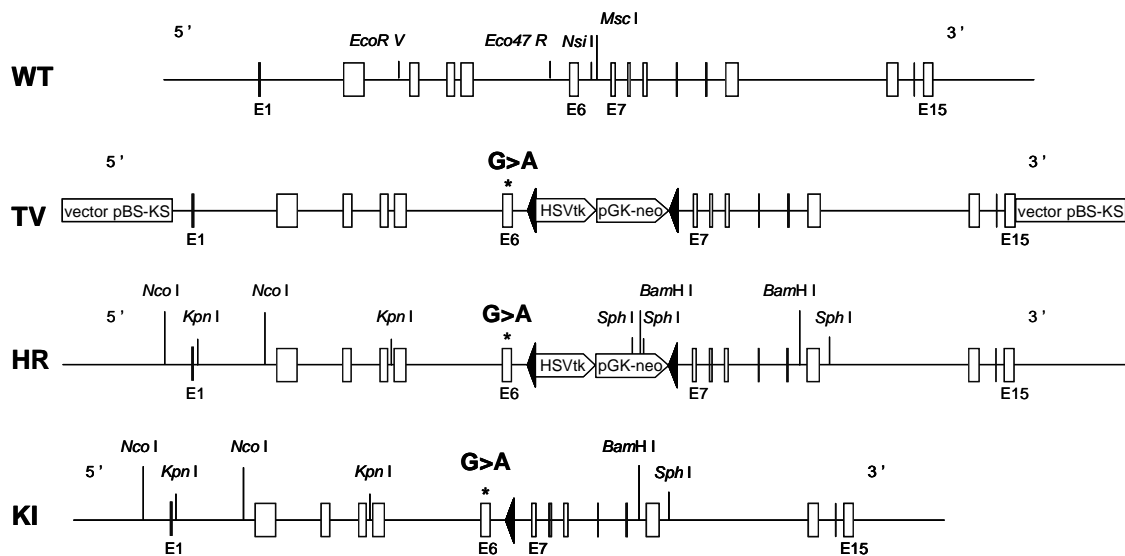


**Figure 2.4: Targeting strategy for the cMyBP-C knock-in mouse model.** WT, schematic structure of the mouse *MYBPC3* gene from exon 1 (E1) to exon 15 (E15); TV, targeting vector containing the G>A transition on the last nucleotide of exon 6 (E6) and the selection cassette (herpes simplex virus thymidine kinase (HSVtk), pGK-neomycin (pGK-neo)) flanked by two loxP sites (black arrows); HR, allele obtained after homologous recombination in AT1 embryonic stem cells; KI, targeted floxed-out knock-in allele.

The targeting vector containing a 12.5-kb insert was obtained in several steps. A 8105-bp fragment containing the 5'-part of the mouse *MYBPC3* gene, which covers 1747-bp upstream of exon 1 up to exon 15, was obtained by long-range polymerase chain reaction (PCR) and cloning from a FIX II genomic library derived from a 129/Svj mouse strain, and then cloned into the pBluescript® II KS+ vector. The G>A transition on the last nucleotide of exon 6 was obtained by site-directed mutagenesis on a 258-bp PCR fragment, which was then cloned into the *Eco47RI*-*NsiI* sites. The

linearized targeting vector, which contained the mutation and a selection cassette composed of the neomycin resistance and herpes simplex virus thymidine kinase genes flanked by two *loxP* sites, was electroporated into AT1 embryonic stem cells and proceeded for homologous recombination (Buchou et al., 2003). Genomic DNA was extracted from G418 resistant clones and screened by long-range PCR to check for 5' and 3' homologous recombination. Two clones with the correct recombination event were used to obtain germ-line transmitting chimeras (Buchou et al., 2003). One chimeric mouse was obtained and crossed with a Black-swiss wild-type mouse to check for germline transmission. Two heterozygous cMyBP-C knock-in females were crossed with a CD1 Sycp1-Cre transgenic male, which expressed the recombinase Cre under the control of the Sycp-1 promoter (Vidal et al., 1998). After Cre-mediated recombination, one *loxP* site remained in the DNA, which resulted in a 94-bp longer PCR fragment. Heterozygous offsprings were further backcrossed to Black-swiss mice. Pups were born in the expected Mendelian ratios of wild-type, heterozygous and homozygous cMyBP-C knock-in mice. Both heterozygous and homozygous cMyBP-C knock-in mice appeared normal and were viable up to two years. Further characterization of this mouse model will be presented in the results.

### **2.1.9.3 The cMyBP-C knock-out mouse model**

The cMyBP-C knock-out mouse model, developed by Lucie Carrier in Paris, is a transcriptional knock-out (Carrier et al., 2004). It was generated by targeted deletion of exons 1 and 2 of the mouse *MYBPC3* gene, which included the transcription initiation site. In homozygous cMyBP-C knock-out mice, no cMyBP-C mRNA and protein were detected, validating the gene inactivation. These mice develop eccentric left ventricular (LV) hypertrophy with decreased fractional shortening and a significant increase of the LV mass to body weight ratio at the age of 3-4 months (mo) compared to corresponding wild-type mice. In addition, histological examination at this age exhibited myocardial disarray, increase of interstitial fibrosis and calcification in the fibrotic areas.



#### 2.1.9.4 The Ub<sup>G76V</sup>-GFP mouse model

The Ub<sup>G76V</sup>-GFP mouse model was kindly given by Nico Dantuma (Microbiology and Tumor Biology Center, Karolinska Institute, Stockholm). This mouse model expresses an Ub<sup>G76V</sup>-GFP reporter protein, which is a N-terminal ubiquitin mutant (Ub<sup>G76V</sup>) in frame with an green fluorescent protein (GFP) and which is widely expressed at high levels by a chimeric cytomegalovirus immediate early (CMV-IE) enhancer and a chicken  $\beta$ -actin promoter (Lindsten et al., 2003) (Fig. 2.5).

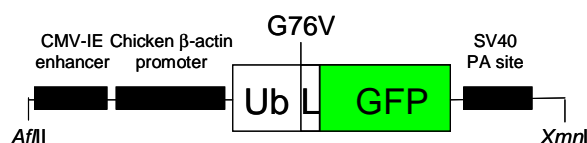


**Figure 2.5: Schematic illustration of the transgenic construct of the Ub<sup>G76V</sup>-GFP mice.** The transgene contains the CMV-IE enhancer, the chicken  $\beta$ -actin promoter, the Ub<sup>G76V</sup>-GFP open reading frame and the SV40 polyadenylation signal. Restriction sites used for transgene excision are indicated (adapted from Lindsten et al., 2003).

Ub<sup>G76V</sup>-GFP transcripts were present in different tissues, with predominant expression in skeletal muscle, heart, testis and cerebellum. The N-terminal-linked ubiquitin molecule serves as an acceptor for polyubiquitin chains, through the canonical Lys48 and the less common Lys29. The G76V substitution prevents the removal of this ubiquitin by cellular ubiquitin C-terminal hydrolases, leading to efficient ubiquitination and proteasomal degradation of the Ub<sup>G76V</sup>-GFP fusion protein. Therefore, no GFP-fluorescence in any of the tissues was obtained in cryosections from adult Ub<sup>G76V</sup>-GFP mice by fluorescence microscopy under normal conditions. In contrast, after treatment with different proteasome inhibitors, pronounced accumulation of the Ub<sup>G76V</sup>-GFP reporter was visualized in primary fibroblasts and neonatal cardiomyocytes. The intraperitoneal (i.p.) injection of the proteasome inhibitor MG262 (5  $\mu$ mol/kg) in adult Ub<sup>G76V</sup>-GFP mice resulted in a detectable GFP fluorescence in the liver, small intestine, pancreas, kidney and to a lower extent in the lung and spleen. No fluorescent cells could be observed in the brain, heart and skeletal muscles (Lindsten et al., 2003).

### 2.1.9.5 The GFPdgn mouse model

The GFPdgn mouse model was kindly provided by Xuejun Wang (Cardiovascular Research Institute, University of South Dakota School of Medicine, South Dakota). This mouse model was engineered by fusion of the CL1 degron, which is a consensus ubiquitination signal sequence, to the C-terminus of the coding sequence of the GFP (Kumarapeli et al., 2005). This modified GFP (GFPdgn) was placed behind a hybrid promoter composed of the human CMV-IE enhancer and the chicken  $\beta$ -actin promoter along with its first intron and in front of the rabbit  $\beta$ -globin poly-adenylation site (Fig. 2.6).

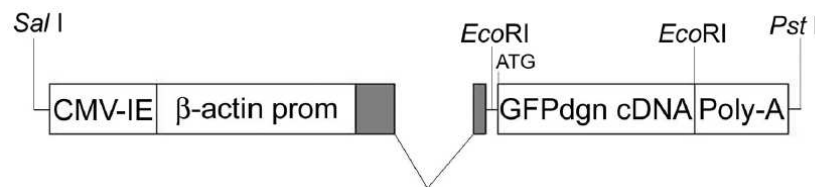


**Figure 2.6: Schematic illustration of the transgenic construct of the GFPdgn mice.** The transgenic construct consists of the CMV-IE enhancer, the chicken  $\beta$ -actin promoter, the GFPdgn cDNA open reading frame and the polyadenylation sequence (Poly-A) from the rabbit  $\beta$ -globin gene. The 2 grey boxes represent noncoding exons of the chicken  $\beta$ -actin promoter. Restriction sites used for transgene excision are indicated (adapted from Kumarapeli et al., 2005).

GFPdgn transcripts were expressed in all major organs. The GFPdgn protein was detected by Western blot in the heart under normal conditions. Proteasome inhibition with different proteasome inhibitors caused marked increase of the GFPdgn protein in isolated adult cardiomyocytes analyzed by Western blot or fluorescence microscopy. Systemic proteasomal inhibition by intravenous (i.v.) injection of MG262 (5  $\mu$ mol/kg) in adult GFPdgn mice revealed increased GFPdgn protein levels in all examined organs (including the heart) analyzed by Western blot or confocal microscopy (Kumarapeli et al., 2005).

## 2.2 Methods

### 2.2.1 Genotyping

#### 2.2.1.1 Genotyping by Southern Blot

Genomic DNA was extracted from mouse tails according to the instruction manual of the DNA isolation reagent for genomic DNA, except that the DNA was dissolved in TE buffer (1 M Tris-HCl, 0.5 M EDTA, pH 7.4) instead of 8 mM NaOH. Extracted DNA was digested overnight with the restriction enzyme *EcoR* I at 37 °C and then separated by electrophoresis at 130 V on a 0.8% agarose gel for 4.5 h. Afterwards, the gel was first treated with 0.25 M HCl for 15 min to depurinate the DNA fragments and then with 0.4 M NaOH for 15 min to denature the DNA. The DNA-gel was transferred overnight to a positively charged nylon membrane by capillary action under alkaline conditions (0.4 M NaOH). The dried membrane was exposed overnight to a hybridization probe at 68 °C in a hybridization solution (ExpressHyb™). The probe (see 2.1.1.1 and Fig. 2.3) was labeled before with  $\alpha$ -<sup>32</sup>P-dCTP by random primer labeling using the Rediprime™ II kit. After washing (75 mM NaCl, 7.5 mM sodium citrate, 1% SDS, pH 7.0), the membrane was exposed overnight to a Phospho-Imager plate. The pattern of hybridization was visualized using a Phospho-Imager-System.

#### 2.2.1.2 Genotyping by PCR

Genomic DNA was extracted and amplified from mouse tails according to the instruction manual of the Extract-N-Amp™ Tissue PCR Kit. PCR amplification was performed using the cycling parameters specified in Table 2.1 and the primers listed in Table 2.2.

**Table 2.1: PCR cycling parameters for genotyping by PCR.**

PCR step	Temperature (°C)	Time (min:sec)	Cycles
Initial denaturation	94	5:00	1
Denaturation	94	0:30	11
Annealing 1	Depending on mouse line (see Table 2.2)	0:30	
Elongation	72	1:00	
Denaturation	94	0:30	24
Annealing 2	Depending on mouse line (see Table 2.2)	0:30	
Elongation	72	1:00	
Final elongation	72	7:00	1
Final hold	4	indefinitely	

**Table 2.2: Primer list for genotyping.**

Mouse line	Primer name	Primer sequence (5'-3')	AT 1/2 (°C)
M7t	M7t-F	GCCAGTCTCAGCCTTTAGCA	60/55
	M7t-R	CCAGCAATGACTGCGTAAGA	
cMyBP-C knock-in	GKI cas F	GTCTGGTCTTGTGGTCTT	55/50
	GKI cas R	GCATTTTCGTTACACCTC	
Ub <sup>G76V</sup> -GFP	TG5-1 (s)	CCTACAGCTCCTGGGCAACGT	65/60
	Ub/G76V/-2	TCGACCAAGCTTCCCCACCAC	
GFPdgn	GFPdgn-F	GCGATGCCACCTACGGCAAGC	70/65
	GFPdgn-R	GTGGTCGGCGAGCTGCACGCT	

AT means annealing temperature (see Table 2.1).

The amplified DNA was loaded on a 1% agarose gel. The Gene Ruler™ 100 bp DNA Ladder was used as molecular weight marker. Gel image was recorded with the Chemie Genius<sup>2</sup> Bio Imaging System.

### **2.2.2 Organ extraction**

Organ extraction was authorized by the Behörde für Soziales, Familie, Gesundheit und Verbraucherschutz der Freien und Hansestadt Hamburg (Org 370). Mice were sacrificed by cervical dislocation in light CO<sub>2</sub> anesthesia and weighted. After median thoracotomy, the hearts were extracted, rinsed in isotonic 0.9% NaCl solution, dried and weighted. After removing the atria, the ventricular weights were determined. If needed other organs like lung, liver and kidney were also excised and their weights noted. After weighing, tissues were frozen in liquid nitrogen and stored at -80 °C until utilization. To equally portion the ventricles for different preparations, frozen ventricles were powdered with a steel mortar in liquid nitrogen. The tissue powder was mainly divided in three portions and also stored at -80 °C until utilization.

### **2.2.3 RNA analysis**

#### **2.2.3.1 RNA isolation**

Total RNA was extracted from ~ 30 mg frozen tissue powder (see 2.2.2) or  $3.3 \times 10^5$  cultured and treated isolated neonatal mouse cardiomyocytes (see 2.2.5.1) according to the instruction manual of the SV Total RNA Isolation Kit. Total RNA was stored at -80 °C until further utilization.

#### **2.2.3.2 RNA concentration determination**

RNA concentration was determined with a spectrophotometer by measuring the absorbance at a wavelength of 260 nm and assuming that 1 unit of absorbance corresponds to 40 µg of RNA. Absorbance was also determined at the wavelength of 280 nm, and the ratio  $A_{260}/A_{280}$  was calculated to test for protein contamination.

### 2.2.3.3 Reverse transcription (RT)

Total RNA (100 ng from cell preparations and 100 ng or 1 µg from tissue preparations) was reverse transcribed into cDNA using oligo(dT)s according to the instruction manual of the SuperScript™ III First-Strand Synthesis System for RT-PCR. For the amplification of the cMyBP-C pre-mRNA, RT was performed using random hexamers instead of oligo(dT)s.

### 2.2.3.4 Classical RT-PCR

To analyze the expression of the transgene in the M7t mouse model, corresponding cDNAs were amplified according to the instruction manual of the Extract-N-Amp™ Tissue PCR Kit with the exception that 1 µl cDNA was applied instead of 4 µl. The same cycling parameters as specified in Table 2.1 were used and the used primers are listed in Table 2.3.

**Table 2.3: Primer list for classical RT-PCR in the M7t mouse model.**

Mouse line	Primer name	Primer sequence (5'-3')	AT 1/2 (°C)
M7t	Myc-M7t-F	TGGAGCTAGCATGGAGCAAA	60/55
	Myc-M7t-R	CAGGCCGTACTTGTTGCTG	

AT means annealing temperature (see Table 2.1).

The amplified cDNA was loaded on a 1% agarose gel. The Gene Ruler™ 100 bp DNA Ladder was used as molecular weight marker. Gel images were recorded with the Chemie Genius<sup>2</sup> Bio Imaging System.

To analyze the different cMyBP-C mRNA species in the cMyBP-C knock-in mouse model, corresponding cDNAs were amplified according to the instruction manual of the AmpliTaq Gold® polymerase using the cycling parameters specified in Table 2.1 and the primers listed in Table 2.4.

**Table 2.4: Primer list for classical RT-PCR in the cMyBP-C knock-in mouse model.**

Mouse line	Primer name	Primer sequence (5'-3')	AT 1/2 (°C)
cMyBP-C	Cprot ex 4-5 (F)	GACCGTGGGCGGCAGCATTG	65/60
knock-in	Cprot ex 8-9 (R)	TGGCTGTCACTGGTTCTCCG	

AT means annealing temperature (see Table 2.1).

The amplified PCR-products were visualized in the same way as described above.

#### 2.2.3.5 Quantitative RT-PCR

The quantitative RT-PCRs were performed on the TaqMan<sup>®</sup> ABI Prism<sup>®</sup> 7900HT sequence detection system using specific TaqMan<sup>®</sup> probes or SYBR<sup>®</sup> Green (Fig. 2.7).

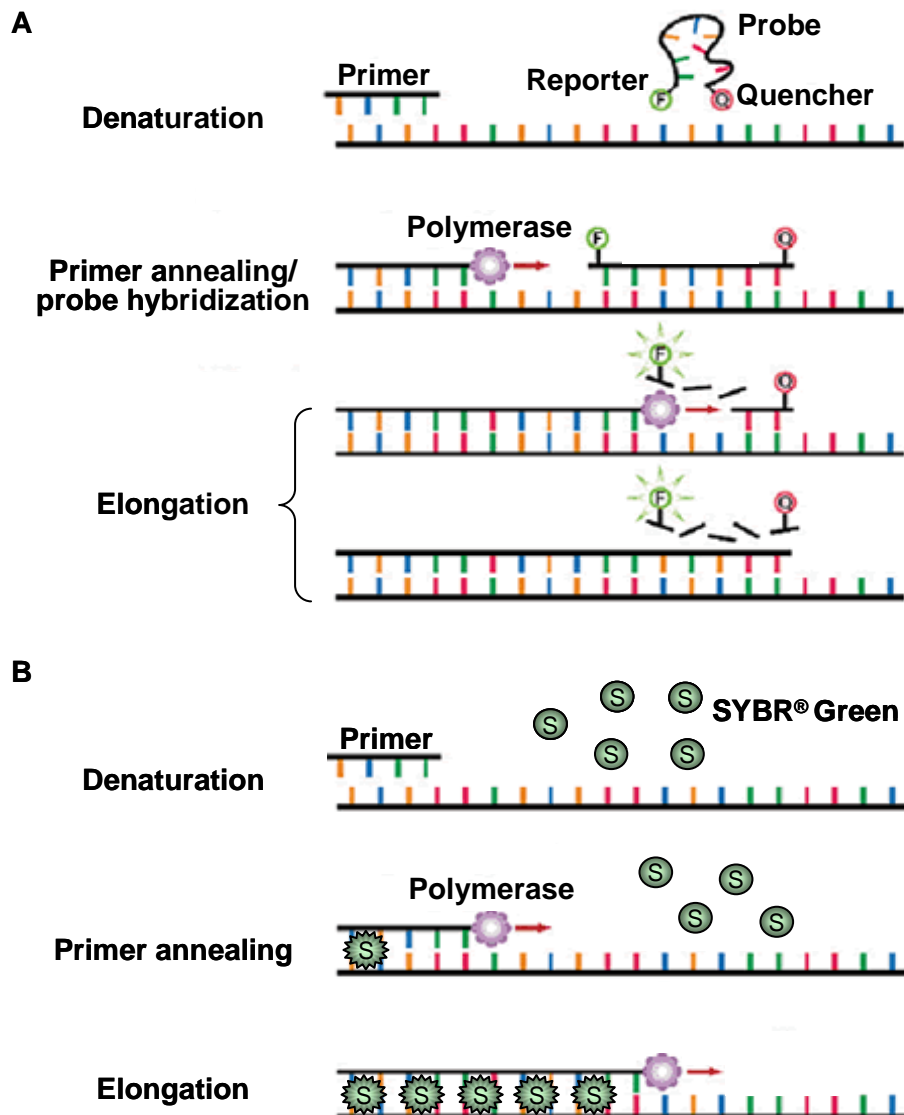


**Figure 2.7: Quantitative RT-PCR using specific TaqMan® probes or SYBR® Green.** **A**, The TaqMan® probe is designed to anneal to a specific sequence of the template between the forward and reverse primers. The probe has a high-energy dye termed reporter at its 5'-end and a low-energy molecule termed quencher at its 3'-end. When the probe is intact and excited by a light source, the reporter's emission is suppressed by the quencher as a result of the close proximity of the dyes. When the probe is cleaved by the 5'-exonuclease activity of the polymerase, the distance between the reporter and quencher increases causing the transfer of energy to stop. The fluorescent emission of the reporter increases and is directly proportional to the amplification factor. **B**, SYBR® Green is a dye that unspecifically intercalate in double-stranded DNA. This intercalation induces a fluorescent emission. After the PCR reaction, a melting curve analysis is required to differentiate between mismatched PCR products (e.g. primer dimers) and perfectly matched fragments (adapted from the Takara Bio USA website).

For all RT-PCRs, glyceraldehyde-3-phosphate dehydrogenase (GAPDH) was used as an endogenous control to normalize the quantification of the target mRNAs for difference in the amount of cDNA added to each reaction (primers and probe see



Table 2.5). For the quantitative determination of the transgene expression in the M7t mouse model, the corresponding cDNAs were diluted 1:10 and amplified using the primer pair and the probe specified in Table 2.6 and the TaqMan<sup>®</sup> Universal PCR Master Mix. The used PCR program is shown in Table 2.7.

**Table 2.5: GAPDH primer and probe sequences for quantitative RT-PCR.**

Primer/Probe name	Primer/Probe sequence (5'-3')
GAPDH-F	ATGTTCCAGTATGACTCCACTCACG
GAPDH-R	GAAGACACCAGTAGACTCCACGACA
GAPDH probe	AAGCCCATCACCATCTTCCAGGAGCGAGA

The probe has the fluorescent reporter 6-carboxy-fluorescein (FAM) at its 5'-end and the quencher 6-carboxy-tetramethyl-rhodamine (TAMRA) at its 3'-end.

**Table 2.6: Primer and probe sequences for quantitative RT-PCR in the M7t mouse model (I).**

Mouse line	Primer/Probe name	Primer/Probe sequence (5'-3')
M7t	hM7t (F)	GGACCAGGCGGTGTTCAA
	hM7t (R)	AGGTGTGACGTCGTCAATGG
	hM7t probe	TGTCCCACATCGGGCGGGTC

The probe has the fluorescent reporter FAM at its 5'-end and the quencher TAMRA at its 3'-end.

**Table 2.7: PCR program for quantitative RT-PCR using the relative quantification method and the TaqMan<sup>®</sup> Universal PCR Master Mix.**

Stage	Temperature (°C)	Time (min:sec)	cycles
Stage 1	50	02:00	1
Stage 2	95	10:00	1
Stage 3	95	00:15	45
	60	01:00	

To analyze the ratio of transgenic to endogenous cMyBP-C mRNA in the M7t mouse model, corresponding cDNAs (diluted 1:10) were amplified with the primer pair and probes depicted in Table 2.8 and the PCR program shown in Table 2.7.

**Table 2.8: Primer and probe sequences for quantitative RT-PCR in the M7t mouse model (II).**

Mouse line	Primer/Probe name	Primer/Probe sequence (5'-3')
M7t	hM7t ex 5-7 (F)	AATGGGTGGACCTGAGCA
	hM7t ex 5-7 (R)	GGCTGATAGGAGGTCCAGGT
	Hum ex 5-7 probe	CCAGCAAGAGGCCATGGGCA
	Mus ex 6 probe	TCACAGATGCTCAGACCACTTCTGCTG

The probes have the fluorescent reporter FAM at their 5'-end and the quencher TAMRA at their 3'-end.

For the quantitative determination of total cMyBP-C mRNA in the cMyBP-C knock-in mouse model, the cDNAs were diluted 1:10 and amplified using the Power SYBR<sup>®</sup> Green PCR Master Mix. PCR primers and cycling parameters are shown in Table 2.9 and 2.10, respectively.

**Table 2.9: Primer sequences for quantitative determination of total cMyBP-C mRNA level in the cMyBP-C knock-in mouse model.**

Mouse line	Primer name	Primer sequence (5'-3')
cMyBP-C knock-in	Cprot ex 2-3 F	GATGCGAGCCCTGATGAC
	Cprot ex 2-3 R	GACTTGAGACACTTTCTTCC

**Table 2.10: PCR program for quantitative RT-PCR using the absolute quantification method and the Power SYBR<sup>®</sup> Green PCR Master Mix.**

Stage	Temperature (°C)	Time (min:sec)	cycles
Stage 1	95	10:00	1
Stage 2	95	00:15	45
	60	01:00	
Stage 3	95	00:15	1
	60	00:15	
	95	00:15	

For amplification of the cMyBP-C pre-mRNA, quantitative RT-PCR was performed in the same way as described above, but with the primer pair shown in Table 2.11.

**Table 2.11: Primer sequences for quantitative determination of cMyBP-C pre-mRNA levels in the cMyBP-C knock-in mouse model.**

Mouse line	Primer name	Primer sequence (5'-3')
cMyBP-C knock-in	Cprot int 1 F	GCAAGTTCCATCTGGCTCTT
	Cprot int 2 R	GCGAGGTCAGCAAGCTCTTA

For the quantitative determination of the nonsense and missense cMyBP-C mRNAs in the cMyBP-C knock-in mouse model, the cDNAs were diluted 1:10 and amplified using the TaqMan<sup>®</sup> Universal PCR Master Mix and the primers and probes depicted in Table 2.12. The used PCR program is shown in Table 2.7.

**Table 2.12: Primer and probe sequences for quantitative determination of nonsense and missense mRNA levels in the cMyBP-C mouse model.**

Mouse line (mRNA species)	Primer/probe name	Primer/Probe sequence (5'-3')
cMyBP-C knock-in (nonsense)	Spe del 6 F	TGGACCTGAGCAGCAAAGTG
	Spe del 6 R	GGTCCAGGTCTCCAGAACCA
	Spe del 6 probe	CCAGCAAGAGGCCA
cMyBP-C knock-in (missense)	Spe WT M F	GTGTCTACCAAGGACAAATTTGACA
	Spe del 6 R	GGTCCAGGTCTCCAGAACCA
	Spe M probe	CTCACTGTCCATAAGG

The probes for the determination of the nonsense and missense mRNA have the fluorescent reporter FAM and VIC, respectively, at their 5'-end. The probe for the nonsense mRNA has the quencher TAMRA at its 3'-end, whereas the probe for the missense mRNA has a nonfluorescent quencher with a minor groove binder (MGB) at its 3'-end.

All analyses were performed in triplicates with the software ABI 7900HT SDS 2.2. The mRNA amount was quantified according to the comparative Ct method with the  $2^{-\Delta\Delta C_t}$  formula. The Ct values of GAPDH (endogenous control) were subtracted from the Ct values of the target gene ( $\Delta C_t$ ). The mean of  $\Delta C_t$  of the reference (mainly WT or DMSO-treated controls) was then subtracted from each single  $\Delta C_t$  resulting in the  $\Delta\Delta C_t$  value. The formula  $2^{-\Delta\Delta C_t}$  provides the amount of mRNA in every sample.

## **2.2.4 Protein analysis**

### **2.2.4.1 Protein extraction**

For Western blot analysis, about 30-50 mg tissue powder (see 2.2.2) were mixed with 5 volumes of lysis buffer I (3% SDS, 30 mM Tris base, pH 8.8, 5 mM EDTA, 30 mM NaF, 10% glycerol) and homogenized with the Tissue Lyser twice for 30 sec at a frequency of 30 Hz. After centrifugation (13200 rpm, 10 min, room temperature), the supernatant was collected and its concentration was determined as described in the next chapter. For protein extraction from cultured cells, 100  $\mu$ l lysis buffer II (500 mM NaCl, 1% Triton X-100, 1 mM EDTA, 1 mM DTT, 50 mM Tris-HCl, pH 7.4, 1 tablet complete mini-proteases inhibitor cocktail (for 10 ml buffer)) were added to  $\sim 3.3 \times 10^5$  cultured isolated neonatal mouse cardiomyocytes (see 2.2.5.1) or isolated adult mouse cardiomyocytes (2.2.5.3). After homogenization by pipetting up and down, the homogenate was centrifuged at 13200 rpm for 10 min at room temperature. The supernatant was collected and its concentration was determined. For measurement of the 20S activity, about 30-50 mg tissue powder (see 2.2.2) were mixed with five volumes of lysis buffer III (1 tablet complete mini-proteases inhibitor cocktail dissolved in 10 ml aqua ad iniectabilia). After three cycles of freezing (in liquid nitrogen) and thawing (at room temperature), the samples were homogenized with the Tissue Lyser as described above. After centrifugation (13200 rpm, 30 min, 4 °C), the supernatant was collected and its concentration was determined.

### **2.2.4.2 Determination of the protein concentration**

The protein concentration was determined by the Bradford protein assay, which is a dye-binding assay in which a differential color change of a dye occurs in response to various concentrations of protein (Bradford, 1976). For determination, 5  $\mu$ l of supernatant of protein samples were added to 795  $\mu$ l 0.1 M NaOH. After admixture of 200  $\mu$ l Coomassie<sup>®</sup> Brilliant Blue G-250 reagent and incubation at room temperature for 5 min, the absorbance at 595 nm was measured with a spectrophotometer. Subtraction of the blank value (800  $\mu$ l 0.1 M NaOH plus 200  $\mu$ l Coomassie<sup>®</sup> Brilliant

Blue G-250 reagent) and comparison to a standard (immunoglobulin G) curve provided a relative measurement of protein concentration. Each protein concentration determination was performed in duplicates.

#### **2.2.4.3 Western blot analysis**

Either 7.5 µg (tissue) or 20 µg (cells) of protein were adjusted to Laemmli buffer composition (2% SDS, 10% glycerol, 10 mM Tris base, pH 6.8, 100 mM DTT and 0.01% bromphenol blue), denatured by heating at 95 °C for 5 min and subsequently separated on 10% or 15% (depending on the target protein) polyacrylamide gels (running gel composition: 375 mM Tris base, pH 8.8, 10% or 15% acrylamide/bis solution (29:1), 0.1% SDS, 0.1% APS, 0.03% TEMED; stacking gel composition: 125 mM Tris base, pH 6.8, 5% acrylamide/bis solution (29:1), 0.1% SDS, 0.1% APS, 0.08% TEMED) by gel electrophoresis. Electrophoresis was carried out first at 80 V for 10 min and then at 150 V as long as needed in electrophoresis buffer (25 mM Tris base, 192 mM glycine, 0.1% SDS) using the Mini Protean 3 electrophoresis system. The Precision Plus Protein Standard™ was used as molecular weight marker. After separation, the proteins were transferred onto a nitrocellulose membrane at 300 mA for 90 min in transfer buffer (50 mM Tris base, 380 mM glycine, 0.1% SDS, 20% methanol) using the Mini Trans-Blot cell system. Afterwards, the membrane was stained with Ponceau S to visualize the transferred proteins. After 3 times washing with TBS-T buffer (100 mM Tris base, pH 7.5, 150 mM NaCl, 0.1% Tween 20), the membrane was blocked in 5% milk solution (milk powder in TBS-T buffer) for 1 h at room temperature and then, after repeated washing, incubated with the primary antibody (Table 2.13) overnight at 4 °C. After 3 times washing with TBS-T buffer, the membrane was then incubated with the secondary antibody (Table 2.13) for 1 h at room temperature. After a final washing with TBS-T buffer, the membrane was incubated with a detection reagent according to the instruction manual of the ECL Plus Western blotting detection system for tissue preparations or the SuperSignal® West Dura extended duration substrate for cell preparations. The produced chemiluminescent signal was detected with the Chemie Genius<sup>2</sup> Bio Imaging System and quantified with the Gene Tools software.

**Table 2.13: Antibodies list for Western blot analysis.**

Investigated protein	Primary antibody	dilution	Secondary antibody	dilution
cMyBP-C	C0C1	1:1000	anti-rabbit IgG peroxidase conjugate	1:6000
Ubiquitinated proteins	Ubiquitin	1:2000	anti-mouse IgG peroxidase conjugate	1:20000
GFP	GFP	1:2000	anti-rabbit IgG peroxidase conjugate	1:10000

The primary antibodies were diluted in TBS-T buffer, whereas the secondary antibodies were diluted in 5% milk solution.

#### 2.2.4.4 Measurement of the 20S proteasome activities

As described in the introduction, the 20S proteasome (Fig. 1.8) contains 3 peptidase activities: the chymotrypsin-like, the trypsin-like and the caspase-like activity. All 3 activities can be determined by measurement of fluorescence generated from enzymatic cleavage of fluorogenic substrates (Fig. 2.7).

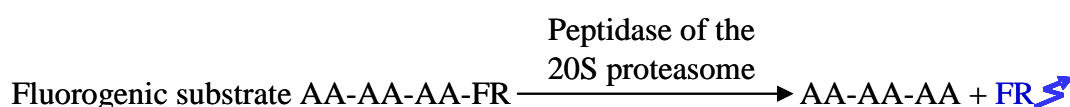


**Figure 2.7: Enzymatic reaction during degradation by the 20S proteasome.** To measure the different activities of the 20S proteasome, specific fluorogenic substrates were used, which are composed of a chain of amino acids (AA) and a fluorescent reporter (FR). After cleavage of these substrates by a specific peptidase, the fluorescent reporter is released, whose fluorescence can be measured.

The method to measure the 20S proteasome activities was adapted from (Ludwig et al., 2005)). For determination, 30 µg of protein (2.2.4.1) were incubated in the dark for 1 h at 37 °C in an incubation buffer (225 mM Tris-HCl, pH 8.2, 45 mM KCl, 7.5 mM Mg(CH<sub>3</sub>COO)<sub>2</sub>·4H<sub>2</sub>O, 7.5 mM MgCl<sub>2</sub>·6H<sub>2</sub>O, 1.1 mM DTT) containing an ATP regenerating system (6 mM ATP, 5 mM phosphocreatine, 0.2 U phosphocreatine-kinase) and a specific fluorogenic substrate (Table 2.14).

**Table 2.14: Fluorogenic substrates used to measure the activities of the 20S proteasome.**

<b>20S activity</b>	<b>Fluorogenic substrate</b>	<b>Concentration (<math>\mu</math>M)</b>
Chymotrypsin-like activity	Succinyl-leucyl-leucyl-valyl-tyrosyl-7-amino-4-methylcoumarin (SUC-Leu-Leu-Val-Tyr-AMC)	60
Trypsin-like activity	Benzoyl-valyl-glycyl-arginyl-7-amino-4-methylcoumarin (Bz-Val-Gly-Arg-AMC)	20
Caspase-like activity	Benzyloxycarbonyl-leucyl-leucyl-glutamyl- $\beta$ -naphthylamide (Z-Leu-Leu-Glu- $\beta$ NA)	200

For each activity of the 20S proteasome, a specific fluorogenic substrate was used. The indicated concentrations were determined in preliminary tests.

Released fluorescence of the fluorescent reporter 7-amino-4-methylcoumarin (AMC) and  $\beta$ -naphthylamide ( $\beta$ NA) was measured using the TECAN Safire<sup>2</sup> microplate reader at an excitation wavelength of 380 and 350 nm, respectively, and an emission wavelength of 460 and 450 nm, respectively. Each sample was measured in triplicates. The mean of the blank (incubation buffer and H<sub>2</sub>O) was subtracted from the mean of each sample triplicate.

In preliminary experiments, the substrate-dependent and protein amount-dependent response of this method was tested for the chymotrypsin-like activity. To investigate the substrate-dependent response, 10  $\mu$ g of protein were incubated in incubation buffer with different concentrations of the fluorogenic substrate, whereas different amounts of protein were incubated in incubation buffer containing 60  $\mu$ M fluorogenic substrate to examine the protein amount-dependent response (Fig. 2.8).

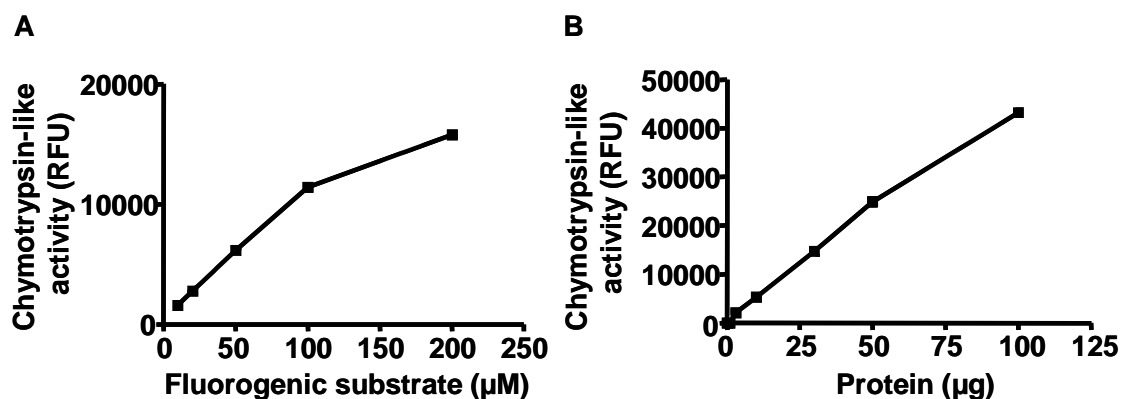


**Figure 2.8: Substrate- and protein amount-dependent response of the chymotrypsin-like activity.** A, Ten  $\mu\text{g}$  of protein were incubated for 1 h in incubation buffers with different concentrations of the fluorogenic substrate (SUC-Leu-Leu-Val-Tyr-AMC). B, Different amounts of protein were incubated for 1 h in incubation buffer containing 60  $\mu\text{M}$  fluorogenic substrate (SUC-Leu-Leu-Val-Tyr-AMC). For A and B, released fluorescence was measured at an excitation wavelength of 380 nm and an emission wavelength of 460 nm.

In both experiments, an almost linear increase of the fluorescence intensity was observed. With regard to the substrate-dependent response, it seems that the system is saturated when high concentrations of fluorogenic substrate (200  $\mu\text{M}$ ) were used. Finally, the sensitivity of this system to MG132, a reversible proteasome inhibitor, was investigated. Ten  $\mu\text{g}$  of protein were incubated in incubation buffers containing 60  $\mu\text{M}$  fluorogenic substrate and different concentrations of MG132 (Fig. 2.9).

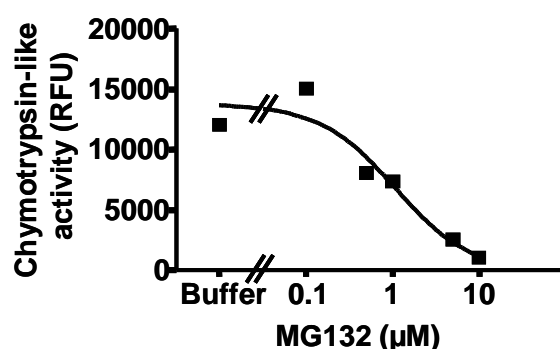


**Figure 2.9: MG132 sensitivity of the chymotrypsin-like activity.** Ten  $\mu\text{g}$  of protein were incubated for 1 h in incubation buffers containing 60  $\mu\text{M}$  fluorogenic substrate (SUC-Leu-Leu-Val-Tyr-AMC) and different concentrations of MG132. Released fluorescence was measured at an excitation wavelength of 380 nm and an emission wavelength of 460 nm.

An inhibition of the proteasome started at a MG132 concentration of 0.5  $\mu\text{M}$  and the 50% inhibitory concentration ( $\text{IC}_{50}$ ) was 1.08  $\mu\text{M}$ . A MG132 concentration of 10  $\mu\text{M}$  resulted in an almost complete blockage of the proteasome.



## 2.2.5 Cell isolation

### 2.2.5.1 Neonatal mouse cardiomyocytes

Neonatal mouse cardiomyocytes (NMCM) were isolated from at least 19 1-4 d-old mice according to a procedure adapted from (Laugwitz et al., 2005). Organ extraction from neonatal mice was authorized by the Behörde für Soziales, Familie, Gesundheit und Verbraucherschutz der Freien und Hansestadt Hamburg (Org 366). Neonatal mice were sacrificed by cervical dislocation. Mouse ventricles were removed aseptically, kept in a  $\text{Ca}^{2+}/\text{Mg}^{2+}$ -free HBSS on ice, washed, minced into small fragments in HBSS, and incubated overnight at 4 °C in 0.5 mg/ml trypsin-HBSS. This trypsin predigestion was followed by five rounds of digestion with 240 U/ml collagenase type II in HBSS solution at 37 °C for 9 min. Cells were collected in an equal volume of cold dark medium (DMEM:M199 3:1, 10% horse serum, 5% FCS, 100 U/ml penicillin-streptomycin, 1 mM HEPES, pH 7.4). The resulting mixture was centrifuged twice (8 and 5 min) at 600 rpm at room temperature and the cells were resuspended in 20-25 ml of dark medium. To exclude nonmuscle cells, the isolated cells were pre-plated twice in T75 flasks at 37 °C and 10%  $\text{CO}_2$  for 75 min. All unattached cells, which were mainly cardiomyocytes, were transferred to a Falcon tube and spinned again twice at 320 rpm for 5 min at room temperature before they were counted using a Neubauer chamber. NMCM were plated on laminin-coated (0.01 mg/ml; in 1x PBS) 12-well dishes at a density of  $10^5$  cells/cm<sup>2</sup> and incubated at 37 °C and 10%  $\text{CO}_2$  for 4 d in the dark medium before treatment (see 2.2.6.1).

### 2.2.5.2 Adult mouse ventricular myocytes

Adult mouse ventricular myocytes (AMVM) were isolated from 3-4 mo-old mice. Heparinised (20000 U/kg) mice were sacrificed by cervical dislocation in light  $\text{CO}_2$  anesthesia. After median thoracotomy, hearts were excised, mounted on a temperature-controlled modified Langendorff perfusion apparatus and retrogradely perfused through the aorta with a  $\text{Ca}^{2+}$ -free modified Tyrode's solution (113 mM NaCl, 4.7 mM KCl, 0.6 mM  $\text{KH}_2\text{PO}_4$ , 0.6 mM  $\text{Na}_2\text{HPO}_4 \cdot 2\text{H}_2\text{O}$ , 1.2 mM  $\text{MgSO}_4 \cdot 7\text{H}_2\text{O}$ ,

12 mM NaHCO<sub>3</sub>, 10 mM KHCO<sub>3</sub>, 10 mM HEPES, pH 7.4, 30 mM taurine, 5.5 mM glucose, 10 mM 2,3-butanedione monoxime (BDM)) at 37 °C for 8 min at 3 ml/min. This perfusion buffer was then switched to a digestion buffer containing the modified Tyrode's solution, 12.5 µM CaCl<sub>2</sub> and 0.1 mg/ml Liberase Blendzyme 3 at 37 °C for 9-10 min. The ventricles were excised, minced with forceps and dissociated by gentle pipetting. The collagenase activity was stopped by the addition of 10% FBS, and CaCl<sub>2</sub> was stepwise reintroduced up to a concentration of 1 mM. After resuspending and counting with a Neubauer chamber, the isolated cells were plated on laminin-coated (0.01 mg/ml in 1x PBS) Lab-Tek™ chambers or coverslips at a density of 20000 cells/ml in 1.8 mM Ca<sup>2+</sup>-plating medium (MEM supplemented with Hanks' salts and 2 mM glutamine, 100 U/ml penicillin-streptomycin, 5% FBS, 10 mM BDM). After 2 h pre-plating, the cells were either used immediately for immunofluorescence analysis (see 2.2.7) or further cultured for treatment in culture medium (MEM supplemented with Hanks' salts and 2 mM glutamine, 0.1 mg/ml BSA, 10 mM BDM, 1% insulin/transferrin/selenium, 100 U/ml penicillin-streptomycin) at 37 °C and 5% CO<sub>2</sub>.

### 2.2.5.3 Mouse fibroblasts

Fibroblasts were isolated from a 9 mo-old Ub<sup>G76V</sup>-GFP mouse. The mouse was sacrificed by cervical dislocation in light CO<sub>2</sub> anesthesia. After median thoracotomy, a piece of the subcutis was excised, minced and cultured in a culture medium (DMEM (4.5 g/l glucose), 10% FCS, 100 U/ml penicillin-streptomycin, 1% glutamine) in a T75 flask at 37 °C and 5% CO<sub>2</sub>. After 6 d, the medium was changed and the fibroblasts were further cultured. When 90% confluence was reached, the fibroblasts were detached from the flask with a trypsin solution (0.25% trypsin in HEPES/EDTA buffer) and split 1 to 2.

## **2.2.6 Treatments**

### **2.2.6.1 Treatment of NMCM**

After 4 d of culture in dark medium (see 2.2.5.1), the medium was removed and NMCM were treated with 10  $\mu$ M MG132 for the times indicated in the results or with 500 nM epoxomicin (irreversible proteasome inhibitor) for 4 h in 0.1% DMSO-containing dark medium at 37 °C and 10% CO<sub>2</sub> for proteasome inhibition. For nonsense-mediated mRNA decay (NMD) inhibition, the cells were treated with 100  $\mu$ g/ml cycloheximide (CHX) or 300  $\mu$ g/ml emetine in 0.1% DMSO-containing dark medium for 4 h at 37 °C and 10% CO<sub>2</sub>. Total RNAs or proteins were extracted from NMCM as described in 2.2.3.1 or 2.2.4.1, respectively.

### **2.2.6.2 Treatment of AMVM**

After pre-plating, AMVM isolated either from a transgenic M7t mouse or a homozygous cMyBP-C knock-in mouse were treated with 10  $\mu$ M MG132 in culture medium (see 2.2.5.2) for 15 h at 37 °C and 5% CO<sub>2</sub>. Afterwards proteins were extracted as described in 2.2.4.1. AMVM isolated from Ub<sup>G76V</sup>-GFP mice were treated with 10  $\mu$ M MG132, 100 nM MG262 (reversible proteasome inhibitor) or 500 nM epoxomicin in culture medium for 20 h at 37 °C and 5% CO<sub>2</sub>. Fluorescence was analyzed by confocal microscopy using a Zeiss Axiovert 200 M microscope with a 40x-oil objective. Confocal images were recorded with a Zeiss LSM 5 Image system. AMVM isolated from GFPdgn mice were treated with 5  $\mu$ M or 10  $\mu$ M MG132 in culture medium for 15 h at 37 °C and 5% CO<sub>2</sub>. Fluorescence was analyzed in the same way as described above.

### **2.2.6.3 Treatment of fibroblasts**

Cultured fibroblasts were plated on Lab-Tek™ chambers and treated either with epoxomicin in a concentration of 5 nM, 50 nM, 500 nM or 5  $\mu$ M or with MG262 in a

concentration of 1 nM, 10 nM, 100 nM or 1  $\mu$ M or with MG132 in a concentration of 0.1  $\mu$ M, 1  $\mu$ M or 10  $\mu$ M in 0.1% DMSO-containing culture medium (2.2.5.3) for 15 h at 37 °C and 5% CO<sub>2</sub>. Fluorescence was analyzed by confocal microscopy using a Zeiss Axiovert 200 M microscope with a 40x-oil objective. Confocal images were recorded with a Zeiss LSM 5 Image system.

#### **2.2.6.4 Treatment of mice**

Systemic application of the reversible proteasome inhibitor MG262 was performed either by i.p. injection (9  $\mu$ mol/kg in a 60% DMSO-NaCl-solution) or by i.v. injection into the lateral tail vein (5  $\mu$ mol/kg in a 38% DMSO-NaCl-solution). The application was authorized by the Behörde für Wissenschaft und Gesundheit der Freien und Hansestadt Hamburg (Org 72/04). Heart and liver were excised 24 h after i.p. injection and 17 h after i.v. injection as described in 2.2.2 and further analyzed by direct fluorescence microscopy using a Zeiss Axiovert 25 microscope and/or Western blot. Systemic inhibition of NMD was performed by subcutaneous (s.c.) injection of cycloheximide (120 mg/kg in a 60% DMSO-NaCl-solution) in the neck fold. The s.c. injection was repeated once per hour four times. The hearts were excised 30 min after the last injection as described in 2.2.2. Total RNA was isolated as described in 2.2.3.1. All applications were performed by using hypodermic needles and insulin syringes. As controls, mice were injected with a 60% or 38% DMSO-NaCl-solution.

#### **2.2.7 Transfection**

Transfection of the final construct pBlue- $\alpha$ -MHC-prom-Myc-M7t-cMyBP-C (Fig. 2.3) into isolated neonatal rat cardiomyocytes (NRCM), which were kindly prepared by Hiroshi Naito, was performed according to the instruction manual of Lipofectamine™ 2000. Immunofluorescence analysis (2.2.8) was made 48 h after transfection.

### 2.2.8 Immunofluorescence analysis

AMVM or transfected NRCM were rinsed twice in 1x PBS and fixed for 7 min at -20 °C in methanol/acetone (20/80). After washing in 1x PBS, cells were permeabilized for 1 h at room temperature in solution A (0.5% Triton X-100, 1% BSA, 10% FCS in 1x PBS). After washing in solution B (0.5% Triton X-100, 1% BSA in 1x PBS), cells were incubated for 40 min at room temperature with the primary antibodies diluted in solution B (anti-cMyBP-C (1:500), anti- $\alpha$ -actinin (1:200), anti-c-myc (1:500), anti-titin-Z1 (1:200)). Cells were rinsed twice in solution B and then incubated for 45 min at room temperature and in the dark with secondary antibodies diluted in solution B (anti-rabbit IgG Alexa 546-conjugated (1:400), anti-mouse IgG Alexa 488-conjugated (1:400), anti-rabbit IgG Cy3-conjugated (1:100)). For nuclear staining, cells were incubated with 1  $\mu$ M ToPro3<sup>®</sup> for 10 min, rinsed three times with 1x PBS and then fixed with Mowiol 4-88. Fluorescence was analyzed by confocal microscopy using a Zeiss Axiovert 200 M microscope with a 40x-oil objective. Confocal images were recorded with a Zeiss LSM 5 Image system.

### 2.2.9 Echocardiography

Transthoracic echocardiography was performed using a Visual Sonics Vevo 770<sup>®</sup> ultrasonograph with a 30-MHz central frequency transducer. Anesthesia of mice with volatile isoflurane was induced at a concentration of 3% and then maintained at 0.5-1% by a face mask. The mice were laid on a heated platform in the supine position with all legs taped to ECG electrodes for heart rate monitoring. Body temperature was monitored via a rectal thermometer and maintained at 36-38 °C. The chest was carefully shaved using a depilatory cream. Afterwards, the mice were placed in a left lateral decubitus position and a prewarmed ultrasound transmission gel was spread over the chest. Two-dimensionally guided EKV<sup>™</sup> (ECG-based kilohertz visualization)-mode images were recorded from the parasternal short axis view at the mid-papillary muscle level. During examination, the level of volatile anesthesia was guided on the basis of the heart rate, which should be close to physiology (500 beats/min). All examinations were recorded digitally and stored for subsequent

off-line analysis. The left ventricular (LV) internal diameter (LVID), the LV posterior wall (LVPW) and the interventricular septum (IVS) thickness were determined in both end-diastolic (d) and end-systolic (s) frames (Fig. 2.10). The end-diastole was defined as the maximal LV diastolic dimension and accordingly, the end-systole was defined as the minimal LV diameter in the same heart cycle. The fractional shortening in % was calculated as  $((\text{LVIDd (mm)} - \text{LVIDs (mm)}) / \text{LVIDd (mm)}) \times 100$ . The left ventricular mass (LVM) in mg was calculated as  $((\text{LVIDd (mm)} + \text{LVPWd (mm)} + \text{IVSd (mm)})^3 - \text{LVIDd (mm)}^3) \times 1.055 \text{ mg/mm}^3$ , in which  $1.055 \text{ mg/mm}^3$  is the density of the myocardium (Gardin et al., 1995). The analysis was made by 2 persons, who were unaware of the genotype during analysis. The final data are presented as the mean of measurements obtained by both observers.

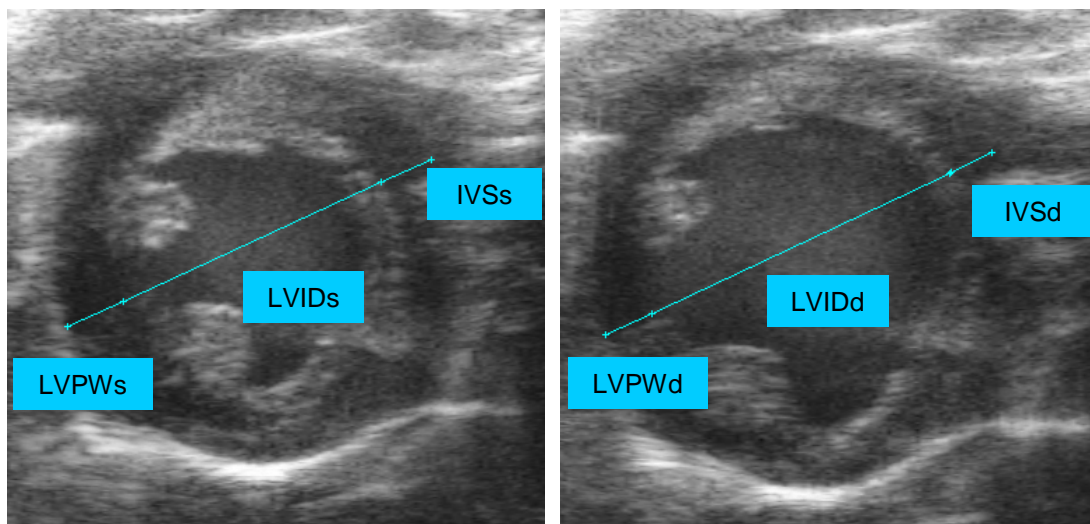


**Figure 2.10: Echocardiographic analysis.** The left ventricular internal diameter (LVID), the left ventricular posterior wall (LVPW) and the interventricular septum (IVS) were determined from EKV™-mode images, which were recorded from the parasternal short axis view at the mid-papillary muscle level. Parameters were determined in both end-systolic (s; left picture) and end-diastolic (d; right picture) frames.

### 2.2.10 Statistical analysis

Data are presented as mean $\pm$ SEM. Statistical analyses were performed using the unpaired Student's t-test. Spearman correlation and linear regression analyses were performed to assess the relationship between hypertrophy, ubiquitination and degradation in the homozygous cMyBP-C knock-in and knock-out mice. Analyses were performed using a commercial software (GraphPad Software, Inc.). A value of  $P < 0.05$  was considered significant.

### 3 Results

#### 3.1 Generation and characterization of targeted cMyBP-C mouse models

Sarikas et al. (2005) showed by adenoviral gene transfer in isolated neonatal rat cardiomyocytes (NRCM) that truncated cMyBP-Cs are rapidly and quantitatively degraded by the UPS and lead to an impairment of this system. To answer the question whether this is also the case *in vivo*, two new targeted cMyBP-C mouse models were generated: the M7t mouse model and the cMyBP-C knock-in mouse model. Both models are based on the same human *MYBPC3* point mutation. This mutation corresponds to a G>A transition on the last nucleotide of exon 6 and is associated with a severe phenotype and a poor prognosis in humans (Richard et al., 2003). The mutation is included in the general consensus sequence for donor splice sites (AG | GTRAGT; (Zhang et al., 2003), which in turn suggests complex molecular mechanisms. The mutation is expected to produce either a missense mRNA (containing the G>A transition), which should lead to a 150-kDa mutant full-length cMyBP-C protein (E256K), or a nonsense mRNA (skipping of exon 6), which should lead to a 32-kDa C-terminal truncated cMyBP-C protein due to a premature termination codon (PTC) in exon 9, or both (Fig. 3.1).

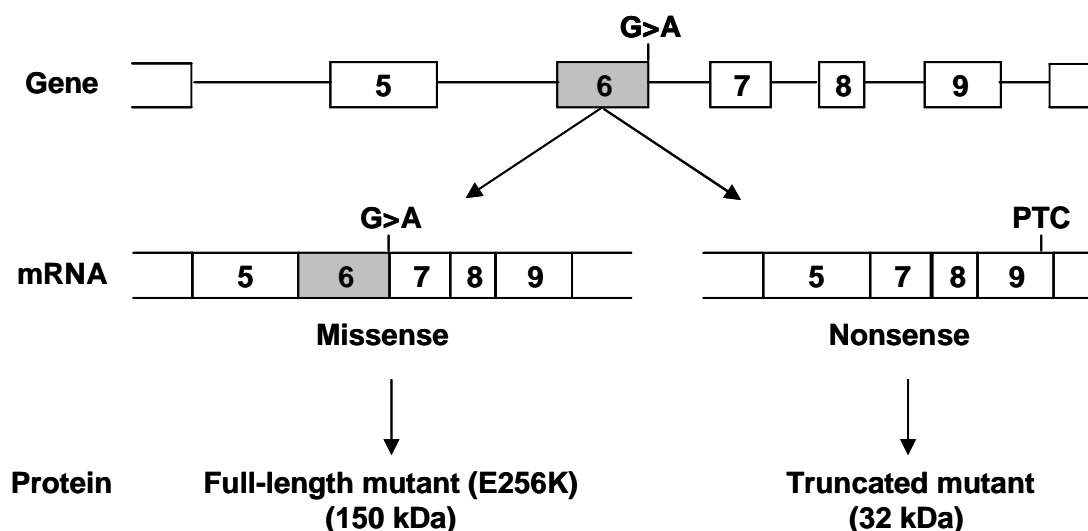


**Figure 3.1: Schematic structure of the consequences of the G>A transition.** The point mutation in exon 6 is expected to result in two different mRNA species and two different proteins. PTC means premature termination codon.

### 3.1.1 Generation and characterization of the M7t mouse model

#### 3.1.1.1 Generation of the M7t mouse model

The M7t mouse model was generated by microinjection of a cDNA construct (Fig. 2.1) in the pronucleus of single-cell mouse embryos (additive transgenesis). The cDNA construct contained the mouse  $\alpha$ -MHC-promoter and the human Myc-M7t-cMyBP-C cDNA deleted of exon 6. Therefore, the M7t mouse model was expected to express a 32-kDa truncated cMyBP-C protein in a heart-specific manner. Nineteen days after the microinjection 23 pups were born, and tail biopsies were taken 3 weeks (wk) after their birth. By Southern blot analysis three transgenic animals were identified (Fig. 3.2).

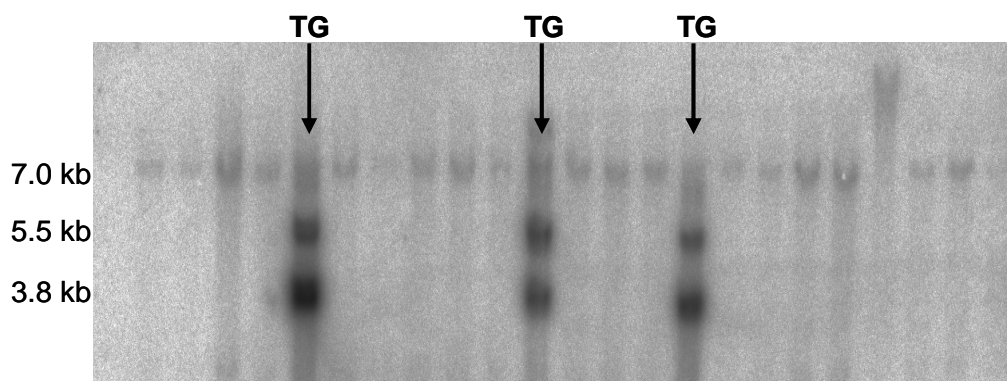


**Figure 3.2: Southern blot analysis of the M7t mouse model.** Southern blot was performed on genomic DNA extracted from mouse tails and digested with *Eco*RI. Three transgenic pups (TG) were found.

To establish the mouse line, the three transgenic animals (founders) were crossed with C57Bl/6J wild-type mice.

#### 3.1.1.2 Genotyping

Genotypes of transgenic M7t (M7t-TG) and wild-type (WT) mice were determined by PCR from genomic tail DNA. The forward and reverse primers were located at the junction between exons 1 and 2 and in exon 2 of the human Myc-M7t-cMyBP-C cDNA, respectively, and were therefore specific for the transgene. PCR products were loaded on a 1% agarose gel (Fig. 3.3).





**Figure 3.3: Genotyping of the M7t mouse model by PCR.** PCR was performed on genomic tail DNA from M7t-TG (TG) and WT mice. As a negative control (-), water was added instead of DNA. MW stands for the 100-bp molecular weight marker. The location of the used primers (black arrows) is indicated in the scheme on the right.

The expected fragment for the transgene at 231 bp was obtained only in the M7t-TG mice.

### 3.1.1.3 Molecular characterization at the mRNA level

To analyze whether the transgene is expressed at the mRNA level, total RNA was isolated from frozen ventricles of one M7t-TG and one WT mouse of each founder line at 6-8 wk of age. Each RNA was reverse transcribed to cDNA. In addition, one approach without adding the reverse transcriptase was performed to detect potential genomic contamination. The cDNAs were amplified by classical RT-PCR using transgene-specific primers located in the Myc-sequence and in exon 2 of the human Myc-M7t-cMyBP-C cDNA. The PCR products were loaded on a 1% agarose gel (Fig. 3.4).

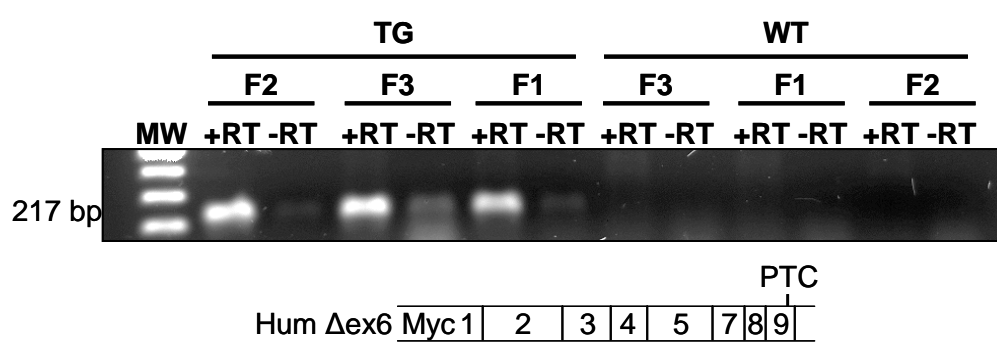


**Figure 3.4: Qualitative analysis of the transgene expression at the mRNA level in the M7t-TG mice.** Total RNA isolated from ventricles of 1 M7t-TG (TG) and 1 WT mouse of each founder line (F1, F2 and F3) was reverse transcribed (+RT) to cDNA. Approaches without adding the reverse transcriptase are indicated as -RT. PCR was performed using the primers indicated in the scheme below (black arrows). MW stands for the 100-bp molecular weight marker.

The expected 217-bp PCR fragment for the transgene was obtained only in the M7t-TG mice. Genomic contamination was present in all three RNA preparations, but in

all three cases the amplified fragments from the –RT samples were clearly less abundant than in the +RT samples.

To quantify the amount of the transgenic mRNA in the three founder lines, a quantitative RT-PCR was performed using the TaqMan<sup>®</sup> method (see 2.2.3.5). Total RNA was isolated from ventricles of three M7t-TG mice of founder lines 1 and 2 (6-13 wk-old) and of one M7t-TG mouse of founder line 3 (7 wk-old). In founder line 3 only one transgene-positive pup was born. Each RNA was reverse transcribed three times and each cDNA was amplified three times by quantitative RT-PCR using transgene-specific primers and a specific probe, which were located in the exons 16 and 17 and at the junction between exons 16 and 17 of the human Myc-M7t-cMyBP-C cDNA, respectively. As an internal standard, glyceraldehyde-3-phosphate dehydrogenase (GAPDH) was used. The different expression levels of the transgene in the three founder lines are shown in Fig. 3.5.

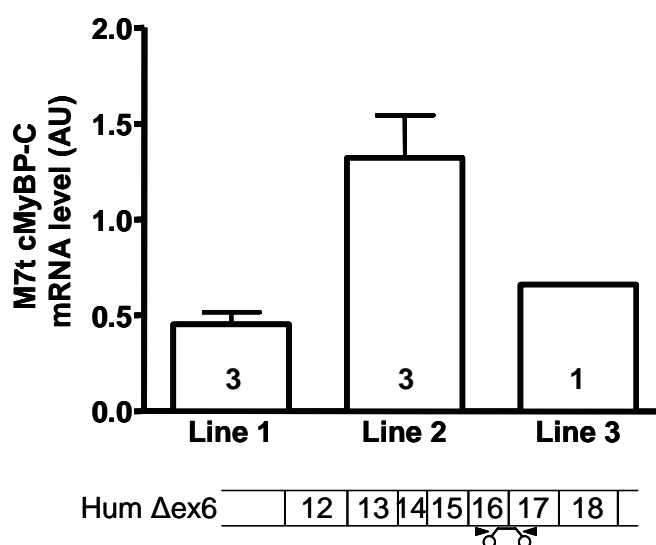


**Figure 3.5: Quantitative analysis of the transgene expression at the mRNA level in the M7t-TG founder lines.** Total RNA isolated from ventricles of 3 M7t-TG mice of founder lines 1 and 2 and of 1 M7t-TG mouse of founder line 3 was reverse transcribed to cDNA. Transcribed cDNA was amplified by quantitative RT-PCR using transgene-specific primers (black arrows) and probe localized as indicated in the scheme below. GAPDH was used as endogenous control. Bars represent the mean±SEM. The number of animals is indicated in the bars.

Based on these results, the founder line 2 was further established, because this line showed the highest transgene expression.

To determine the level of overexpression of the transgene in comparison to the endogenous cMyBP-C in founder line 2, a quantitative RT-PCR analysis was

performed in three WT and M7t-TG mice using primers located in exons 5 and 7 of cMyBP-C cDNA (recognizing both human and mouse) and two different probes. One probe was located in exon 6 of mouse cMyBP-C cDNA and was therefore specific for the endogenous cMyBP-C. The other probe matched exactly the junction between exons 5 and 7 of human Myc-M7t-cMyBP-C cDNA, which is only present in the transgene. The efficiency of the two different PCR reactions should be the same, because the identical primer pair was used. Thus, both PCR reactions should be comparable, and in Fig. 3.6 the results are summarized and related all to the cMyBP-C expression in the WT mice.

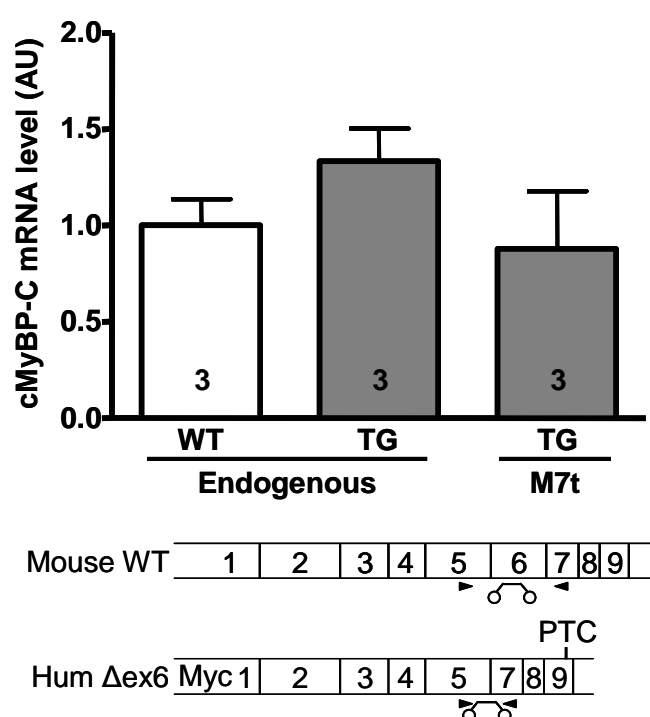


**Figure 3.6: Quantitative analysis of the transgene expression at the mRNA level in comparison to endogenous cMyBP-C in the M7t-TG mice.** Total RNA isolated from ventricles of three WT and M7t-TG (TG) mice was reverse transcribed to cDNA. Transcribed cDNA was amplified by quantitative RT-PCR using primers (black arrows; recognizing both human and mouse) and specific probes as indicated in the scheme below. GAPDH was used as endogenous control. Values were related to the cMyBP-C expression of the WT. Bars represent the mean±SEM. The number of animals is indicated in the bars.

The endogenous cMyBP-C mRNA level was similar in WT and M7t-TG mice. The ratio of transgenic to endogenous cMyBP-C mRNA was 0.63 in the M7t-TG mice. Taken the endogenous and the transgenic cMyBP-C expression together, the level of total cMyBP-C mRNA was 2-fold higher in the M7t-TG mice than in the WT mice.

### 3.1.1.4 Molecular characterization at the protein level

The expression of the endogenous and transgenic cMyBP-C at the protein level was analyzed by Western blot using an antibody that recognizes both the full-length and the truncated isoforms (Fig. 3.7). The analysis was performed on myocardial tissue from M7t-TG and WT mice at the age of 9 mo (n=6).

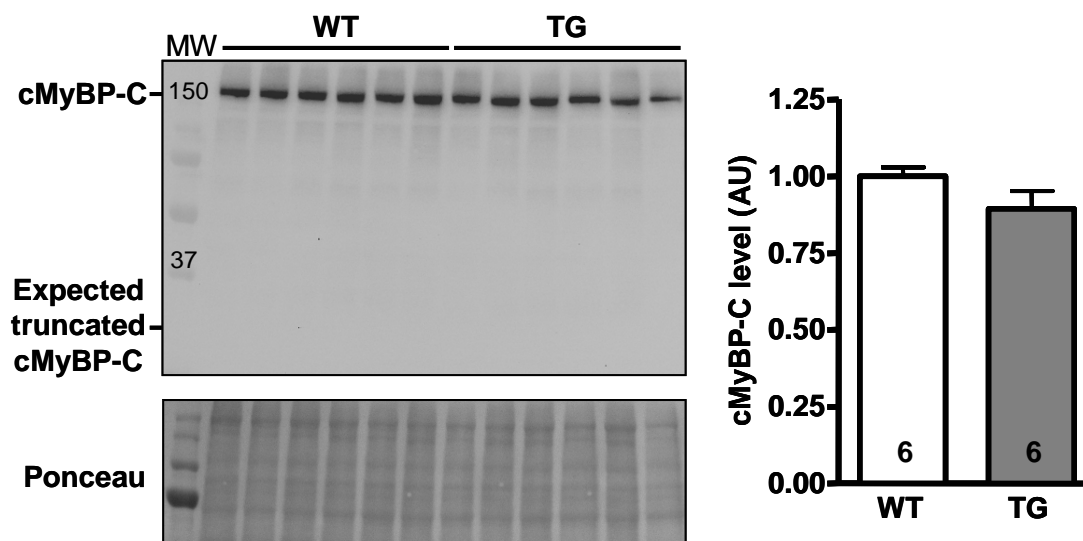


**Figure 3.7: Determination of the cMyBP-C protein expression in the M7t-TG mice.** Proteins were extracted from ventricles of 9 mo-old WT and M7t-TG (TG) mice. On the left, a Western blot stained with an antibody directed against the C0C1-domains of cMyBP-C, which recognizes both the full-length and truncated protein, is shown. Below is the corresponding Ponceau. MW stands for molecular weight marker. On the right, bars represent the quantitative analysis normalized to Ponceau and related to WT. Data are expressed as mean $\pm$ SEM. The number of animals is indicated in the bars.

The level of full-length cMyBP-C protein was similar between WT and M7t-TG mice. The truncated protein at 32 kDa was not detected suggesting that it is either translated at a very low level or highly unstable.

To examine whether the final cDNA construct (Fig. 2.3), which was used for the microinjection, resulted in principle in the Myc-M7t-cMyBP-C protein, NRCM were transfected with the final cDNA construct using lipofectamine and double-stained with anti-myc- and anti-titin-antibodies 48 h after transfection (Fig. 3.8).

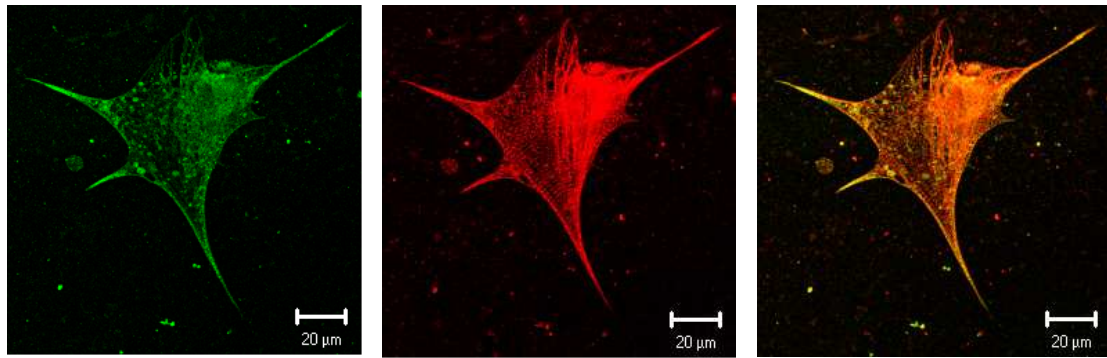


**Figure 3.8: Immunofluorescence analysis of neonatal rat cardiomyocytes transfected with the final transgenic Myc-M7t-cMyBP-C cDNA construct.** Neonatal rat cardiomyocytes were transfected with the final cDNA construct (Fig. 2.3). Forty-eight hours after transfection, cells were double-stained with an anti-myc-antibody, which should detect the transgene (green), and an anti-titin-Z1-antibody, which is directed against the Z1-domain of titin (red) and therefore showing the Z-band. Scale bars represent 20 µm.

A titin-striation was observed indicating that the examined cells were cardiomyocytes. By scanning four coverslips, only one myc-positive NRCM was found (Fig. 3.8). This indicated that in principle the transgene was intact at protein level. The low level of transgene expression is compatible with i) the well known low transfection efficiency in primary cardiomyocytes, ii) the use of the  $\alpha$ -MHC-promoter, which is less strong than the most frequently used CMV promoter and iii) the assumption that truncated proteins are subject to rapid degradation by the UPS.

Finally, cardiomyocytes were isolated from an adult M7t-TG mouse and stained either with antibodies directed against cMyBP-C and  $\alpha$ -actinin to analyze whether the sarcomere is normally organized or with an anti-myc-antibody, which should detect the transgene (Fig. 3.9).

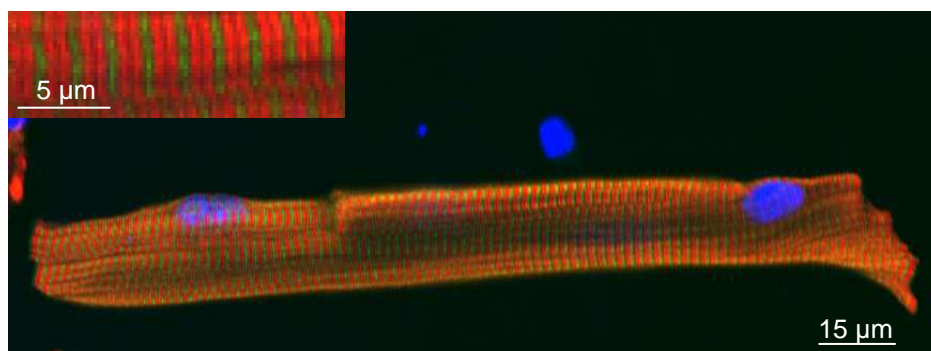


**Figure 3.9: Immunofluorescence analysis of the sarcomere structure in M7t-TG mice.** Cardiomyocytes were isolated from an adult M7t-TG mouse and stained with antibodies directed against cMyBP-C (red) and  $\alpha$ -actinin (green). Nuclei were stained with ToPro3<sup>®</sup> (blue). Scale bars represent 15 µm and 5 µm in the full cell and in the higher magnification, respectively.

The classical alternation of  $\alpha$ -actinin (Z-band) and cMyBP-C (A-band doublets) was revealed in the M7t-TG mouse indicating a correct organization of the sarcomere. No myc-positive cardiomyocyte was found, which was compatible with data obtained by Western blot (Fig. 3.7).

#### **3.1.1.5 Functional characterization**

To investigate whether the transgene expression was associated with a cardiac phenotype, echocardiography was performed each month in WT and M7t-TG mice (n=8) at the age of 9 to 24 mo. The main parameters of the echocardiography analysis are depicted in Fig. 3.10.

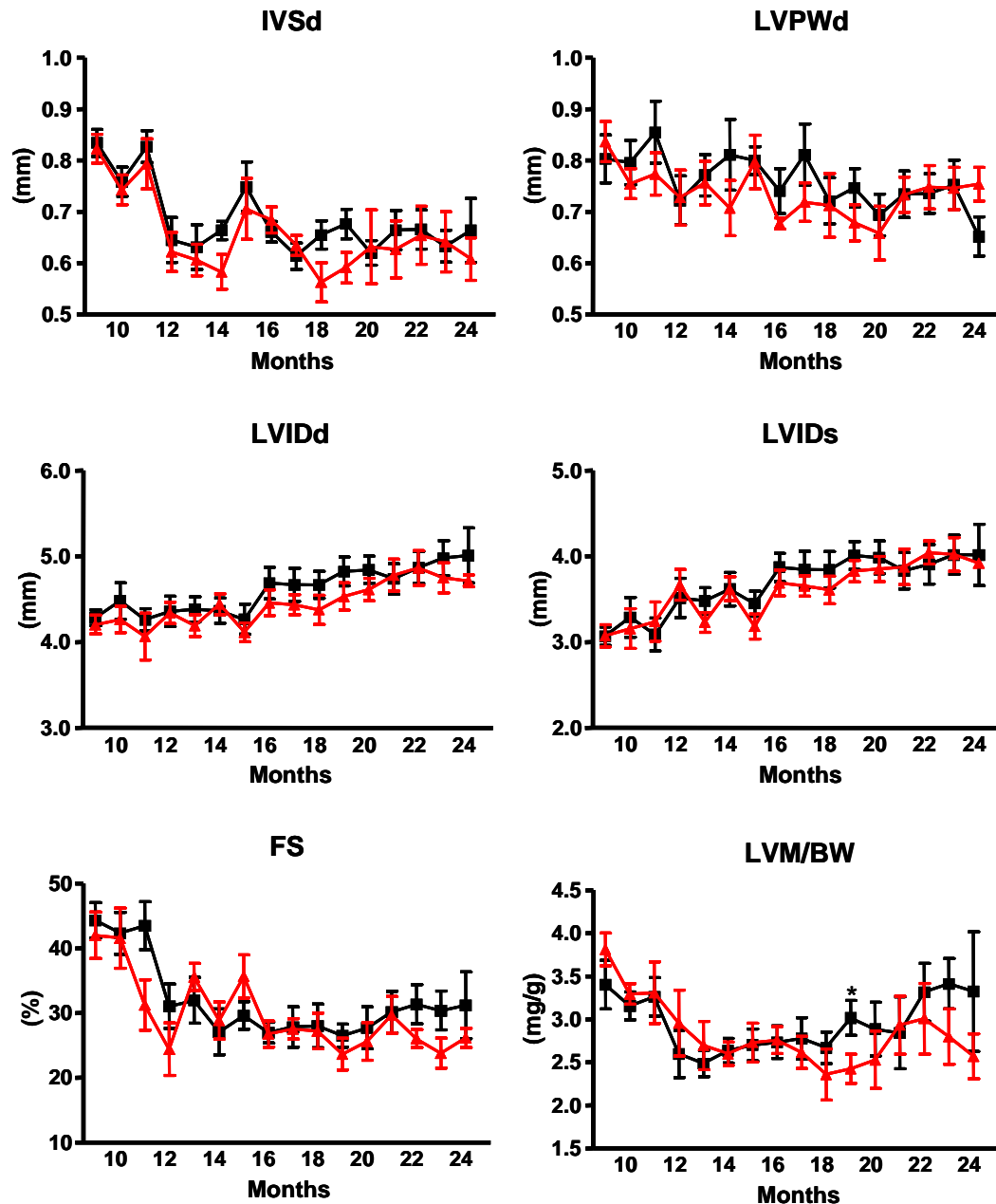


**Figure 3.10: Transthoracic echocardiography in WT and M7t-TG mice.** Cardiac function was evaluated every month between 9 to 24 mo of age. Results were plotted in black for the WT (4 males, 4 females) and in red for the M7t-TG (4 males, 4 females). Comparison was assessed for each time point by Student's t-test. d and s indicate diastole and systole, respectively. IVS stands for interventricular septum thickness, LVPW for left ventricular posterior wall thickness, LVID for left ventricular internal diameter, FS for fractional shortening, LVM for left ventricular mass and BW for body weight.

Both the interventricular septum and the left ventricular (LV) posterior wall thickness decreased with age and were similar between WT and M7t-TG mice. This together with a similar LV mass to body weight ratio (compared to WT) indicated that the M7t-TG mice did not develop LV hypertrophy. The LV internal diameter in diastole and systole increased with age and was similar between WT and M7t-TG mice.

Therefore, the M7t-TG mice did not develop LV dilation. The fractional shortening decreased with age and was also similar between WT and M7t-TG mice. Thus, no cardiac dysfunction or morphological abnormality was observed in the M7t-TG mice up to the age of 24 mo. The echocardiographic analysis was stopped at the age of 24 mo, because some of the mice died or had to be killed due to the occurrence of tumors. Thus, only five M7t-TG and five WT mice could be examined at the end, and in these remaining animals the recording was difficult, because the mice were very fat.

In addition, the ventricular weight to body weight ratio (VW/BW) was determined after sacrifice from hearts of 9 mo-old WT and M7t-TG mice (Fig. 3.11).

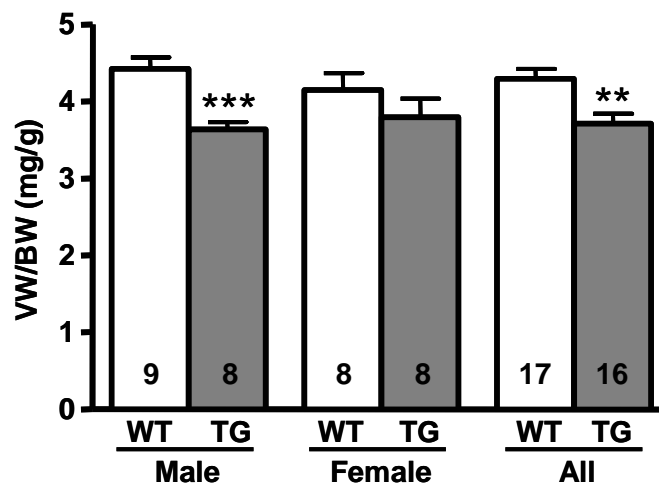


**Figure 3.11: Ventricular weight to body weight ratio in WT and M7t-TG mice.** The ventricular weight to body weight ratio (VW/BW) was determined in 9 mo-old WT and M7t-TG (TG) mice. Bars represent the mean $\pm$ SEM with \*\* $P$ <0.01 and \*\*\* $P$ <0.001 vs. WT mice, Student's t-test. The number of animals is indicated in the bars.

Unexpectedly, the VW/BW was significantly lower (-14%) in the M7t-TG vs. WT mice. This decrease in VW/BW resulted from a decreased VW in the M7t-TG mice, whereas the BW was similar between WT and M7t-TG mice. Therefore, the M7t-TG mice and particularly the males developed LV atrophy.



### 3.1.2 Generation and characterization of the cMyBP-C knock-in mouse model

#### 3.1.2.1 Generation of the cMyBP-C knock-in mouse model

This mouse model was developed by Nicolas Vignier and Lucie Carrier in Paris. It was generated by the targeted knock-in of the G>A transition (on the last nucleotide of exon 6) in the genomic DNA using the Cre/lox system (see 2.1.1.2). The cMyBP-C knock-in mice were expected to produce a missense and/or a nonsense mRNA leading to the 150-kDa mutant full-length cMyBP-C protein (E256K) and/or the 32-kDa C-terminal truncated protein, respectively (Fig. 3.1).

#### 3.1.2.2 Genotyping

Genotypes of wild-type (WT), heterozygous (Het) and homozygous (KI) cMyBP-C knock-in mice were determined by PCR from genomic tail DNA using primers located in intron 7 of the *MYBPC3* gene. PCR products were loaded on a 1% agarose gel (Fig. 3.12).

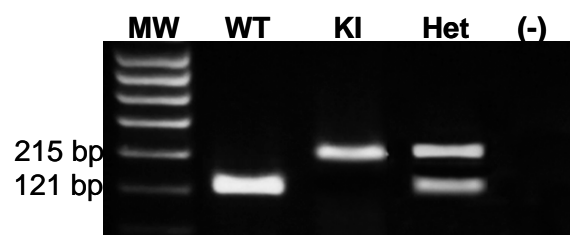


**Figure 3.12: Genotyping of the cMyBP-C knock-in mouse model by PCR.** PCR was performed on genomic tail DNA from WT, Het and KI mice using primers located in intron 7 of the *MYBPC3* gene. As a negative control (-), water was added instead of DNA. MW stands for the 100-bp molecular weight marker.

In the WT mice, the expected 121-bp fragment was obtained, whereas in the KI mice, which still have 1 *loxP* site (see 2.1.1.2), a 94-bp longer PCR fragment (215-bp) was amplified. Both PCR fragments were obtained in the Het mice.

### 3.1.2.3 Molecular characterization at the mRNA level

The level of total cMyBP-C transcripts was determined in 3 mo-old WT, Het and KI mice by quantitative RT-PCR using the SYBR<sup>®</sup> Green strategy (see 2.2.3.5) and primers located in exons 2 and 3 of the mouse cMyBP-C cDNA, i.e. upstream of the mutation (Fig. 3.13).

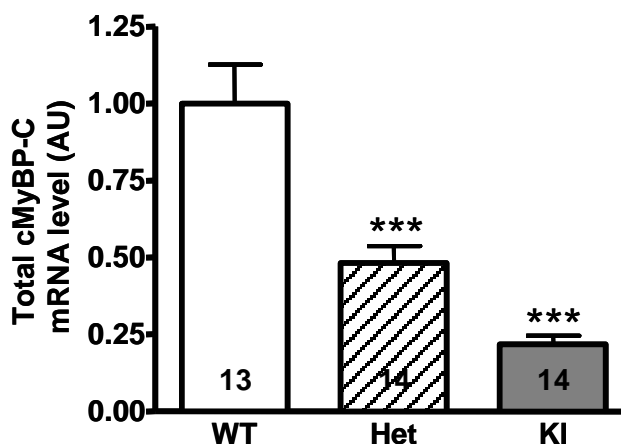


**Figure 3.13: Determination of the level of total cMyBP-C mRNAs in the cMyBP-C knock-in mouse model.** The level of total cMyBP-C transcripts was analyzed in 3 mo-old WT, Het and KI mice by quantitative RT-PCR using the SYBR<sup>®</sup> Green strategy and primers located in exons 2 and 3 of the mouse cMyBP-C cDNA. Bars represent the mean $\pm$ SEM with \*\*\* $P$ <0.001 vs. WT, Student's t-test. The number of animals is indicated in the bars. This analysis was performed by Nicolas Vignier.

Statistical analysis revealed that the amount of total cMyBP-C mRNAs was 52% and 78% lower in the Het and KI mice, respectively, as compared with WT.

To analyze whether the decrease in total cMyBP-C mature RNAs results from a decrease in the level of pre-mRNA, quantitative RT-PCR was performed in 6-10 wk-old WT, Het and KI mice using the SYBR<sup>®</sup> Green strategy and primers located in introns 1 and 2 of the *MYBPC3* gene (Fig. 3.14).

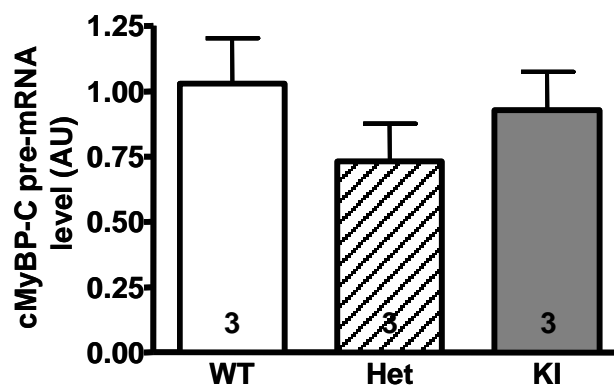


**Figure 3.14: Determination of the level of cMyBP-C pre-mRNA in the cMyBP-C knock-in mouse model.** The level of cMyBP-C pre-mRNA was analyzed in 6-10 wk-old WT, Het and KI mice by quantitative RT-PCR using the SYBR® Green strategy and primers located in introns 1 and 2 of the *MYBPC3* gene. Bars represent the mean±SEM. The number of animals is indicated in the bars.

The amount of cMyBP-C pre-mRNA did not differ between the three groups, which indicated that the markedly lower total cMyBP-C mRNA levels in the Het and KI mice did not result from a lower transcription efficiency. To exclude genomic contamination, similar experiments were performed without adding the reverse transcriptase. No amplification was obtained (data not shown).

By classical RT-PCR using primers around the mutation, the expected fragment at 363 bp was obtained in the WT mice, two different mRNAs (at 363 bp and 245 bp) in the KI mice and only one fragment at 363 bp in the Het mice (Fig. 3.15).

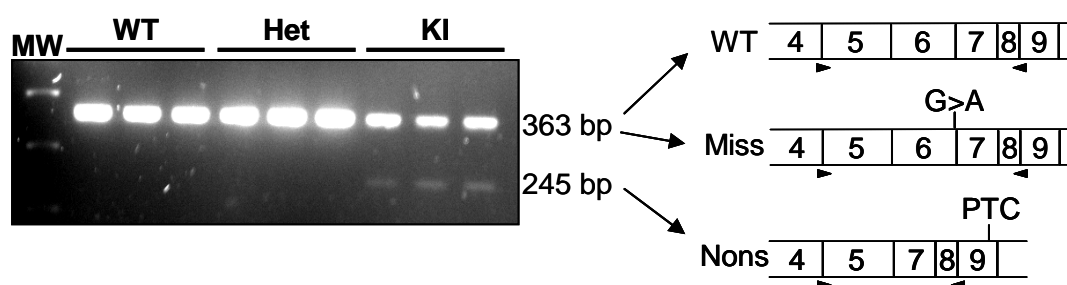


**Figure 3.15: Determination of the different cMyBP-C mRNA species in the cMyBP-C knock-in mouse model.** The different cMyBP-C mRNA species were analyzed in 60 wk-old WT, Het and KI mice by classical RT-PCR using primers (black arrows) as indicated in the scheme on the right (miss means missense mRNA and nons nonsense mRNA). MW stands for the 100-bp molecular weight marker.

Restriction analysis (performed by Nicolas Vignier) indicated that the 363-bp fragment in the Het mice represented both the WT and the missense mRNA. Cloning and sequencing (performed by Nicolas Vignier) of KI products revealed that the 363-bp product contained the missense mRNA and the 245-bp fragment the nonsense

mRNA deleted of exon 6. The level of nonsense mRNA was estimated to be  $\frac{1}{3}$  of the total mRNA species in the KI mice (Fig. 3.15). The low level may explain, why no nonsense mRNA fragment was observed in the Het mice, which also contained the WT allele. By nested RT-PCR using primers around the mutation, the 245-bp product could indeed be amplified in one out of three Het mice (Fig. 3.16).

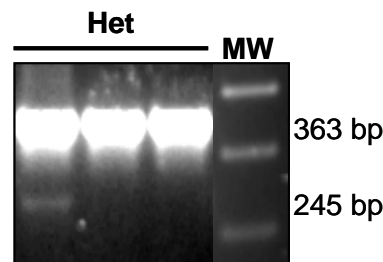


**Figure 3.16: Determination of the nonsense mRNA in the Het mice.** The different cMyBP-C mRNA species were analyzed in 60 wk-old Het mice by nested classical RT-PCR using primers as indicated in the scheme in Fig. 3.15. MW stands for the 100-bp molecular weight marker.

The presence of the nonsense mRNA in one out of three Het mice was confirmed by quantitative RT-PCR using primers located in exons 5 and 7 of the cMyBP-C cDNA and a TaqMan<sup>®</sup> probe, which exactly matches the junction between exons 5 and 7 and is therefore specific for the nonsense mRNA (data not shown). As expected, amplification was never found in WT, but in all KI mice.

### 3.1.2.4 Molecular characterization at the protein level

It was investigated whether the point mutation indeed lead to the full-length mutant (150-kDa) and the truncated (32-kDa) cMyBP-C protein. Western blot analyses were performed using an antibody directed against the C0C1-domains of cMyBP-C, which recognizes both mutants (Fig. 3.17).

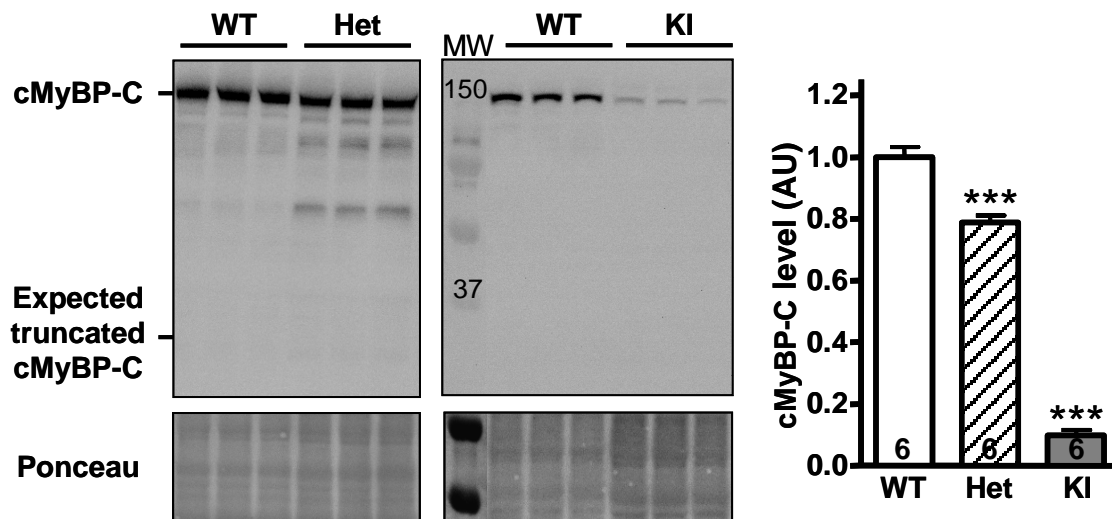


**Figure 3.17: Determination of the cMyBP-C protein expression in the cMyBP-C knock-in mouse model.** Proteins were extracted from ventricles of 60 wk-old WT, Het and KI mice. On the left, representative Western blots stained with an antibody directed against the COC1-domains of cMyBP-C are shown. Below each blot is the corresponding Ponceau. MW stands for molecular weight marker. On the right, bars represent the quantitative analysis normalized to Ponceau and related to WT. Data are expressed as mean±SEM with \*\*\* $P$ <0.001 vs. WT, Student's t-test. The number of animals is indicated in the bars.

The full-length cMyBP-C protein was detected in both the Het and KI mice, but the truncated protein at 32 kDa was not. Quantitative analysis revealed a 21% and 90% reduction of the full-length protein amount in the Het and KI mice, respectively, as compared to WT mice. In the Het mice, the bands at 60 and 100 kDa were likely degradation products.

Cardiomyocytes were isolated from adult WT, Het and KI mice and stained with antibodies directed against cMyBP-C and  $\alpha$ -actinin to analyze whether the low amount of full-length cMyBP-C, especially in the KI mice, was associated with sarcomeric disorganization (Fig. 3.18).

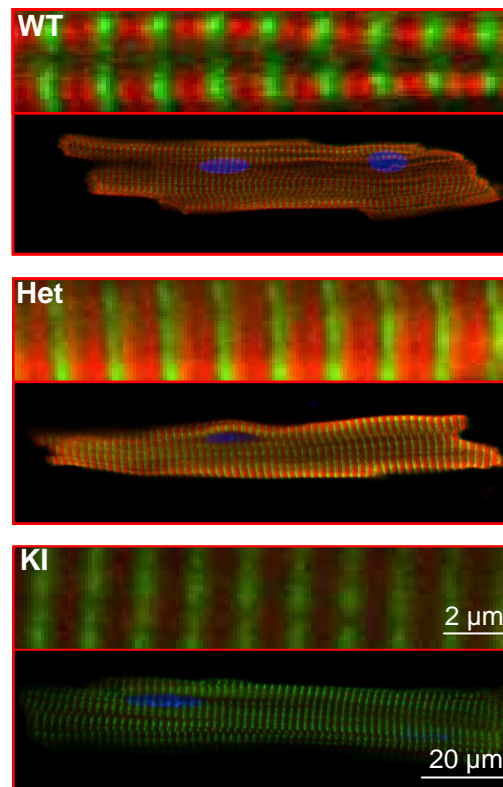


**Figure 3.18: Immunofluorescence analysis of cMyBP-C in cardiomyocytes of cMyBP-C knock-in mice.** Cardiomyocytes were isolated from adult WT, Het and KI mice and stained with antibodies directed against cMyBP-C (red) and  $\alpha$ -actinin (green). Nuclei were stained with ToPro3<sup>®</sup> (blue). The lower part of each panel corresponds to the entire cell, the upper part to a 10x magnification. Scale bars represent 20  $\mu$ m and 2  $\mu$ m in full cells and in the 10x-magnification, respectively.

In KI cardiomyocytes, cMyBP-C protein was almost not detected. In contrast,  $\alpha$ -actinin appeared normal, suggesting correct organization of the sarcomere. In both WT and Het cardiomyocytes, the classical alternation of  $\alpha$ -actinin (Z-band) and cMyBP-C (A-band doublets) was revealed.

### 3.1.2.5 Functional characterization

The characterization of mouse cardiac function was done by Nicolas Vignier. Transthoracic echocardiography was performed at 3, 12 and 18 mo of age in WT, Het and KI mice. No major differences were obtained between Het and WT during all postnatal windows (data not shown), but eccentric LV hypertrophy (LVH) accompanied by a reduced FS was identified in the KI mice (Fig. 3.19 A). Histological examination confirmed enlargement of the LV and exhibited

accumulation of interstitial fibrosis in the KI mice (Fig. 3.19 B and C). The heart to body weight ratio (HW/BW) was 34% higher in the KI mice as compared to WT (Fig. 3.19 D). In contrast, no changes in both myocardial morphology and HW/BW were observed in the Het mice. The cardiomyocyte area, calculated as cardiomyocyte length x width, was 41% and 4% greater in KI and Het mice, respectively, as compared to WT (data not shown). The mRNA level of hypertrophic markers ( $\beta$ -myosin heavy chain ( $\beta$ -MHC),  $\alpha$ -skeletal actin, brain natriuretic peptide (BNP) and atrial natriuretic peptide (ANP)) was 8- to 14-fold higher in the KI mice as compared to WT. In contrast, the Het mice exhibited just a slight, not significant increase in  $\beta$ -MHC mRNA (data not shown).

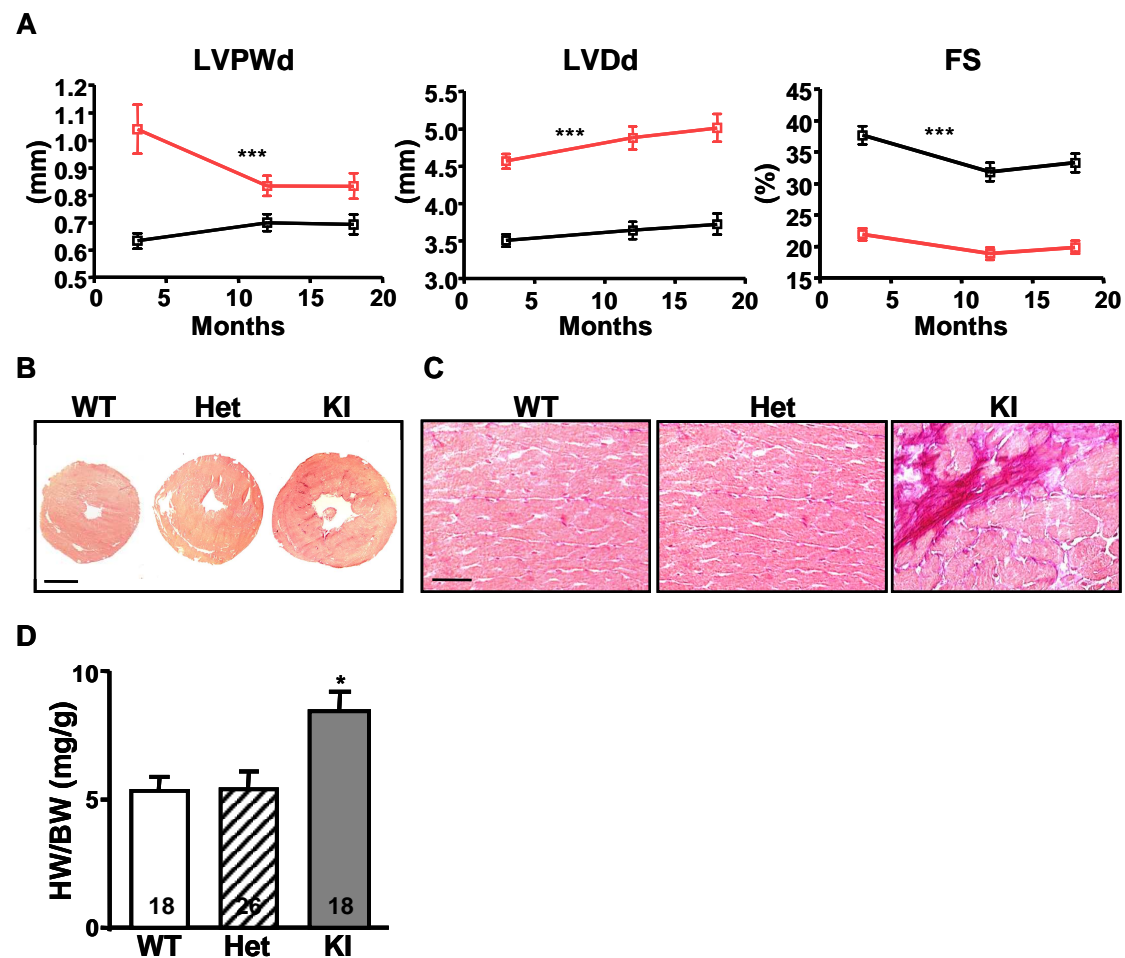


**Figure 3.19: Determination of the cardiac phenotype in the cMyBP-C knock-in mouse model.** **A**, Transthoracic echocardiography was evaluated at 3, 12 and 18 mo of age in WT and KI mice. Results were plotted in black for the WT (8 males, 7 females) and in red for the KI (8 males, 7 females). Differences were assessed by two-way ANOVA with Bonferroni post-tests with \*\*\* $P < 0.001$  vs. WT. d indicates diastole. LVPW stands for left ventricular posterior wall thickness, LVID for left ventricular internal diameter, FS for fractional shortening. **B**, Transversal ventricular sections of WT, Het and KI mice stained with Sirius Red. Bar = 0.5 cm. **C**, Detail of a transversal section stained with Sirius Red. Bar = 10  $\mu$ m. **D**, The HW/BW was calculated of 3 mo-old WT, Het and KI mice. Bars represent the mean  $\pm$  SEM with \* $P < 0.05$  vs. WT, Student's t-test. The number of animals is indicated in the bars. All analyses were performed by Nicolas Vignier.

### 3.1.3 Summary

The major findings of this chapter are the following:

- In M7t-TG compared to WT mice, the level of total cMyBP-C mRNA was 2-fold higher, but the level of full-length cMyBP-C protein was similar and the truncated protein was not detected. The hearts of M7t-TG mice did not show signs of cardiac dysfunction or hypertrophy, but unexpectedly cardiac atrophy, particularly in the male M7t-TG mice. The absence of the truncated cMyBP-C protein is compatible with an involvement of the UPS in the M7t-TG mice.
- In the KI mice, the total amount of cMyBP-C mRNA and protein was markedly lower compared to WT. In the Het mice, the total amount of cMyBP-C mRNA was 50% lower than in WT, and a slight, but significant decrease of the full-length cMyBP-C protein was detected compared to WT. In both KI and Het mice, the truncated protein was not detected. The KI mice developed eccentric LVH with reduced FS, whereas no LVH and cardiac dysfunction were observed in the Het mice. These data show that the cMyBP-C knock-in mouse model is more related to changes at the mRNA level and suggest that the NMD is likely involved in the degradation of the nonsense mRNA in the KI and Het mice. Additionally, the UPS could be involved in the degradation of the full-length mutant cMyBP-C protein and the truncated protein.



## 3.2 Analysis of the UPS involvement *ex vivo*

As mentioned above, the absence of the truncated protein in both the M7t-TG and the KI mice and the quite low level of the full-length mutant in the KI mice could be due to a rapid degradation by the UPS as shown before after gene transfer in cardiomyocytes (Sarikas et al., 2005). Thus, cardiomyocytes were isolated from neonatal and adult mice, cultured and treated with different proteasome inhibitors. After treatment, extracted proteins were analyzed by Western blot to investigate whether the treatment resulted in the detection of the truncated mutant in both M7t-TG and KI mice and/or an increase of the full-length mutant in the KI mice.

### 3.2.1 Inhibition of the UPS in M7t-TG mice

Cardiomyocytes were isolated from neonatal M7t-TG mice and treated with the reversible proteasome inhibitor MG132 (10  $\mu$ M) for different times (Fig. 3.20). Afterwards, proteins were extracted and analyzed by Western blot using the antibody directed against the C0C1-domains of cMyBP-C, which recognizes both the full-length and the truncated proteins. To confirm the inhibition of the UPS, a second membrane with the same loading was stained with an antibody directed against ubiquitin.

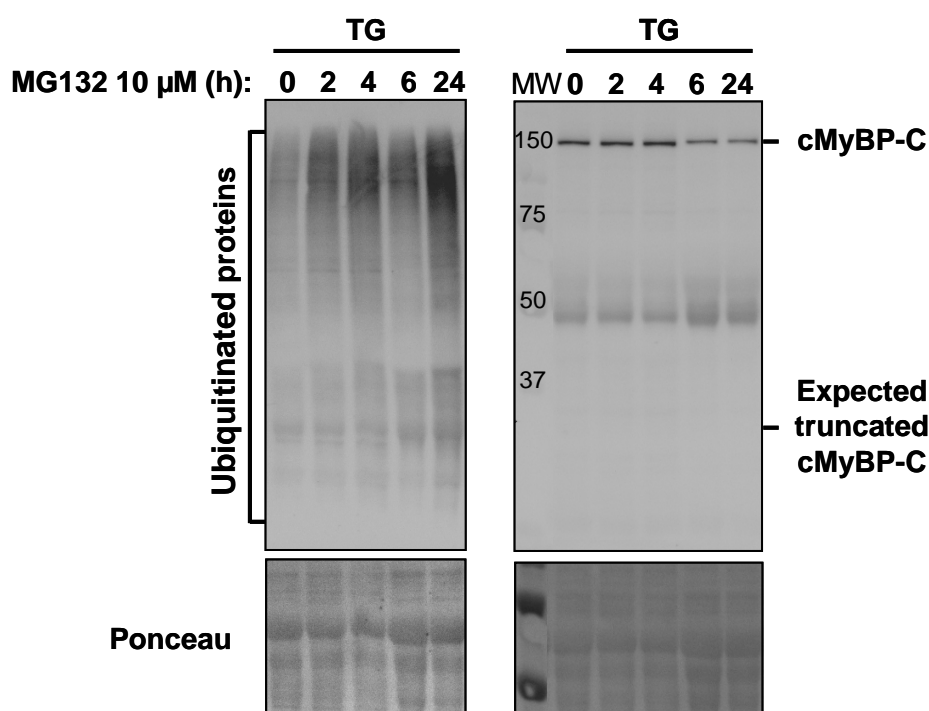


**Figure 3.20: Effect of the reversible UPS inhibition on the cMyBP-C amount in cardiomyocytes of neonatal M7t-TG mice.** Cardiomyocytes were isolated from neonatal M7t-TG (TG) mice and treated with 10  $\mu$ M MG132 for the indicated periods. The left blot was stained with an antibody directed against ubiquitin. The right blot was stained with an antibody directed against the C0C1-domains of cMyBP-C, i.e. both cMyBP-C isoforms could be recognized. The first lane corresponds to the molecular weight marker (MW). Below each blot is the corresponding Ponceau.

The inhibition of the UPS by MG132 was confirmed by the accumulation of ubiquitinated proteins. But unexpectedly, the treatment with MG132 did not reveal the truncated protein at 32 kDa. The amount of the full-length cMyBP-C did not change until 4 h of treatment, but decreased after 6 and 24 h treatment. The reason for this is not known, but could be related to the beginning of apoptosis.

Similar results were obtained by treating neonatal cardiomyocytes of M7t-TG mice with the irreversible proteasome inhibitor epoxomicin (500 nM) for 4 h (Fig. 3.21).

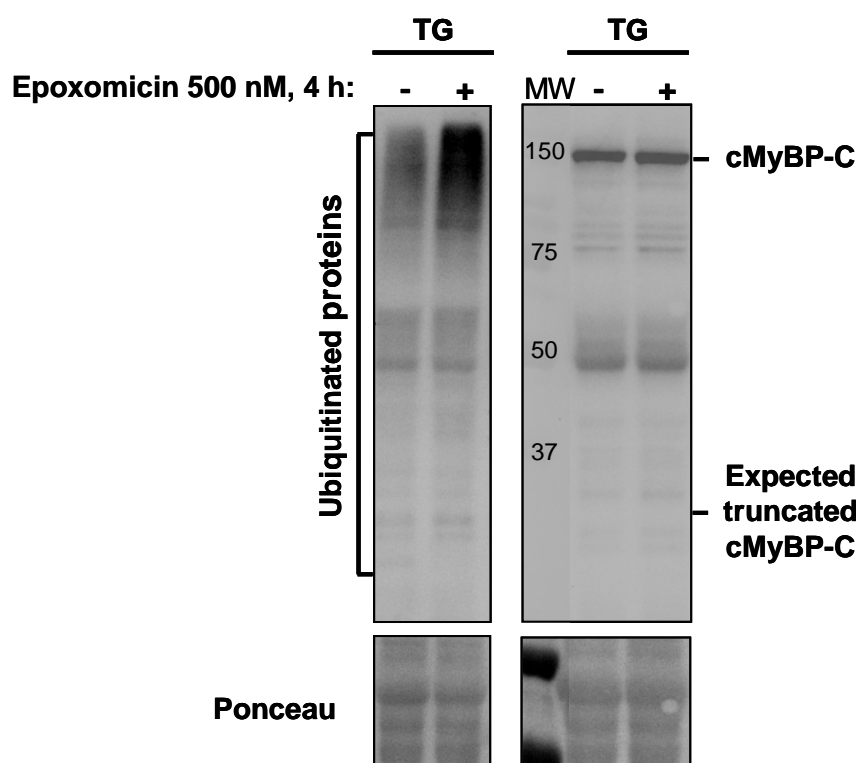


**Figure 3.21: Effect of the irreversible UPS inhibition on the cMyBP-C amount in neonatal cardiomyocytes of M7t-TG mice.** Cardiomyocytes were isolated from neonatal M7t-TG (TG) mice and cultured in the absence (-) or presence (+) of 500 nM epoxomicin for 4 h. The left blot was stained with an antibody directed against ubiquitin. The right blot was stained with an antibody directed against the C0C1-domains of cMyBP-C, i.e. both cMyBP-C isoforms could be recognized. The first lane corresponds to the molecular weight marker (MW). Below each blot is the corresponding Ponceau.

Epoxomicin treatment effectively inhibited the UPS as indicated by an accumulation of ubiquitinated proteins, but did not result in the detection of the truncated protein at 32 kDa. The amount of the full-length cMyBP-C protein did not change by the treatment.

Cardiomyocytes were also isolated from adult M7t-TG mice and cultured in the absence or presence of 10  $\mu$ M MG132 for 15 h. The extracted proteins were analyzed in the same way as above. The UPS inhibition did not reveal the truncated protein (data not shown).

In Fig. 3.20 and 3.21, diffuse bands at ~50 kDa were obtained. To investigate the identity of these bands, proteins were extracted from different preparations (cultured neonatal and adult cardiomyocytes and whole ventricles) and analyzed by Western blot. The blots were stained with the antibody directed against the C0C1-domains of

cMyBP-C and with an antibody directed against  $\alpha$ -actinin to test whether these bands are cMyBP-C-related or not (Fig. 3.22).

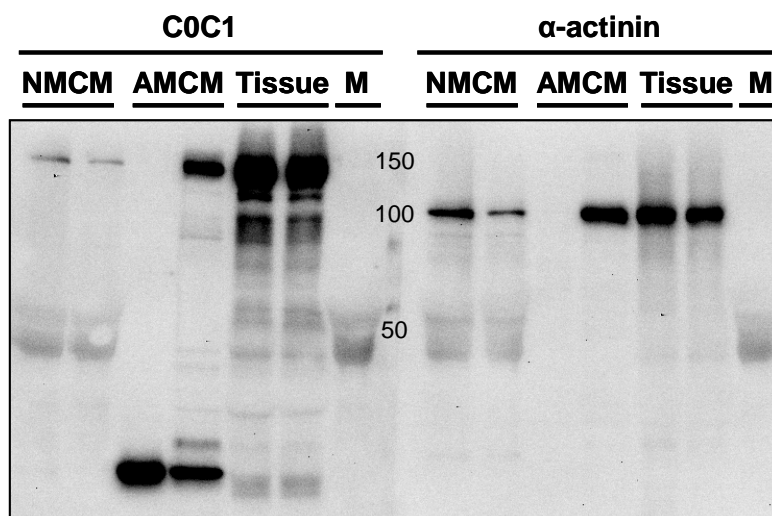


**Figure 3.22: Comparison of cMyBP-C protein levels in different protein preparations.** Proteins were extracted from cultured neonatal or adult mouse cardiomyocytes (NMCM and AMCM, respectively) or from ventricles (tissue). Western blot analysis was performed using either an antibody directed against the C0C1-domains of cMyBP-C (left part) or an antibody directed against  $\alpha$ -actinin (right part). In the M lane, pure NMCM culture medium was loaded. In the middle of the blot the molecular weight marker is shown.

The diffuse bands at  $\sim 50$  kDa were detected with both antibodies, but only in the NMCM preparations and in the NMCM culture medium indicating that these bands derive from components of this culture medium. Interestingly, the level of cMyBP-C was lower in neonatal than in adult cardiomyocytes. One of the AMCM samples (the first one) was obviously degraded: The antibody directed against the C0C1-domains of cMyBP-C could only detect a degradation product at low molecular weight, whereas no signal was detected with the antibody directed against  $\alpha$ -actinin.

### 3.2.2 Inhibition of the UPS in KI mice

Cardiomyocytes were isolated from neonatal KI mice and treated with the reversible proteasome inhibitor MG132 (10  $\mu$ M) for 2 h (Fig. 3.23). Afterwards, the extracted proteins were analyzed in the same way as described for the M7t-TG mice.

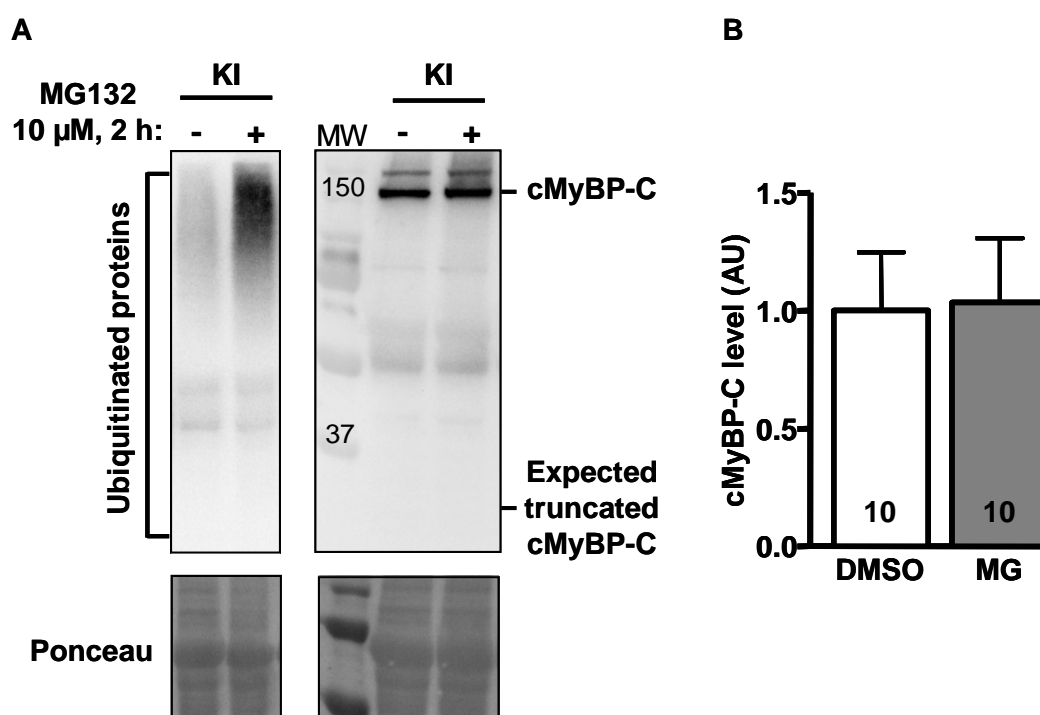


**Figure 3.23: Effect of the reversible UPS inhibition on the cMyBP-C amount in neonatal cardiomyocytes of KI mice.** **A**, Cardiomyocytes were isolated from neonatal KI mice and cultured in the absence (-) or presence (+) of 10  $\mu$ M MG132 for 2 h. The left blot was stained with an antibody directed against ubiquitin. The right blot was stained with the antibody directed against the C0C1-domains of cMyBP-C. MW stands for the molecular weight marker. Below each blot is the corresponding Ponceau. **B**, Quantitative analysis of the full-length cMyBP-C normalized to Ponceau and related to DMSO-treated NMCM. Bars represent the mean $\pm$ SEM. The number of experiments is indicated in the bars.

The ubiquitinated proteins accumulated after treatment with MG132 confirming the inhibition of the UPS. However, despite successful UPS inhibition, the truncated protein was not detected. Quantitative analysis of ten different experiments showed no increase in the amount of the full-length mutant protein after UPS inhibition.

Similar experiments were performed by treating neonatal cardiomyocytes of KI mice with the irreversible proteasome inhibitor epoxomicin (500 nM) for 4 h (Fig. 3.24).

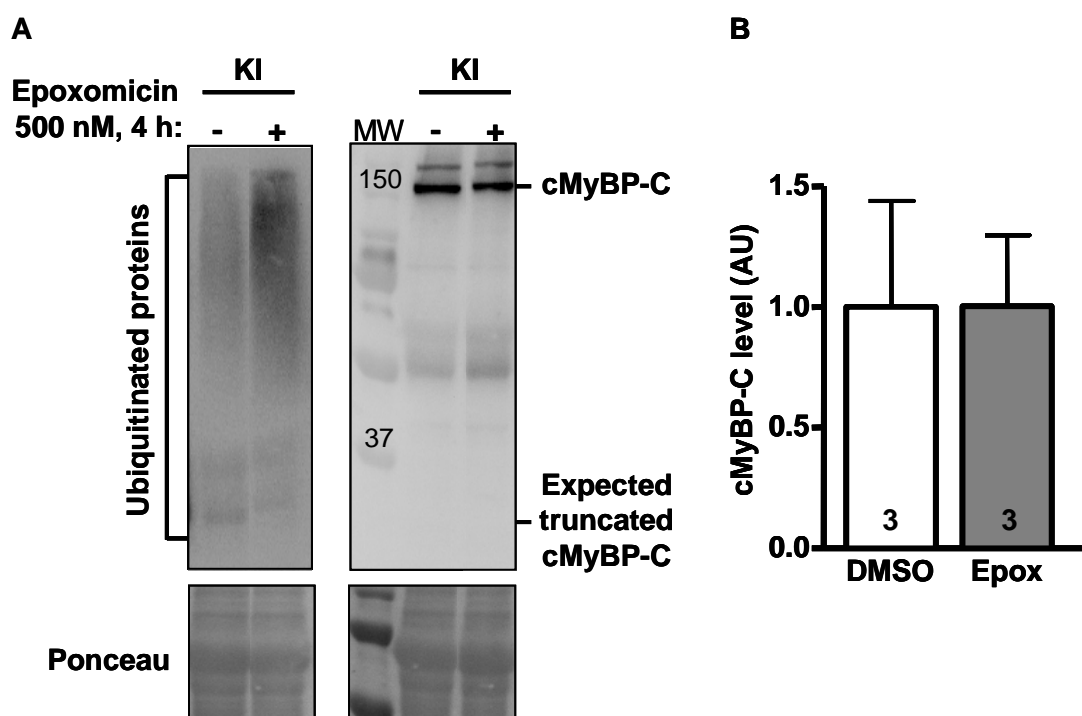


**Figure 3.24: Effect of the irreversible UPS inhibition on the cMyBP-C amount in neonatal cardiomyocytes of KI mice.** **A**, Cardiomyocytes were isolated from neonatal KI mice and cultured in the absence (-) or presence (+) of 500 nM epoxomicin (epox) for 4 h. The left blot was stained with an antibody directed against ubiquitin. The right blot was stained with the antibody directed against the COC1-domains of cMyBP-C. MW stands for the molecular weight marker. Below each blot is the corresponding Ponceau. **B**, Quantitative analysis of the full-length cMyBP-C normalized to Ponceau and related to DMSO-treated NMCM. Bars represent the mean $\pm$ SEM. The number of experiments is indicated in the bars.

Epoxomicin effectively blocked the UPS as confirmed by the accumulation of ubiquitinated proteins, but did not reveal the truncated protein. Quantitative analysis of three different experiments showed no increase in the amount of the full-length mutant protein after UPS inhibition.

Cardiomyocytes were also isolated from adult KI mice and cultured in the absence or presence of 10  $\mu$ M MG132 for 15 h. Extracted proteins were analyzed in the same way as above. The truncated protein was not detected after proteasome inhibition (data not shown).

### 3.2.3 Summary

In contrast to the study of Sarikas et al. (2005), the inhibition of the proteasome with both a reversible and an irreversible inhibitor did neither reveal the truncated protein nor increased the level of the full-length protein in both M7t-TG and KI cardiomyocytes. Thus, these data failed to show evidence for a major UPS involvement in the M7t-TG or KI mice *ex vivo*.

### 3.3 Investigation of the UPS function *in vivo*

#### 3.3.1 Investigation of ubiquitination and degradation in myocardial tissue of M7t-TG and KI mice

Despite these negative results it was possible that the UPS function was altered by the presence of the mutants. Thus, the function of the UPS was investigated at the level of both ubiquitination and degradation in myocardial tissue from M7t-TG and KI mice (Fig. 3.25).

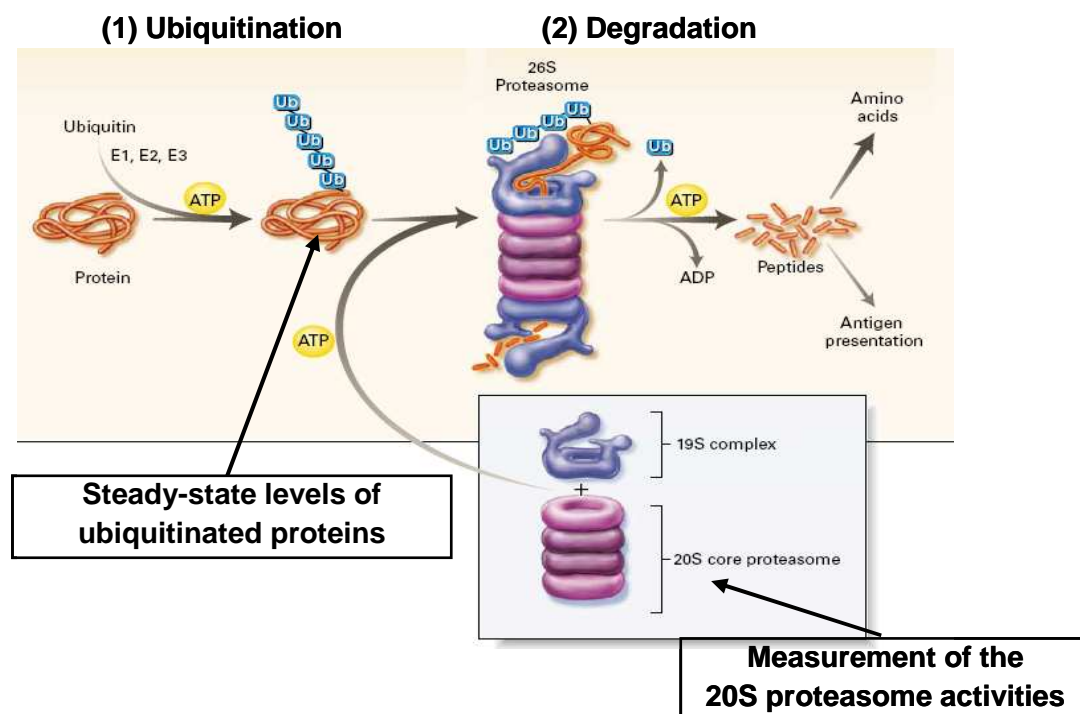


**Figure 3.25: Investigation of the UPS function.** The level of ubiquitination was investigated by determining the steady-state levels of ubiquitinated proteins using an antibody directed against ubiquitin. The level of degradation was analyzed by measuring the three different 20S proteasome activities (chymotrypsin-like, trypsin-like and caspase-like activity) using for each activity a specific, fluorogenic substrate (see 2.2.4.4).

##### 3.3.1.1 Investigation of ubiquitination and degradation in the M7t-TG mice

In the M7t-TG mice, the UPS function was investigated in 9 mo-old mice. The steady-state levels of ubiquitinated proteins are shown in Fig. 3.26.



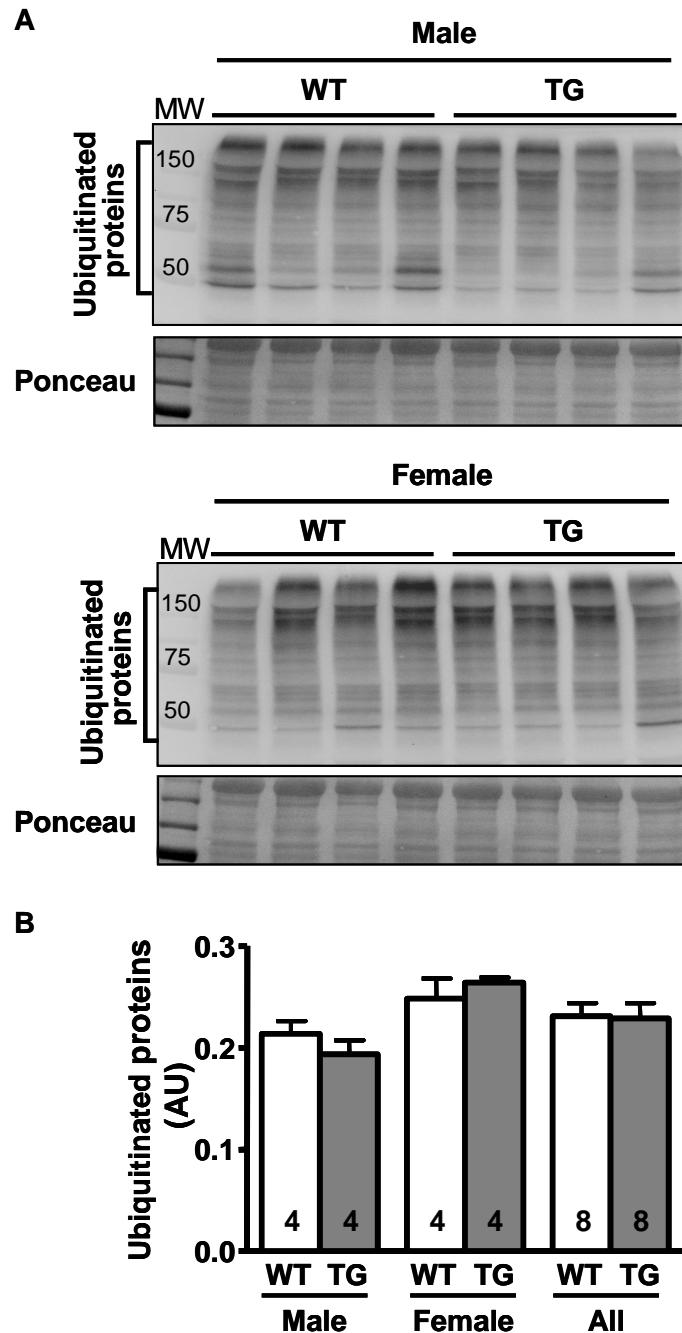


**Figure 3.26: Investigation of ubiquitination in the M7t-TG mice.** **A**, Proteins were extracted from ventricles of 9 mo-old WT and M7t-TG (TG) mice. The blots were stained with an antibody directed against ubiquitin. MW stands for the molecular weight marker. Below each blot is the corresponding Ponceau. **B**, Quantitative analysis normalized to Ponceau. Bars represent the mean $\pm$ SEM. The number of animals is indicated in the bars.

The antibody directed against ubiquitin is able to detect ubiquitin, mono-ubiquitinated and poly-ubiquitinated proteins resulting in the typical pattern of various bands represented in Fig. 3.26 A. For both males and females, the pattern of ubiquitinated proteins was similar between WT and M7t-TG mice. Quantitative analysis did not reveal major differences between the groups.

For investigation of the UPS at the level of degradation, the chymotrypsin-like activity was measured in the M7t-TG mice (Fig. 3.27).

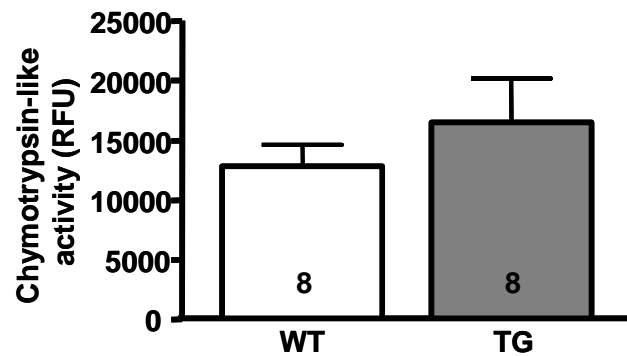


**Figure 3.27: Investigation of the chymotrypsin-like activity of the 20S proteasome in the M7t-TG mice.** The chymotrypsin-like activity was measured in 9 mo-old WT and M7t-TG (TG) mice. Bars represent the mean $\pm$ SEM. Number of animals is indicated in the bars.

The chymotrypsin-like activity of the 20S proteasome was not significantly altered in the M7t-TG mice as compared to WT.

### 3.3.1.2 Investigation of ubiquitination and degradation in the KI and KO mice

In the KI mice, the UPS function was investigated from birth to 50 wk of age and compared to the corresponding WT mice. To prove that an UPS alteration, if present, is cMyBP-C-dependent, also the KO mouse model, which does not express any cMyBP-C, was analyzed in the same way. The determination of the steady-state levels of ubiquitinated proteins was investigated by Karim Sultan (for the KI mice) and Daniel Englmann (for the KO mice). Ventricular proteins from KI, KO and corresponding WT mice were extracted for each time point (0 (birth), 2, 4, 6, 9, 13, 27 and 50 wk of age) and analyzed by Western blot (Fig. 3.28).

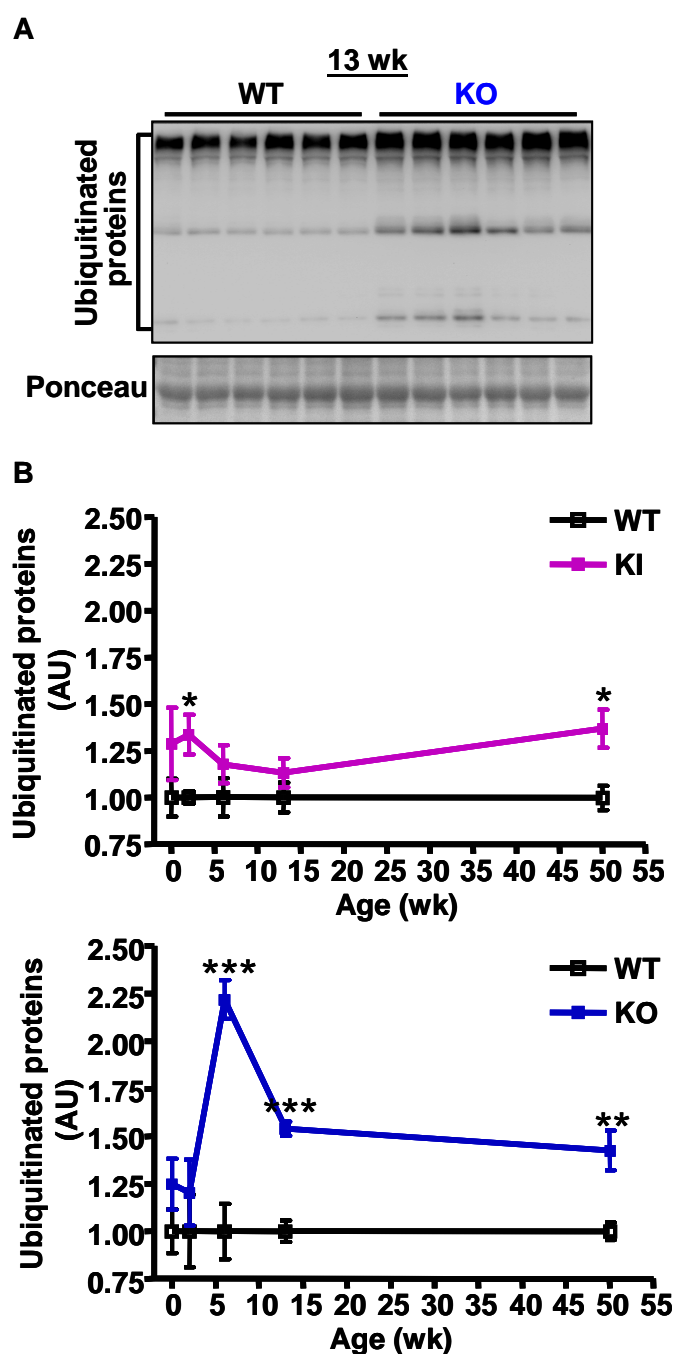


**Figure 3.28: Investigation of ubiquitination in the KI and KO mice.** Ventricular proteins were extracted from KI, KO and corresponding WT mice. **A**, A representative blot (13 wk-time point in the KO mice) stained with an antibody directed against ubiquitin is shown. Below is the corresponding Ponceau. **B**, Representative time courses of the steady-state levels of ubiquitinated proteins in KI and KO mice related to WT are shown with \* $P < 0.05$ , \*\* $P < 0.01$  and \*\*\* $P < 0.001$  vs. WT, Student's t-test. These analyses were performed by Karim Sultan and Daniel Englmann.

In Fig. 3.28 A, the ubiquitination pattern for the 13 wk-time point of the KO mice is representatively shown. With the known limitations of quantifying Western blots for many samples a few statements can be made with confidence for the representative time courses of the steady-state levels of ubiquitinated proteins in KI and KO mice,

shown in Fig. 3.28 B. First, the steady-state levels of ubiquitinated proteins stayed overall elevated during development for both KI and KO mice. Second, the average steady-state level of ubiquitinated proteins was 26% and 53% higher in KI and KO mice, respectively, as compared to their respective WT. In particular in the KI mice, there was no clear cut increase in the steady-state levels of ubiquitinated proteins in 50 wk-old mice compared to neonatal mice.

All three 20S proteasome activities were measured in cytosolic protein extracts from the same mice as above, i.e. 8 KI, KO and corresponding WT mice were analyzed (Fig. 3.29-3.31).

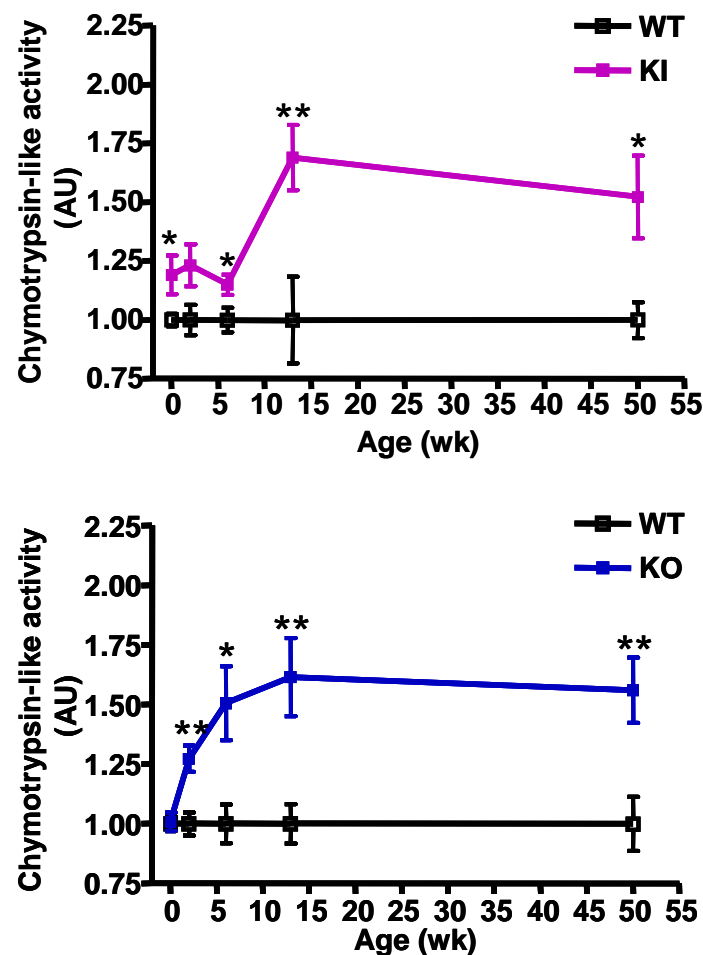


**Figure 3.29: Investigation of the chymotrypsin-like activity in the KI, KO and corresponding WT mice.** Ventricular cytosolic proteins were extracted from 8 KI, KO and respective WT mice. Representative time courses of the chymotrypsin-like activity (related to WT) are shown with  $*P < 0.05$  and  $**P < 0.01$  vs. WT, Student's t-test.

In KI compared to WT mice, the chymotrypsin-like activity was already increased by 19% at birth. At 13 wk of age, the chymotrypsin-like activity was elevated by 69% and remained highly elevated (>50%) until the age of 50 wk. In KO compared to WT mice, the chymotrypsin-like activity was not altered at birth, but increased by 27% at the age of 2 wk. A >50% greater chymotrypsin-like activity was observed at the age of 6 wk and remained until the age of 50 wk.

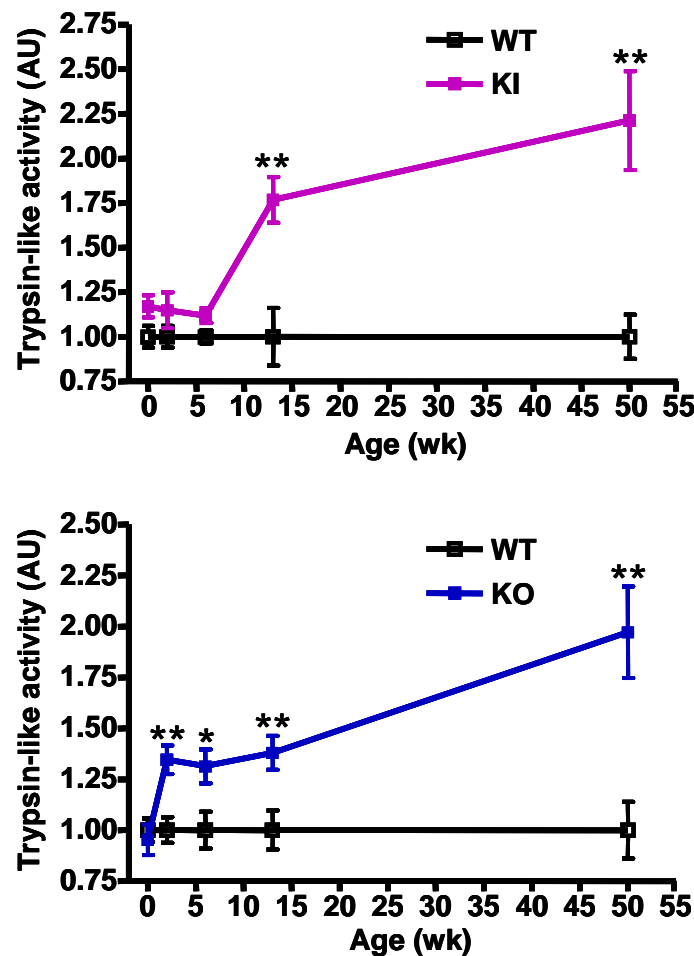


**Figure 3.30: Investigation of the trypsin-like activity in the KI, KO and corresponding WT mice.** Ventricular cytosolic proteins were extracted from 8 KI, KO and respective WT mice. Representative time courses of the trypsin-like activity (related to WT) are shown with \* $P < 0.05$  and \*\* $P < 0.01$  vs. WT, Student's t-test.

The trypsin-like activity was not significantly altered at birth and until the age of 6 wk in KI vs. WT mice. An elevated trypsin-like activity by 77% and 121% was observed in 13 and 50 wk-old KI mice, respectively, compared to WT. In KO compared to WT mice, the trypsin-like activity was not altered at birth, but increased by 35% at the age of 2 to 13 wk. An almost 2-fold greater trypsin-like activity was observed in 50 wk-old KO vs. WT mice.

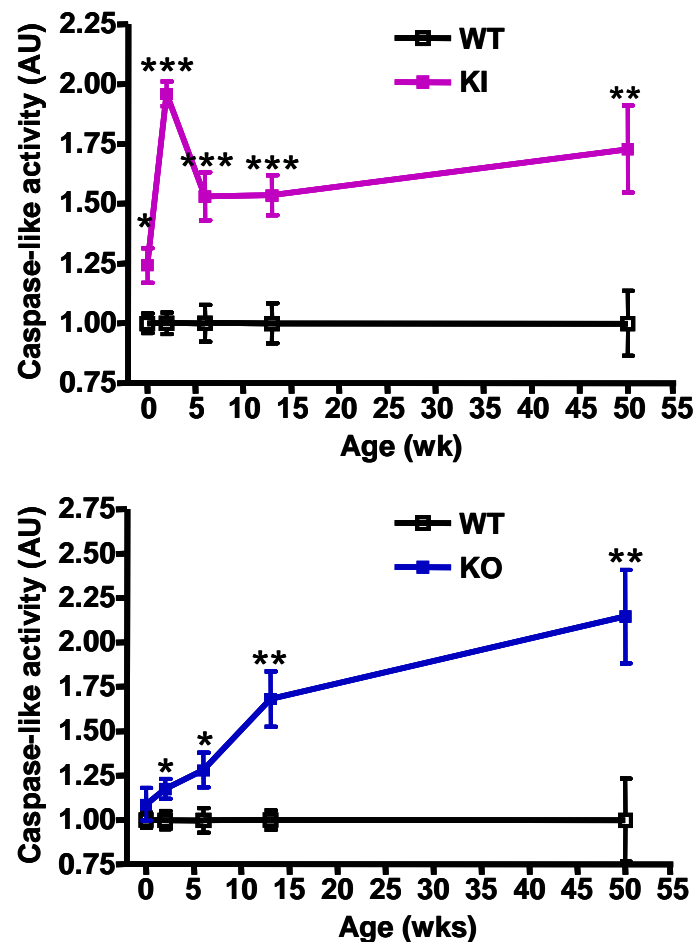


**Figure 3.31: Investigation of the caspase-like activity in the KI, KO and corresponding WT mice.** Ventricular cytosolic proteins were extracted from 8 KI, KO and respective WT mice. Representative time courses of the caspase-like activity (related to WT) are shown with \* $P < 0.05$ , \*\* $P < 0.01$  and \*\*\* $P < 0.001$  vs. WT, Student's t-test.

Like the chymotrypsin-like activity, the caspase-like activity was elevated (+24%) at birth in KI vs. WT mice. At the age of 2 wk, an almost 2-fold greater caspase-like activity was observed. From 6 to 50 wk of age, the caspase-like activity was increased by >50%. In KO compared to WT mice, the caspase-like activity was not altered at birth. At the age of 2 wk, the caspase-like activity was 18% greater and increased continuously during development. At the age of 50 wk, the caspase-like activity was more than 2-fold greater in KO vs. WT mice.

It was then investigated whether there are correlations between the degree of hypertrophy, the steady-state levels of ubiquitinated proteins and the 20S proteasome activities in the KI, KO and corresponding WT mice. First, the correlation between the steady-state levels of ubiquitinated proteins and the degree of hypertrophy, determined by the HW/BW, was evaluated (Fig. 3.32).

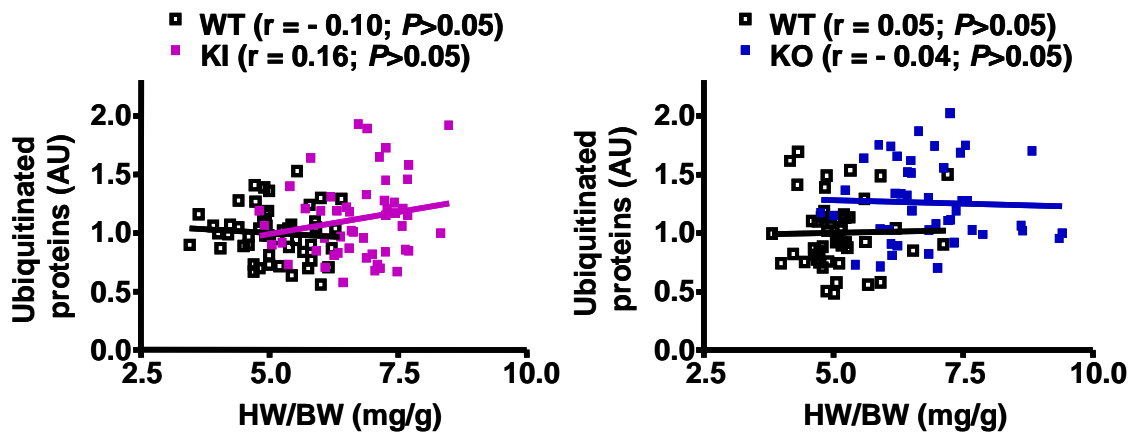


**Figure 3.32: Correlation between the steady-state levels of ubiquitinated proteins and the degree of hypertrophy in KI and KO mice.** The steady-state level of ubiquitinated proteins was plotted against the HW/BW and checked for correlation using the nonparametric correlation (Spearman =  $r$ ) test.

No correlation could be seen in KI, KO and corresponding WT mice concerning these examined parameters. This means that the steady-state levels of ubiquitinated proteins did not increase with the degree of hypertrophy or vice versa.

Next, the correlation between the 20S proteasome activities and the degree of hypertrophy was analyzed (Fig. 3.33).

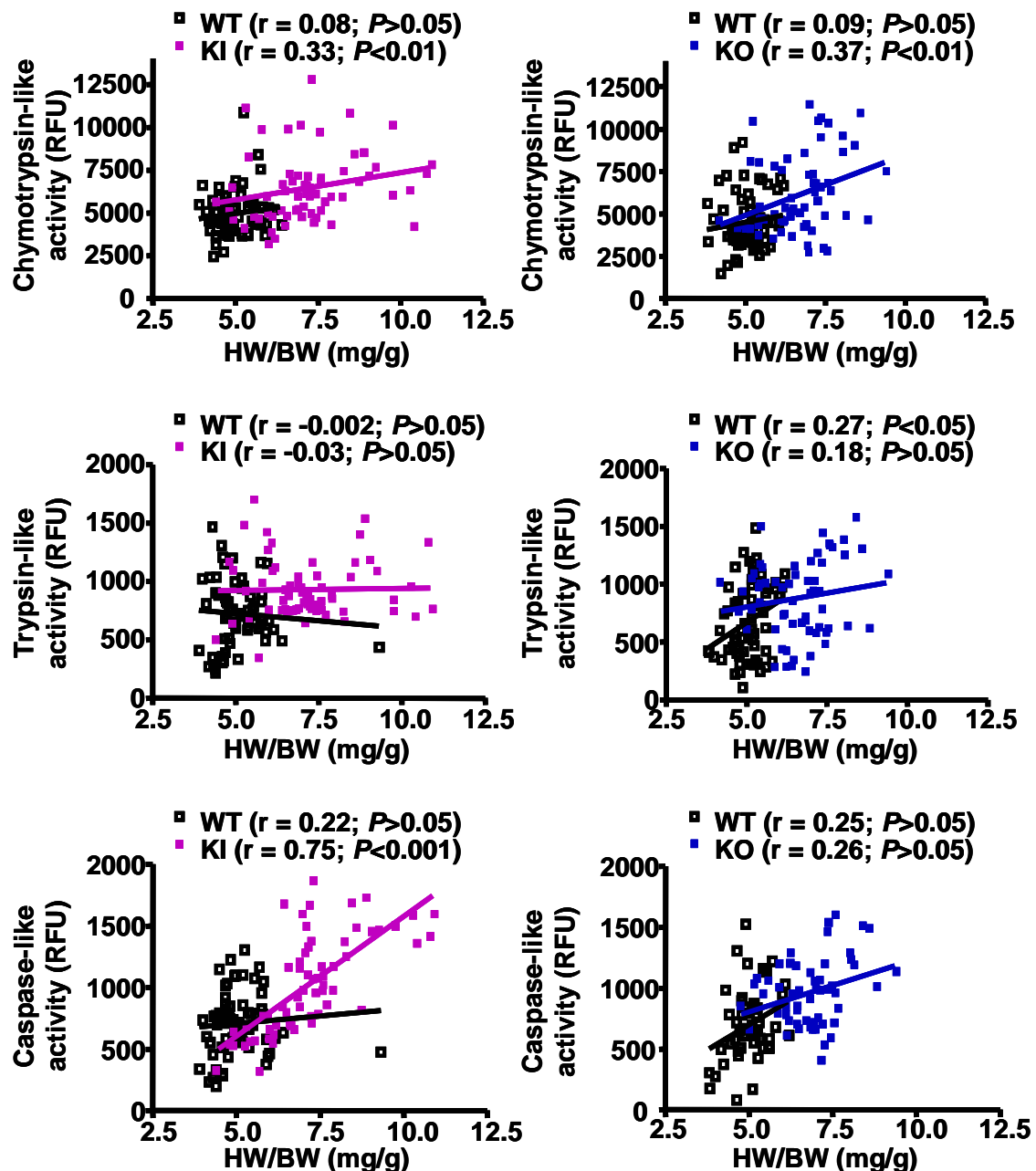


**Figure 3.33: Correlation between the 20S proteasome activities and the degree of hypertrophy in KI and KO mice.** All three 20S proteasome activities were plotted against the HW/BW and checked for correlation using the nonparametric correlation (Spearman =  $r$ ) test.

As expected, no correlation was found between the chymotrypsin-like and caspase-like activities and the HW/BW in the WT mice. Just between the trypsin-like activity and the HW/BW a positive correlation was found in the WT mice (from the KO line), which is not explainable. In both KI and KO mice, the chymotrypsin-like activity was positively correlated to the degree of hypertrophy, i.e. the chymotrypsin-like activity was high, when the HW/BW was high. Only in the KI mice, a positive correlation between the caspase-like activity and the HW/BW was obtained, whereas no



significant correlation between these 2 parameters was found in the KO mice. Between the trypsin-like activity and the degree of hypertrophy, no correlation was found in both KI and KO mice.

Finally, the correlation between the steady-state levels of ubiquitinated proteins and the 20S proteasome activities was evaluated (Fig. 3.34).

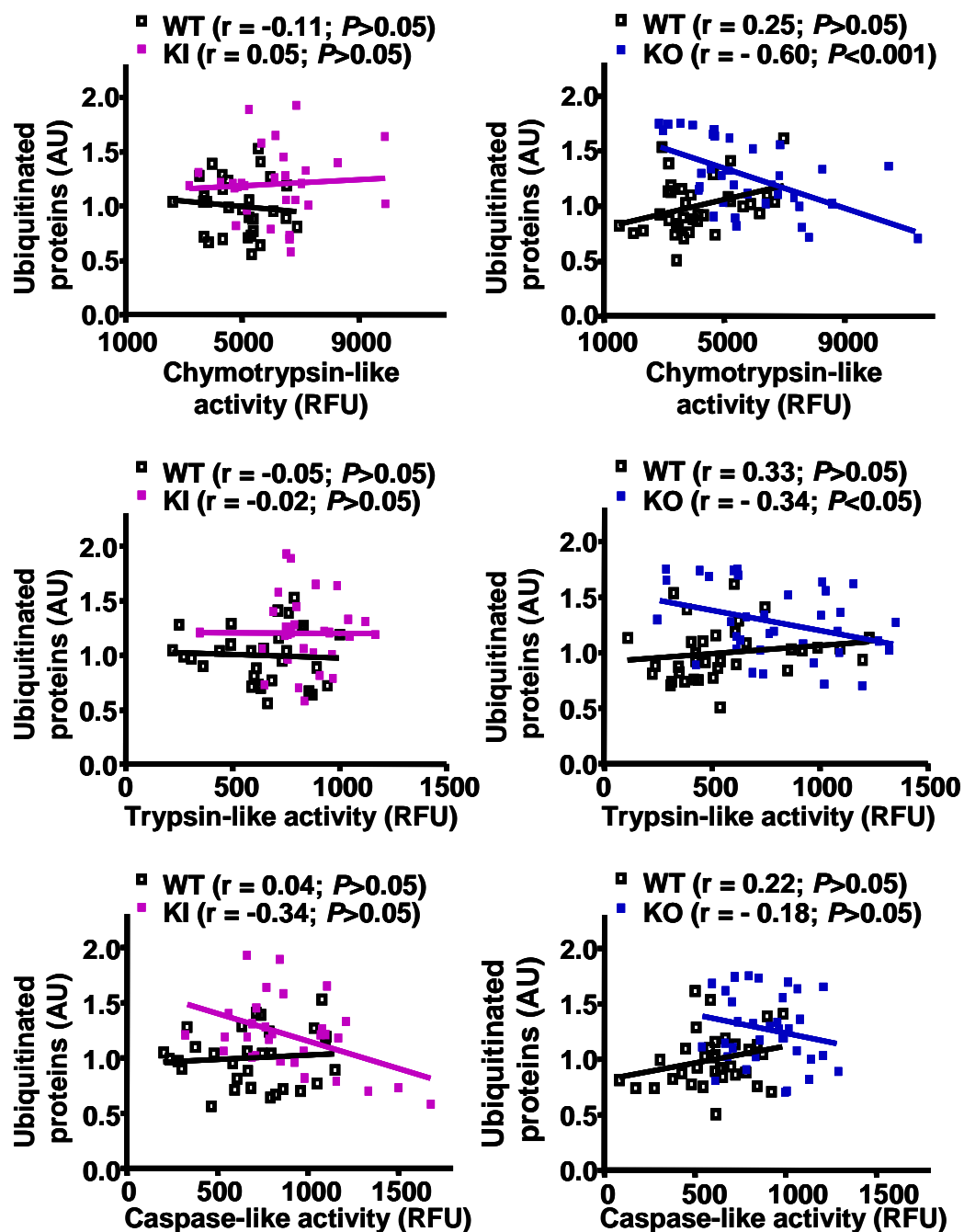


Figure 3.34: Correlation between the steady-state levels of ubiquitinated proteins and the 20S proteasome activities in KI and KO mice. The steady-state level of ubiquitinated proteins was plotted against all three 20S proteasome activities and checked for correlation using the nonparametric correlation (Spearman =  $r$ ) test.

As expected, no correlation was found between the steady-state level of ubiquitinated proteins and all three 20S proteasome activities in the WT mice. Only in the KO mice, the steady-state levels of ubiquitinated proteins correlated inversely with the chymotrypsin-like and the trypsin-like activity, i.e. the steady-state levels of ubiquitinated proteins were low, when the two activities were high or vice versa. No correlation was found in the KI mice concerning these parameters. Between the steady-state levels of ubiquitinated proteins and the caspase-like activity, no correlation was observed in both KI and KO mice.

### 3.3.2 Investigation of the UPS reporter mouse models

Crossing mutant cMyBP-C mice with the so-called UPS reporter mice should provide the opportunity to monitor the UPS function *in vivo*. Two different UPS reporter mice were investigated: the Ub<sup>G76V</sup>-GFP mice (Lindsten et al. 2003; see 2.1.1.4) and the GFPdgn mice (Kumarapeli et al. 2005; see 2.1.1.5). Both mouse models ubiquitously express a modified green fluorescent protein (GFP) that is constitutively targeted for proteasomal degradation. This GFP reporter protein should be degraded at normal UPS function. Administration of proteasome inhibitors should result in a substantial accumulation of GFP, which could be investigated by Western blot or direct fluorescence microscopy. Similarly, an impairment of the UPS by cMyBP-C mutants should also lead to increased GFP levels. First, it was investigated whether the two mouse models were suitable to monitor the UPS function in the heart.

#### 3.3.2.1 Investigation of the Ub<sup>G76V</sup>-GFP mouse model

Genotypes of transgenic Ub<sup>G76V</sup>-GFP and corresponding WT mice were determined by PCR from genomic tail DNA using primers, which were specific for the transgene. PCR products were loaded on a 1% agarose gel (Fig. 3.35).

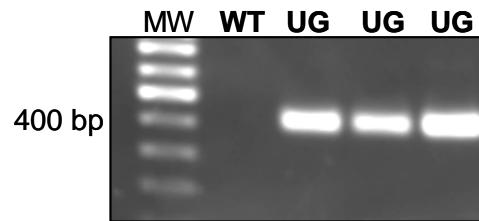


**Figure 3.35: Genotyping of the Ub<sup>G76V</sup>-GFP mouse model by PCR.** PCR was performed on genomic tail DNA from transgenic Ub<sup>G76V</sup>-GFP (UG) and WT mice using transgene-specific primers. MW stands for the 100-bp molecular weight marker.

The expected 400 bp-fragment for the transgene was only amplified in the transgenic Ub<sup>G76V</sup>-GFP mice.

Fibroblasts were isolated from subcutis biopsies of an adult Ub<sup>G76V</sup>-GFP mouse, propagated for several weeks, plated on Lab-Tek™ chamber slides and treated with different proteasome inhibitors for 15 h. The reversible proteasome inhibitor MG132 was used in a concentration of 0.1 μM, 1 μM or 10 μM, the reversible proteasome inhibitor MG262 in a concentration of 1 nM, 10 nM, 100 nM or 1 μM and the irreversible proteasome inhibitor epoxomicin in a concentration of 5 nM, 50 nM, 500 nM or 5 μM. Afterwards, the GFP fluorescence was analyzed by confocal microscopy (Fig. 3.36).

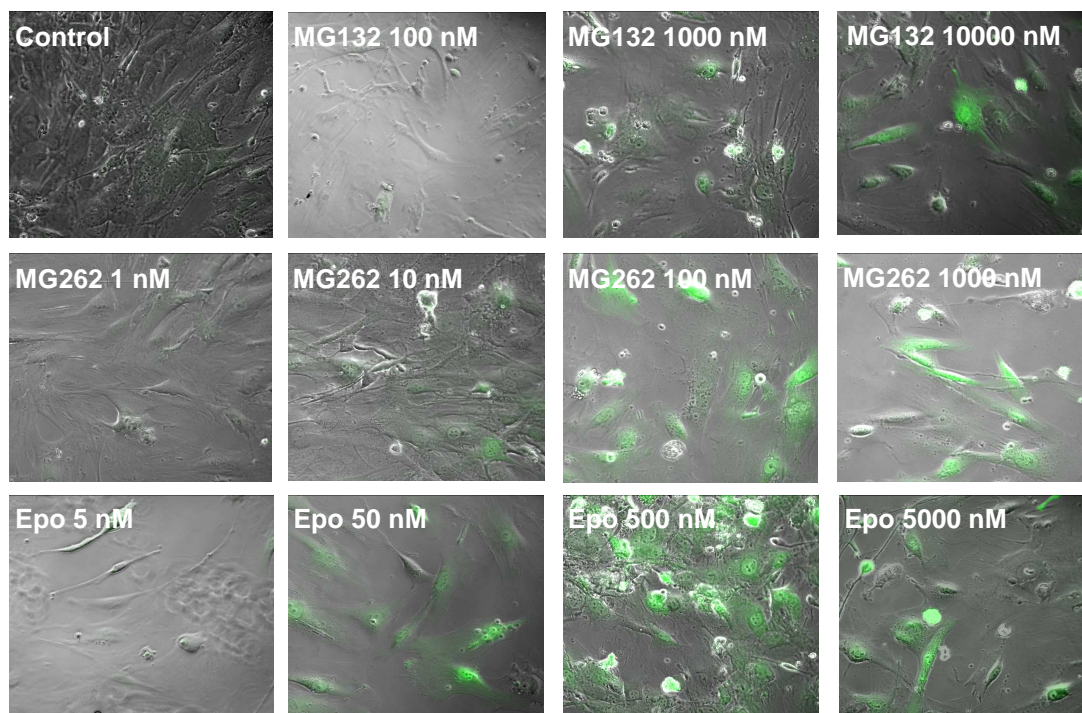


**Figure 3.36: Direct fluorescence micrographs of treated fibroblasts from an adult Ub<sup>G76V</sup>-GFP mouse.** Fibroblasts were untreated (control) or treated with the proteasome inhibitors MG132, MG262 or epoxomicin (epo) in the indicated concentrations. Confocal images were recorded after 15 h treatment with a Zeiss LSM 5 Image system using a Zeiss Axiovert 200 M microscope.

Without proteasome inhibition, no GFP-positive fibroblasts could be found, which proved that the reporter was rapidly degraded by the UPS under normal conditions. In contrast, after proteasome inhibition an increase of GFP-positive fibroblasts was observed in a concentration-dependent manner. This was found with all 3 inhibitors; the inhibition by MG262 and epoxomicin was more potent than by MG132.

To analyze whether proteasome inhibition leads to the same effect in cardiomyocytes, cardiomyocytes were isolated from adult Ub<sup>G76V</sup>-GFP mice, plated on laminin-coated Lab-Tek™ chamber slides and treated with 10 µM MG132, 100 nM MG262 or 500 nM epoxomicin for 20 h. Afterwards, GFP-positive, rod-shaped cardiomyocytes were counted under the confocal microscope (Fig. 3.37).

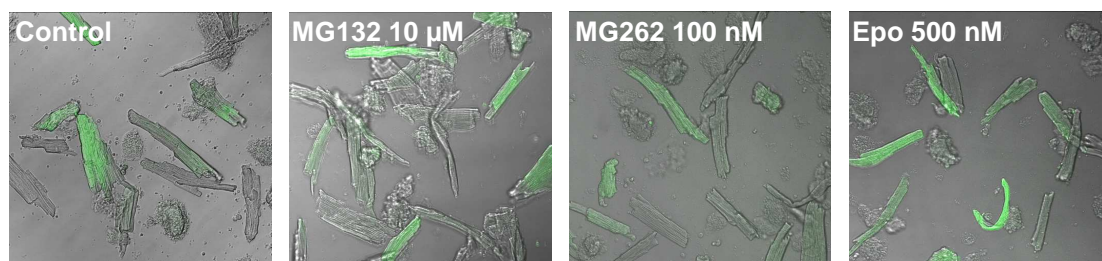


**Figure 3.37: Direct fluorescence micrographs of treated cardiomyocytes from adult Ub<sup>G76V</sup>-GFP mice.** Cardiomyocytes were untreated (control) or treated with the proteasome inhibitors MG132, MG262 or epoxomicin (epo) in the indicated concentrations. Confocal images were recorded after 20 h treatment with a Zeiss LSM 5 Image system using a Zeiss Axiovert 200 M microscope.

GFP-positive cells were found in the untreated cardiomyocytes, and the number of GFP-positive cardiomyocytes did not increase after UPS inhibition. This suggests that the adult cardiomyocytes were exposed to stress during isolation and responded with a stress-induced GFP accumulation already visible without proteasome inhibition.

Finally, 9 µmol/kg MG262, which is a high dose (Lindsten et al., 2003), was injected intraperitoneally (i.p.) into an adult Ub<sup>G76V</sup>-GFP mouse. As a control, a 60% DMSO-NaCl-solution (vehicle) was i.p. injected into a second Ub<sup>G76V</sup>-GFP mouse. Both mice were killed 24 h after injection, and the liver and heart were examined by direct fluorescence microscopy (Fig. 3.38).

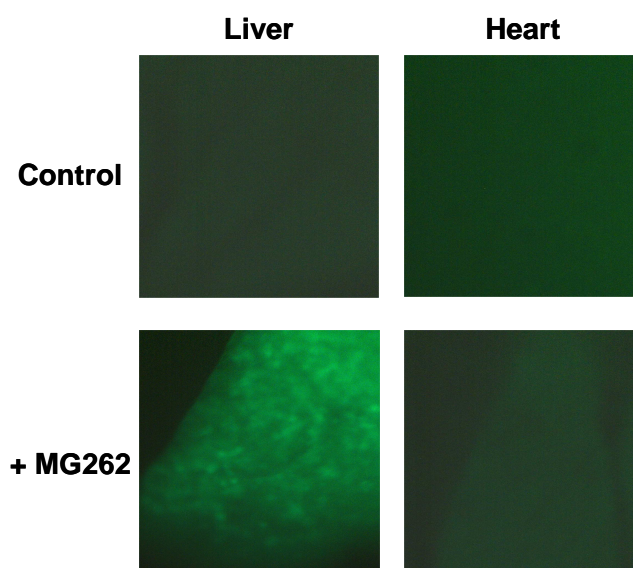


**Figure 3.38: Direct fluorescence micrographs of tissues from treated adult Ub<sup>G76V</sup>-GFP mice.** MG262 (9  $\mu\text{mol/kg}$ ) or vehicle only (60% DMSO-NaCl-solution; control) were injected i.p. into adult Ub<sup>G76V</sup>-GFP mice. Direct fluorescence micrographs were taken from both liver and heart 24 h after injection.

No GFP-fluorescence was detected in the control liver and heart, which indicated that the reporter was rapidly degraded by the UPS. After proteasome inhibition by MG262, a GFP-fluorescence was obtained in the liver, but not in the heart. Moreover, proteins were extracted from the heart and liver of these treated mice and analyzed by Western blot using an antibody directed against ubiquitin (Fig. 3.39).

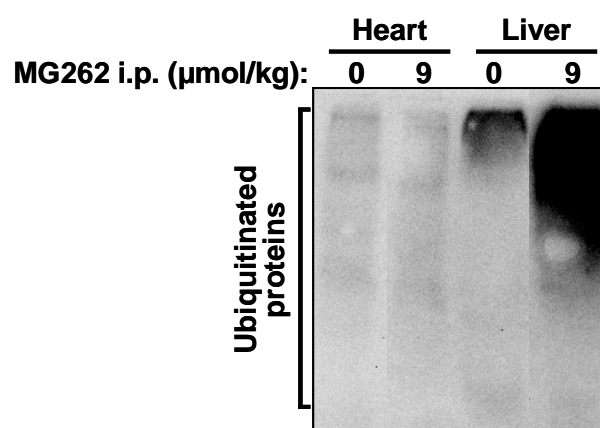


**Figure 3.39: Ubiquitination in treated adult Ub<sup>G76V</sup>-GFP mice.** Proteins were extracted from both heart and liver of adult Ub<sup>G76V</sup>-GFP mice treated i.p. with MG262 (9  $\mu\text{mol/kg}$ ) or vehicle only (60% DMSO-NaCl-solution). The blot was stained with an antibody directed against ubiquitin.

First, the Western blot analysis showed that the steady-state level of ubiquitinated proteins was much higher in the liver than in the heart under normal conditions. Second, no increase in the amount of ubiquitinated proteins was observed in the heart

after treatment. This suggests that the concentration of MG262 that reached the heart after i.p. injection was insufficient to inhibit the proteasome. This would explain why no GFP fluorescence was visualized by fluorescence microscopy in the heart of the MG262-treated Ub<sup>G76V</sup>-GFP mouse. In contrast, a strong increase in the steady-state level of ubiquitinated proteins was revealed in the liver of the MG262-treated mouse compared to the control, which was in line with the strong GFP-accumulation examined by the fluorescence microscopy.

### 3.3.2.2 Investigation of the GFPdgn mouse model

Genotypes of transgenic GFPdgn and corresponding WT mice were determined by PCR from genomic tail DNA using primers, which were specific for the transgene. PCR products were loaded on a 1% agarose gel (Fig. 3.40).

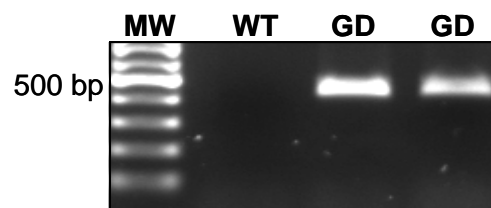


**Figure 3.40: Genotyping of the GFPdgn mouse model by PCR.** PCR was performed on genomic tail DNA from transgenic GFPdgn (GD) and WT mice using transgene-specific primers. MW stands for the 100-bp molecular weight marker.

The expected 500 bp-fragment for the transgene was obtained only in the transgenic GFPdgn mice.

To analyze whether cardiomyocytes from adult GFPdgn mice are useful for *ex vivo* studies of the UPS function, cardiomyocytes were isolated from adult GFPdgn mice, plated on laminin-coated Lab-Tek™ chamber slides and treated with 5 and 10  $\mu$ M MG132. After 15 h incubation, the cells were analyzed by confocal microscopy to check for accumulation of GFP-positive cells after proteasome inhibition (Fig. 3.41).





**Figure 3.41: Direct fluorescence micrographs of treated cardiomyocytes from adult GFPdgn mice.** Cardiomyocytes were untreated (control) or treated with the proteasome inhibitor MG132 in the indicated concentrations. Confocal images were recorded after 15 h treatment with a Zeiss LSM 5 Imager system using a Zeiss Axiovert 200 M microscope.

Like in the cardiomyocytes isolated from the Ub<sup>G76V</sup>-GFP mice, GFP-positive cells were found already in the untreated cardiomyocytes isolated from GFPdgn mice, and the number of GFP-positive cardiomyocytes did not increase after UPS inhibition. This was the second time that adult cardiomyocytes seemed to be stress-sensitive during isolation, and they are therefore maybe not the best tool for treatment with proteasome inhibitors. Thus, the experiment was repeated in cardiomyocytes isolated from neonatal GFPdgn mice, which are less subjected to stress during isolation. The cells were treated with 10  $\mu$ M MG132 for 2, 8 and 24 h, and proteins were extracted and analyzed by Western blot using antibodies directed against ubiquitin and GFP (Fig. 3.42 A). Furthermore, the chymotrypsin-like activity of the 20S proteasome was measured (Fig. 3.42 B).

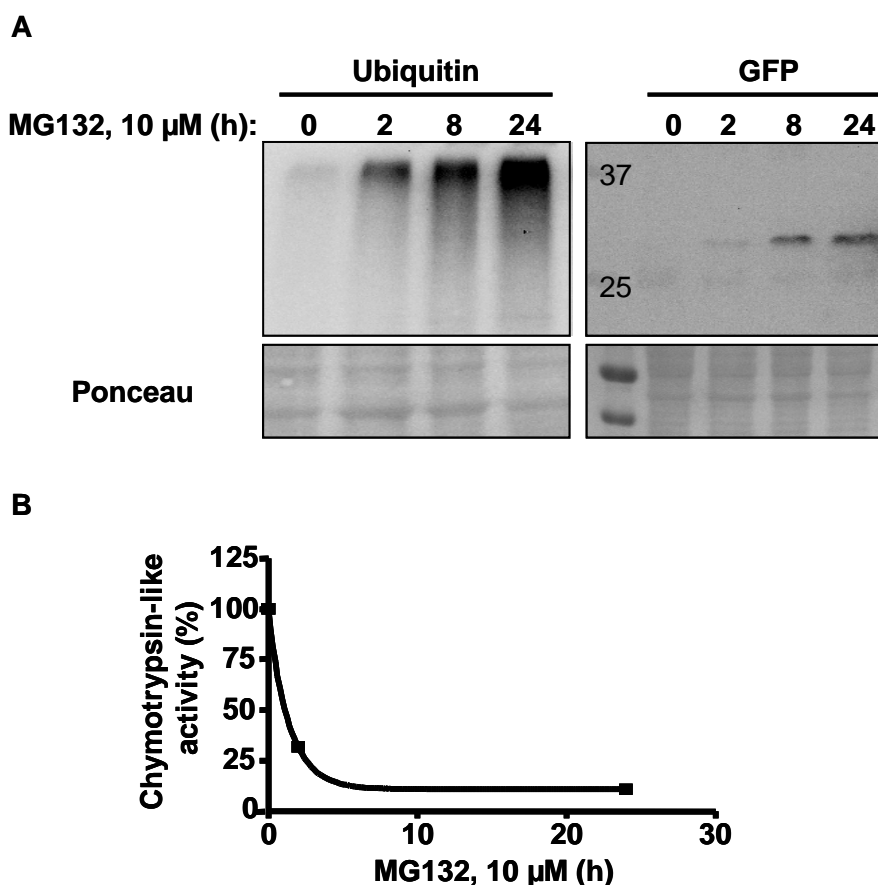


**Figure 3.42: Ubiquitination, GFP-accumulation and chymotrypsin-like activity in cardiomyocytes from neonatal GFPdgn mice.** **A**, Proteins were extracted from cardiomyocytes isolated from neonatal GFPdgn mice and treated with 10  $\mu$ M MG132 for 2, 8 or 24 h. The left blot was stained with an antibody directed against ubiquitin, the right blot with an antibody directed against GFP. The first lane of the right blot represents the molecular weight marker. Below each blot is the corresponding Ponceau. **B**, The chymotrypsin-like activity of the 20S proteasome was measured in a cystolic protein extract from the cardiomyocytes described in A.

Densitometric analysis of the Western blots revealed a 7-fold increase of the steady-state level of ubiquitinated proteins and a 9-fold increase of the GFP level after 24 h-treatment with MG132 compared to control. By measuring the chymotrypsin-like activity, a decrease by 89% after 24 h treatment was obtained vs. control. These data proved that the proteasome was blocked by MG132 and that this inhibition resulted in a GFP accumulation. Therefore, cardiomyocytes isolated from neonatal mice appear to be a useful tool for *ex vivo* investigations of the UPS function.

Finally, it was evaluated whether systemic injection of MG262 inhibited the proteasome *in vivo*. MG262 (5  $\mu$ mol/kg) was intravenously (i.v.) injected into one adult GFPdgn mouse. As a control, a 60% DMSO-NaCl-solution (vehicle) was i.v. injected into a second GFPdgn mouse. Both mice were sacrificed 17 h after injection,



and the heart and liver were excised. Extracted proteins were examined by Western blot using antibodies directed against ubiquitin and GFP (Fig. 3.43).

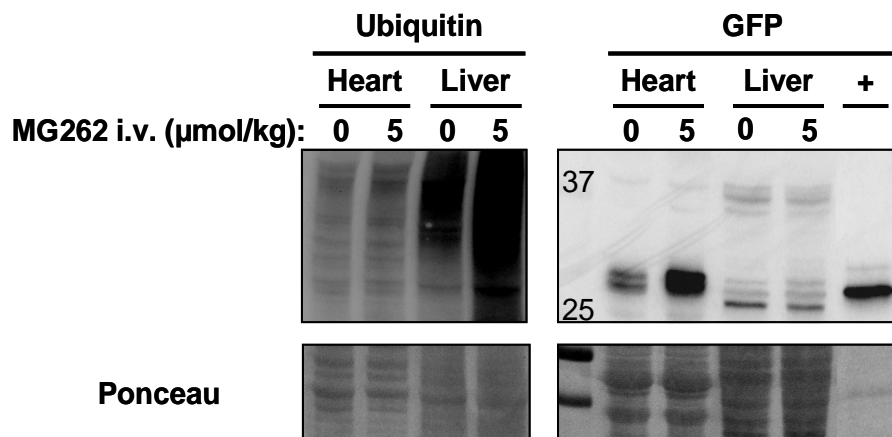


**Figure 3.43: Ubiquitination and GFP-accumulation in tissue from treated adult GFPdgn mice.** Proteins were extracted from both heart and liver of adult GFPdgn mice treated i.v. with MG262 (5 μmol/kg) or vehicle only (60% DMSO-NaCl-solution). The left blot was stained with an antibody directed against ubiquitin, the right blot with an antibody directed against GFP. The first lane of the right blot represents the molecular weight marker. The last lane of the right blot was loaded with proteins extracted from neonatal rat cardiomyocytes infected with a GFP-encoding virus and served as a positive control for GFP. Below each blot is the corresponding Ponceau.

First, this Western blot analysis showed again that the steady-state levels of ubiquitinated proteins are much higher in the liver than in the heart under normal conditions. Second, systemic proteasomal inhibition resulted in increased levels of ubiquitinated proteins and GFP, both in the heart and the liver. Unexpectedly, the GFP-antibody detected several bands around 29 kDa, two bands in the heart samples and even three bands in the liver samples. The reason for this is not known at the moment.

### 3.3.3 Investigation of the UPS function in the KI and KO mice crossed with Ub<sup>G76V</sup>-GFP mice

In chapter 3.3.1.1, an alteration of the UPS at the level of ubiquitination and degradation was found in the KI and KO mice. Using small fluorogenic substrates, which are degraded by the 20S proteasome in an ubiquitination-independent manner, allows detecting alterations in the proteolytic activities, but will fail to detect alterations at any other level of the UPS. An approach, which allows monitoring the

function of the UPS in an ubiquitination-dependent manner and in the whole animal (*in vivo*), was to cross the KI and KO mice with the Ub<sup>G76V</sup>-GFP mice, which express a reporter protein with a tag for efficient degradation by the UPS. To investigate whether an alteration or even an impairment of the UPS by the cMyBP-C mutants was present, the steady-state levels of ubiquitinated proteins and GFP were determined by Western blot and the 20S proteasome activities were measured.

### 3.3.3.1 Investigation of the UPS function in the KI mice crossed with Ub<sup>G76V</sup>-GFP mice

Proteins were extracted from ventricles of very old WT x Ub<sup>G76V</sup>-GFP (age ~ 79 wk, two males and females) and KI x Ub<sup>G76V</sup>-GFP (age ~ 62 wk, four males and females) mice and analyzed by Western blot using an antibody directed against GFP (Fig. 3.44).

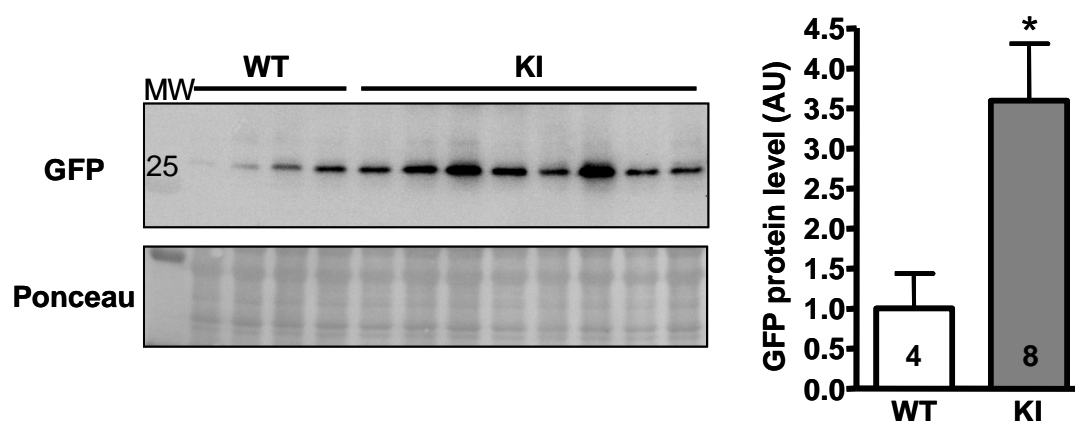


**Figure 3.44: Determination of the GFP level in ventricles of WT and KI mice crossed with Ub<sup>G76V</sup>-GFP mice.** Proteins were extracted from ventricles of WT and KI mice crossed with Ub<sup>G76V</sup>-GFP mice. On the left, a blot stained with an antibody directed against GFP is shown. The first lane represents the molecular weight marker (MW). Below is the corresponding Ponceau. On the right, the quantitative analysis normalized to Ponceau and related to WT is shown. Bars represent the mean±SEM with \**P*<0.05 vs. WT, Student's t-test. The number of animals is indicated in the bars.

A 3.6-fold increase of the GFP level was found in the KI x Ub<sup>G76V</sup>-GFP mice compared to WT indicating an impairment of the UPS. It was then investigated whether the GFP-accumulation was associated with changes in the steady-state levels of ubiquitinated proteins. A blot with the same loading was stained with an antibody directed against ubiquitin (Fig. 3.45).

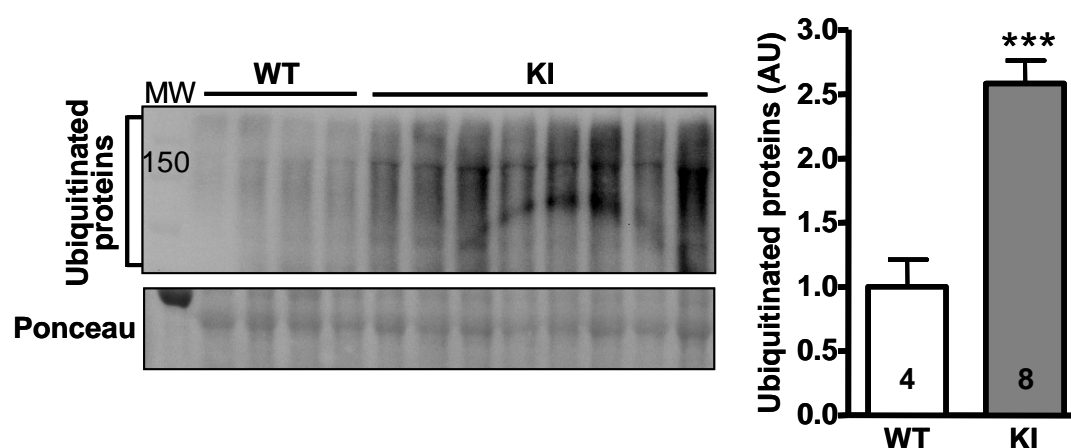


**Figure 3.45: Ubiquitination in ventricles of WT and KI mice crossed with Ub<sup>G76V</sup>-GFP mice.** Proteins were extracted from ventricles of WT and KI mice crossed with Ub<sup>G76V</sup>-GFP mice. On the left, a blot stained with an antibody directed against ubiquitin is shown. The first lane represents the molecular weight marker (MW). Below is the corresponding Ponceau. On the right, the quantitative analysis normalized to Ponceau and related to WT is shown. Bars represent the mean±SEM with \*\*\* $P<0.001$  vs. WT, Student's t-test. The number of animals is indicated in the bars.

The steady-state levels of ubiquitinated proteins were elevated in the KI x Ub<sup>G76V</sup>-GFP mice as compared to WT mice. Quantitative analysis showed a 2.6-fold increase in the amount of ubiquitinated proteins. Thus, the UPS was altered at the ubiquitination level in old KI x Ub<sup>G76V</sup>-GFP mice.

To examine whether there is also an alteration of the UPS at the degradation level in these old mice, all three 20S proteasome activities were measured in the same animals as above (Fig. 3.46).

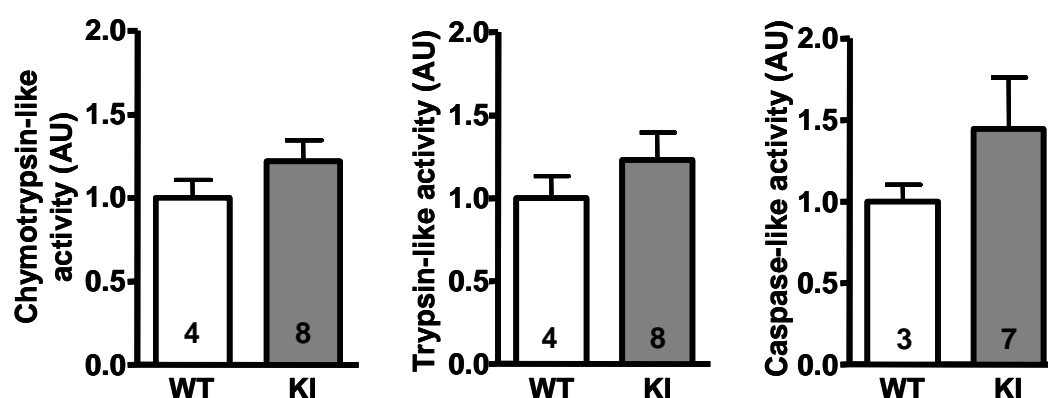


**Figure 3.46: The 20S proteasome activities in ventricles of WT and KI mice crossed with Ub<sup>G76V</sup>-GFP mice.** Proteins were extracted from ventricles of WT and KI mice crossed with Ub<sup>G76V</sup>-GFP mice. The 20S proteasome activities were measured using specific, fluorogenic substrates. Bars represent the mean±SEM. The number of animals is indicated in the bars.

All three 20S proteasome activities had a tendency to be elevated in old KI x Ub<sup>G76V</sup>-GFP vs. WT mice, but the elevations were not significant. Thus, no significant alteration of the UPS was detected at the degradation level in old KI x Ub<sup>G76V</sup>-GFP mice.

### 3.3.3.2 Investigation of the UPS function in the KO mice crossed with Ub<sup>G76V</sup>-GFP mice

Proteins were extracted from very old WT x Ub<sup>G76V</sup>-GFP (age ~ 83 wk, all females) and KO x Ub<sup>G76V</sup>-GFP (age ~ 77 wk, all females) mice and analyzed by Western blot using an antibody directed against GFP (Fig. 3.47).

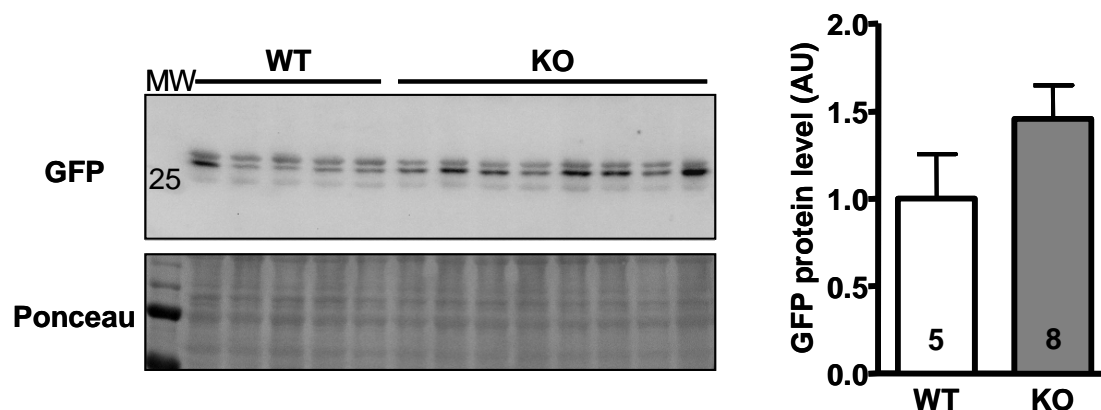


**Figure 3.47: Determination of the GFP level in ventricles of WT and KO mice crossed with Ub<sup>G76V</sup>-GFP mice.** Proteins were extracted from ventricles of WT and KO mice crossed with Ub<sup>G76V</sup>-GFP mice. On the left, a blot stained with an antibody directed against GFP is shown. The first lane represents the molecular weight marker (MW). Below is the corresponding Ponceau. On the right, the quantitative analysis normalized to Ponceau and related to WT is shown. Bars represent the mean ± SEM. The number of animals is indicated in the bars.

The GFP protein level was increased (1.5-fold) in old KO x Ub<sup>G76V</sup>-GFP mice vs. WT mice, but not significantly. As in Fig. 3.43, the GFP-antibody detected unexpectedly two bands around 29 kDa. The reason for this is not known at the moment.

To investigate whether this increase was associated with changes in the steady-state level of ubiquitinated proteins, a blot with the same loading was stained with an antibody directed against ubiquitin (Fig. 3.48).

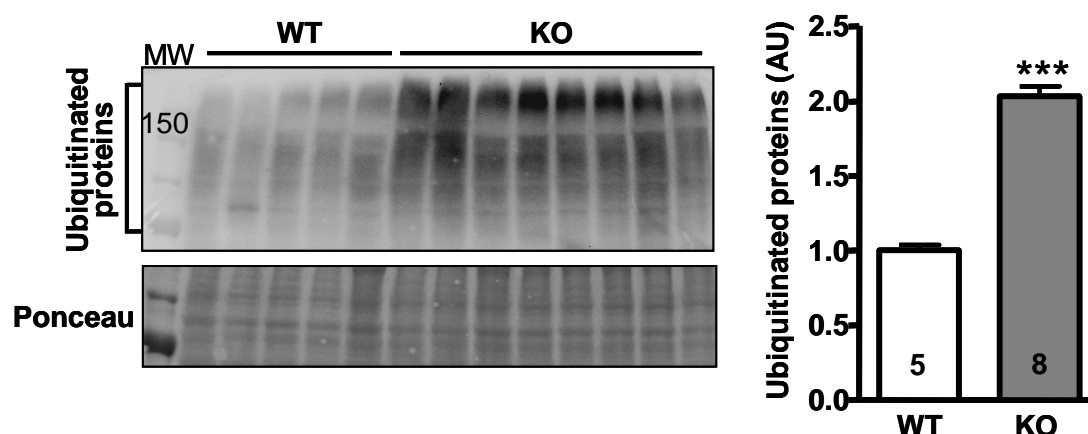


**Figure 3.48: Ubiquitination in ventricles of WT and KO mice crossed with Ub<sup>G76V</sup>-GFP mice.** Proteins were extracted from ventricles of WT and KO mice crossed with Ub<sup>G76V</sup>-GFP mice. On the left, a blot stained with an antibody directed against ubiquitin is shown. The first lane represents the molecular weight marker (MW). Below is the corresponding Ponceau. On the right, the quantitative analysis normalized to Ponceau and related to WT is shown. Bars represent the mean±SEM with \*\*\**P*<0.001 vs. WT, Student's *t*-test. The number of animals is indicated in the bars.

The level of ubiquitinated proteins was 2-fold higher in old KO x Ub<sup>G76V</sup>-GFP mice vs. WT mice. Thus, like in the old KI x Ub<sup>G76V</sup>-GFP mice, the UPS was altered at the ubiquitination level in old KO x Ub<sup>G76V</sup>-GFP mice.

Finally, all three 20S proteasome activities were measured in the same animals as above to analyze whether there is also an alteration of the UPS at the degradation level (Fig. 3.49).

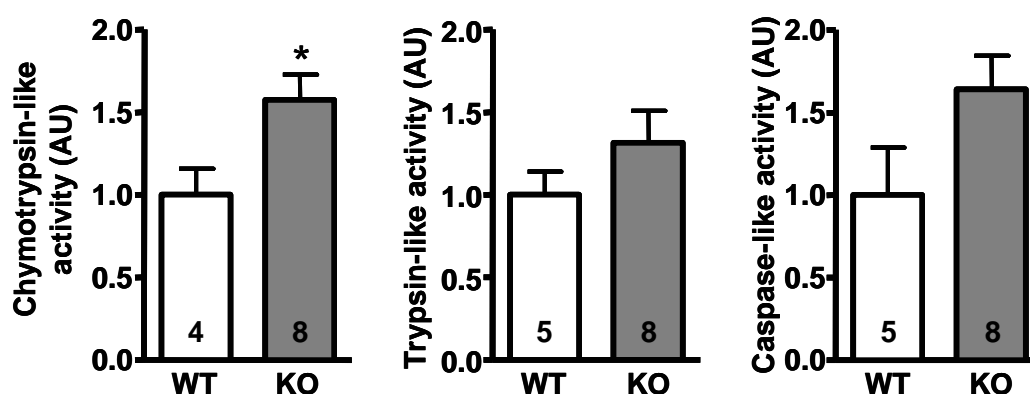


**Figure 3.49: The 20S proteasome activities in ventricles of WT and KO mice crossed with Ub<sup>G76V</sup>-GFP mice.** Proteins were extracted from ventricles of WT and KO mice crossed with Ub<sup>G76V</sup>-GFP mice. The 20S proteasome activities were measured using specific, fluorogenic substrates. Bars represent the mean±SEM with \**P*<0.05 vs. WT, Student's *t*-test. The number of animals is indicated in the bars.

All three 20S proteasome activities tended to be higher in old KO x Ub<sup>G76V</sup>-GFP mice as compared to WT, but only the chymotrypsin-like activity was significantly higher.

### 3.3.4 Summary

The major findings of this chapter are the following:

- The M7t-TG mice did not exhibit alterations in the steady-state level of ubiquitinated proteins or in the 20S proteasome activities, indicating that the UPS function was overall unchanged.
- The KI and KO mice exhibited increased steady-state levels of ubiquitinated proteins and 20S proteasome activities.
- The chymotrypsin-like activity, which is the main 20S proteasome activity, was positively correlated with the degree of hypertrophy in both KI and KO mice. In contrast, the steady-state levels of ubiquitinated proteins did not correlate with the degree of hypertrophy. Thus, one could speculate that the increase in the chymotrypsin-like activity with the increased degree of hypertrophy prevents further increases in the steady-state levels of ubiquitinated proteins. Accordingly, the chymotrypsin-like activity was negatively correlated with the steady-state level of ubiquitinated proteins in the KO mice.
- Crossing of KI and KO mice with UPS reporter mice gave further support for alterations at the level of ubiquitination and degradation in old animals. In old KI and KO mice, the 20S proteasome activities just tended to be higher, whereas the steady-state levels of ubiquitinated proteins were significantly increased. The level of GFP protein was also increased in old KI and KO mice, but only significantly in old KI mice. These data suggests that a likely age-dependent exhaustion of the proteasome may participate in the greater accumulation of ubiquitinated proteins and GFP.

### 3.4 Investigation of the nonsense-mediated mRNA decay

#### 3.4.1 Investigation of the nonsense-mediated mRNA decay in the KI and Het mice

The experiments described in chapter 3.2.2 failed to provide evidence that the level of cMyBP-C mutants is regulated at the protein level in the KI mice. UPS inhibition did neither reveal the truncated protein nor increased the amount of the full-length mutant protein. On the other hand, the 78% decrease in the amount of total cMyBP-C mRNA in the KI mice (3.1.2.3) suggested that a strong regulation for the cMyBP-C mutants existed at the mRNA level. Thus, the nonsense-mediated mRNA decay (NMD; 1.5.1), which is assumed to play a key role in cell quality control by removal of PTC-containing nonsense mRNAs, was investigated in the KI and also in the Het mice, in which the nonsense mRNA was randomly detected. NMD occurs when the PTC is located more than 50-55 nt upstream of the last exon-exon junction (Nagy and Maquat, 1998). In KI and Het mice, the PTC is located in exon 9 within the nonsense mRNA and is therefore more than 55 nt upstream of the last junction between exons 34 and 35. Because NMD requires a pioneer round of translation in mammalian cells, it can be prevented by translation inhibitors like cycloheximide (CHX) or emetine (see 1.5.1). Therefore, cardiomyocytes were isolated from neonatal WT and KI mice, cultured and treated with CHX (100 µg/ml; Fig. 3.50) or emetine (300 µg/ml; Fig. 3.51) for 4 h. After treatment, total RNA was isolated and analyzed by classical and quantitative RT-PCR. The level of total cMyBP-C transcripts was determined by quantitative RT-PCR using the SYBR<sup>®</sup> Green strategy and primers located in exons 2 and 3 of the cMyBP-C cDNA. The level of nonsense mRNA was analyzed by quantitative RT-PCR using primers located in exons 5 and 7 of the cMyBP-C cDNA and a TaqMan<sup>®</sup> probe, which matches the junction between exons 5 and 7 and is therefore specific for the nonsense mRNA. The level of missense mRNA was determined by quantitative RT-PCR using primers located in exons 6 and 7 of the cMyBP-C cDNA and a specific TaqMan<sup>®</sup> probe located at the junction between exons 6 and 7 matching the G>A transition.

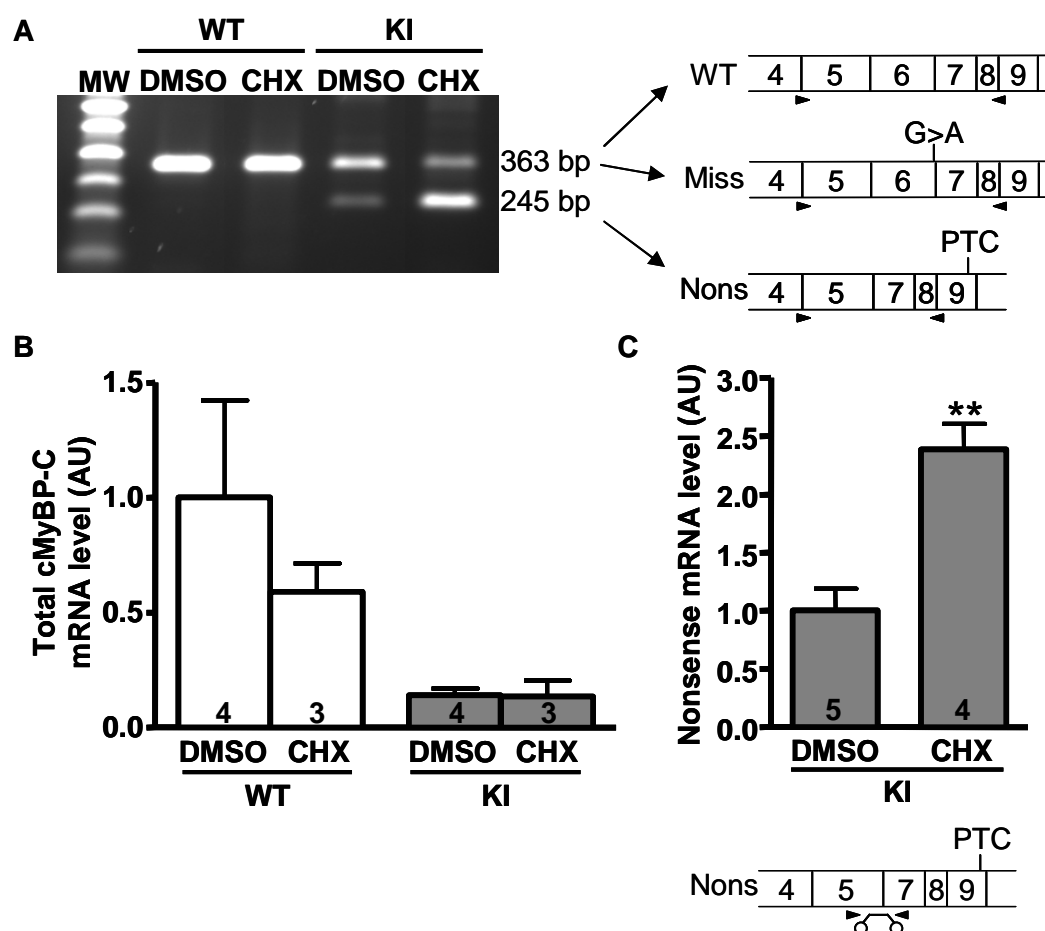


**Fig. 3.50: Effect of NMD inhibition by CHX on the mRNA level in cardiomyocytes of neonatal WT and KI mice.** Cardiomyocytes were isolated from neonatal WT and KI mice, cultured and treated with CHX (100  $\mu$ g/ml) or 0.1% DMSO for 4 h. **A**, The different cMyBP-C mRNA species were determined by classical RT-PCR using primers (black arrows) as indicated in the scheme on the right (miss means missense mRNA and nons nonsense mRNA). MW stands for the 100-bp molecular weight marker. **B**, The level of total cMyBP-C mRNA was determined by quantitative RT-PCR using the SYBR<sup>®</sup> Green strategy and primers located in exons 2 and 3. **C**, The level of nonsense mRNA was determined by quantitative RT-PCR using primers (black arrows) and probe as indicated in the scheme below. Bars represent the mean $\pm$ SEM with \*\* $P$ <0.01 vs. DMSO-treated cells, Student's t-test. The number of preparations is indicated in the bars. These analyses were performed by Nicolas Vignier.

The basal level of total cMyBP-C transcripts was  $\sim$  80% lower in KI than in WT cardiomyocytes (Fig. 3.50 A and B), which was comparable to the data obtained in adult hearts (Fig. 3.13). CHX treatment did not significantly affect the level of total cMyBP-C mRNA in both WT and KI cardiomyocytes (Fig. 3.50 A and B), but increased the amount of the nonsense mRNA 2.5-fold in KI cells (Fig. 3.50 C).



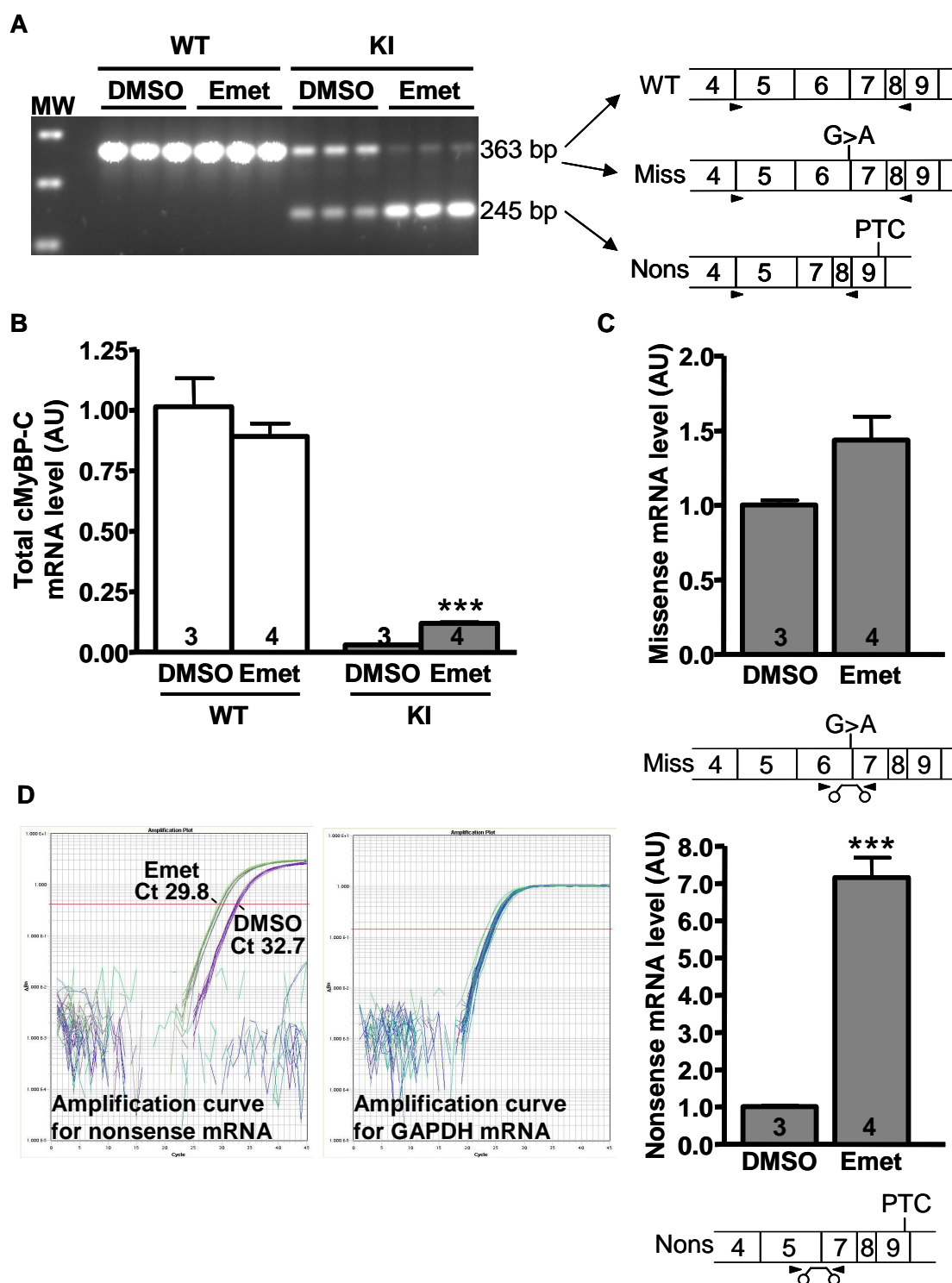


**Fig. 3.51: Effect of NMD inhibition by emetine on the mRNA level in cardiomyocytes of neonatal WT and KI mice.** Cardiomyocytes were isolated from neonatal WT and KI mice, cultured and treated with emetine (300  $\mu\text{g/ml}$ ; emet) or 0.1% DMSO for 4 h. **A**, The different cMyBP-C mRNA species were determined by classical RT-PCR using primers (black arrows) as indicated in the scheme (miss means missense and nons nonsense mRNA). MW stands for the 100-bp molecular weight marker. **B**, The level of total cMyBP-C mRNA was determined by quantitative RT-PCR using the SYBR<sup>®</sup> Green strategy and primers located in exons 2 and 3. **C**, The level of missense mRNA was determined by quantitative RT-PCR using primers (black arrows) and probe as indicated in the scheme. **D**, The level of nonsense mRNA was determined by quantitative RT-PCR using primers (black arrows) and probe as indicated in the scheme. On the left, amplification curves of nonsense and GAPDH mRNA are shown. On the right, the statistical analysis is presented. Bars represent the mean $\pm$ SEM with \*\*\* $P$ <0.01 vs. DMSO-treated cells, Student's t-test. The number of preparations is indicated in the bars.

Emetine did not change the level of total cMyBP-C mRNA in WT cells, but increased the level of total cMyBP-C transcripts 4-fold in KI cells (Fig. 3.51 A and B). Quantitative analysis of the nonsense mRNA level in KI cells revealed a 7-fold increase after treatment with emetine as compared to DMSO (Fig. 3.51 D), whereas the missense mRNA level was not significantly changed after treatment (Fig. 3.51 C). Both CHX and emetine treatment seemed to decrease the missense mRNA level as determined by the classical RT-PCR (Fig. 3.50 A and Fig. 3.51 A). However, this effect was likely due to a competition in the PCR reaction, because the specific TaqMan<sup>®</sup> assay showed that emetine rather increased the missense mRNA level than decreased it (Fig. 3.51 C).

To analyze whether NMD is also involved in the degradation of the nonsense mRNA *in vivo*, CHX (120 mg/kg) or DMSO were 4 times (once per hour) subcutaneously injected in 3 WT, Het and KI mice. The animals were sacrificed 30 min after the last injection. Total RNA was isolated from the ventricles and analyzed by qualitative and quantitative RT-PCR (Fig. 3.52).

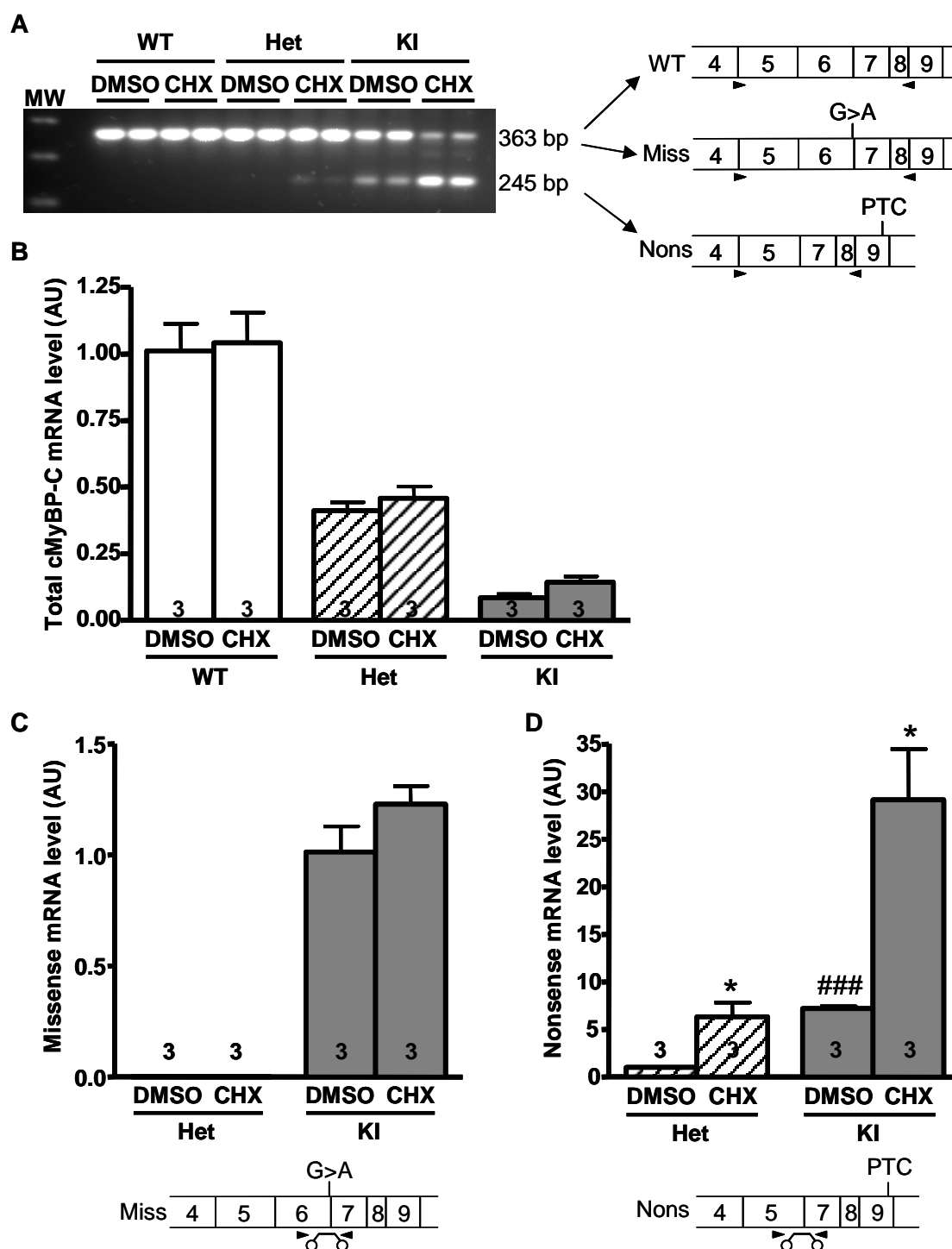


**Fig. 3.52: Effect of NMD inhibition on the mRNA level in ventricles of CHX-treated WT, Het and KI mice.** WT, Het and KI mice were subcutaneously injected with CHX (120 mg/kg, 4 times, once a hour) or 60% DMSO-NaCl-solution. Total ventricular RNA was then isolated. **A**, The different cMyBP-C mRNA species were determined by nested classical RT-PCR using primers (black arrows) as indicated in the scheme on the right (miss means missense mRNA and nons nonsense mRNA). MW stands for the 100-bp molecular weight marker. **B**, The level of total cMyBP-C mRNA was determined by quantitative RT-PCR using the SYBR<sup>®</sup> Green strategy and primers located in exons 2 and 3. **C**, The level of missense mRNA was determined by quantitative RT-PCR using primers (black arrows) and probe as indicated in the scheme below. **D**, The level of nonsense mRNA was determined by quantitative RT-PCR using primers (black arrows) and probe as indicated in the scheme below. Bars represent the mean $\pm$ SEM with \* $P$ <0.05 vs. DMSO-treated mice and ### $P$ <0.001 vs. DMSO-treated Het mice, Student's t-test. The number of animals is indicated in the bars.

*In vivo* treatment with CHX did not significantly affect the level of total cMyBP-C transcripts in the WT and Het mice, but induced a tendency towards an increase ( $P=0.09$ ) in the KI mice (Fig. 3.52 A and B). Quantitative analysis of the nonsense mRNA level revealed a 4-fold increase in the KI and a 6-fold increase in the Het mice after treatment with CHX as compared to the DMSO-treated mice (Fig. 3.52 D). Like in cells, the level of the missense mRNA was not changed by CHX in the KI (Fig. 3.52 C). Surprisingly, the missense mRNA was not detectable in the Het mice by TaqMan<sup>®</sup> analysis, which would suggest that its level was very low compared to the WT mRNA (Fig. 3.52 C).

### 3.4.2 Summary

The major findings of this chapter are the following:

- NMD inhibition stabilized the nonsense mRNA level in cells and *in vivo*.
- The missense mRNA level was not changed by the treatment with NMD inhibitors.

Thus, these data suggest that the low level of nonsense mRNA in cells and *in vivo* is attributed to NMD in KI and Het mice.

## 4 Discussion

The goal of this thesis was to investigate molecular mechanisms regulating the expression of cMyBP-C mutants in FHC. Only two papers have analyzed so far the consequences of cMyBP-C mutations in FHC-patients, and in both cases the truncated cMyBP-C proteins were not detected although the aberrant mRNAs were present (Rottbauer et al., 1997; Moolman et al., 2000). It has been recently shown by adenoviral gene transfer of human mutant cDNAs in rat cardiomyocytes that truncated cMyBP-C proteins were rapidly and quantitatively degraded by the UPS, which was associated with an impairment of the proteolytic capacity of the UPS (Sarikas et al., 2005). In addition, it was proposed that this impairment leads or contributes subsequently to cardiac hypertrophy. The main question studied in this thesis was whether truncated cMyBP-C proteins are also subject to degradation by the UPS *in vivo* and whether this alters the function of the UPS. The analyses were performed in two new targeted cMyBP-C mouse models: the M7t mouse model and the cMyBP-C knock-in mouse model.

The transgenic M7t mouse model was generated to specifically express in the heart a human truncated cMyBP-C. The Myc-M7t-cMyBP-C is deleted of exon 6 leading to a premature termination codon in exon 9. The plasmid, which contains the sequence for this transgene, was already used before by Sarikas et al. (2005) to create the recombinant adenovirus expressing the Myc-M7t-cMyBP-C. Thus, the M7t mouse model represents the appropriate *in vivo* model with regard to the *ex vivo* experiments from Sarikas et al. (2005). But the transgenic M7t mouse model is of limited value for directly comparing the consequences of FHC-causing mutations, because it is not exactly mimicking the situation found in humans. FHC-patients are heterozygous for the mutation, whereas the M7t-TG mice express the transgene in addition to two healthy alleles. Therefore, to investigate the molecular mechanisms of FHC in a genomic context as close to the human situation as possible, the cMyBP-C knock-in mouse model was developed. This mouse model was generated by targeted knock-in of the G>A transition on the last nucleotide of exon 6 and was expected to express the missense and/or nonsense mRNA and the corresponding proteins.

The expected 32-kDa truncated protein in both the M7t and the cMyBP-C knock-in mouse model is not only lacking the titin and myosin binding sites but also the MyBP-C motif, which contains the myosin subfragment 2 binding site and the three phosphorylation sites. Previous interaction studies have shown that small cMyBP-C mutants do not interact with  $\beta$ -MHC and suggested that in particular the C-terminal domains are important for the correct localization of cMyBP-C in the sarcomere (Gruen and Gautel, 1999; Flavigny et al., 2003). Thus, it was assumed that due to its structural and functional deficits the truncated protein would be rapidly recognized and degraded by the UPS in both the M7t and the cMyBP-C knock-in mouse model.

The fundamental assumptions for the M7t mouse model were the following: i) the truncated protein is not or at a low level present under normal conditions due to its rapid degradation by the UPS, ii) the truncated protein is detectable after UPS inhibition, iii) impairment of the UPS occurs late in life and iv) cardiac hypertrophy occurs late in life, possibly due to an impairment of the UPS.

The fundamental assumptions for the cMyBP-C knock-in mouse model were the following: i) the missense as well as the nonsense (exon 6 skipped) mRNAs are expressed, ii) the full-length E256K protein is present, but the truncated protein not or only at a low level due to its rapid degradation by the UPS, iii) inhibition of the UPS results in the detection of the truncated protein, iv) impairment of the UPS occurs early in life in the KI and later in the Het mice and v) cardiac hypertrophy occurs early in life in the KI and later in the Het mice.

**Hypothesis 1: Truncated cMyBP-C proteins are rapidly and quantitatively degraded by the UPS.**

In the M7t-TG mice, the truncated protein was detected neither by Western blot nor by immunofluorescence analysis, despite the presence of the transgene at mRNA level. In the same way, the truncated protein was not detected in both the Het and KI mice. These findings support the data obtained by adenoviral gene transfer of the Myc-M7t-cMyBP-C cDNA in cardiomyocytes (Sarikas et al., 2005) and in human myocardial tissue of FHC-patients with other frameshift mutations (Rottbauer et al., 1997;

Moolman et al., 2000), in which the truncated cMyBP-C proteins were hardly or not detected. Similar observations were also made in a transgenic mouse model expressing a mutant cMyBP-C lacking the myosin binding site (MyBP-C.mut2-mice; (Yang et al., 1999). Despite high expression levels of the transgene at the mRNA level (1.5- to 5-fold of endogenous cMyBP-C), the level of the truncated MyBP-C.mut2 protein was very low.

In the Het and KI mice, a strong regulation of the cMyBP-C mutant levels was observed already at the transcriptional level. The level of total cMyBP-C transcripts was reduced by 52% and 78% in the Het and KI mice, respectively, compared to WT. The level of nonsense mRNA was calculated to be ~7% ( $\frac{1}{3}$  of 22%) in the KI mice and therefore only low level of truncated protein could result. Similar levels of mutant cMyBP-C transcripts as in the KI and Het mice were obtained in mice bearing a neomycin resistance gene inserted in exon 30 of the *MYBPC3* gene (McConnell et al., 1999; McConnell et al., 2001). The insertion resulted in the skipping of exon 30 and the production of a PTC. The level of cMyBP-C transcripts was reduced by 50% and ~86% in heterozygous cMyBP-C<sup>t/+</sup> (expressing mutant and WT mRNA) and homozygous cMyBP-C<sup>t/t</sup> (expressing only mutant mRNA) mice, respectively. In contrast to the KI mice, the truncated (only 15 kDa smaller than full-length) protein was detected in myofilament extracts in homozygous cMyBP-C<sup>t/t</sup> mice and represented 9.5% of the cMyBP-C amount found in WT mice (McConnell et al., 1999). Interestingly, truncated cMyBP-C in total protein homogenates of cMyBP-C<sup>t/t</sup> mice was only 2.3% of the amount found in analogous WT extracts. Thus, myofilament protein preparations should be analyzed in the KI mice to increase the sensitivity and detect the truncated protein. But probably even this approach will fail to detect the truncated protein in the KI mice. Since ~14% mutant transcripts lead to ~10% truncated protein in myofilament extracts of cMyBP-C<sup>t/t</sup> mice, the ~7% nonsense mRNA in the KI mice are expected to result in ~5% truncated protein in myofilament extracts or even less, because it has also to be considered that the truncated protein in the cMyBP-C<sup>t/t</sup> mice is only 15 kDa smaller than the WT protein and therefore expected to be more stable and functional than the truncated protein resulting from the nonsense mRNA in the KI mice. In the Het mice, it will be even more difficult to detect the truncated protein, because the nonsense mRNA is even less expressed than in the KI mice.

Taken together, both the data in the M7t and cMyBP-C knock-in mouse models are compatible with the notion that truncated cMyBP-C proteins are rapidly degraded by the UPS.

To analyze directly whether the UPS was indeed involved in the degradation of the truncated protein, NMCM of M7t-TG and KI mice were isolated and treated with a reversible or an irreversible proteasome inhibitor. It was expected that the proteasome inhibition resulted in the accumulation and detection of the truncated protein. But in contrast to the study of Sarikas et al. (2005), this was not the case, despite the proof for proteasome inhibition by the accumulation of ubiquitinated proteins. Thus, these data failed to show evidence for a major UPS involvement in the degradation of truncated proteins *ex vivo*.

The discrepancy to the cell culture data is maybe explainable by several facts. First, it has to be noted that by adenoviral gene transfer in cardiomyocytes markedly higher levels of mutant mRNAs are reachable than in transgenic mice for two reasons. First, the CMV promoter is stronger than the  $\alpha$ -MHC promoter used for the M7t-TG mice or the endogenous cMyBP-C promoter. Second, adenoviral infection leads to several copies of adeno-genomes in the infected cells. This becomes also clear by the fact that the truncated proteins were detectable by Western blot in the adenovirally transfected cardiomyocytes already without proteasome inhibition (Sarikas et al., 2005). In the M7t-TG mice, the level of mutant mRNA was quite low when compared to the adenoviral approach or even to the similar transgenic MyBP-C.mut2-mice. Related to the considerations from above, it is not really surprising that the proteasome inhibition in KI NMCM did not reveal the truncated protein in total protein extracts, because even with proteasome inhibition the level of this protein was likely very low. A second point is that the conditions, in which the experiments were performed, are maybe not yet fully matured. For instance, the Western blot analysis was performed on Triton X-100-extracts isolated from treated NMCM. In an attempt to increase sensitivity, it could be helpful to analyze rather myofilament protein preparations like it was done by McConnell et al. (1999) for the cMyBP-C<sup>t/t</sup> mice and by Yang et al. (1999) for the MyBP-C.mut2-mice. In addition, protein fractions from nuclear extract and nuclear pellet should be analyzed, because a previous study showed that proteasome inhibition could lead to translocation of proteins into specific subnuclear



compartments (Sano et al., 2007). A third point, especially for the M7t-TG mice, is that cardiomyocytes derived from neonatal mice may not be the optimal model to study the involvement of the UPS. According to preliminary experiments with a number of transgenic constructs, the group around Jeffrey Robbins found that 1-2 mo is the earliest age, at which the maximal amount of transgenic protein is present in the hearts (Yang et al., 1998). Thus, low expression levels will have further decreased the sensitivity of the experiments performed in the neonatal M7t-Tg mice.

In contrast to the truncated protein, the full-length protein was detected in total protein extracts of M7t-TG, Het and KI mice. The level of endogenous cMyBP-C protein was not changed in the M7t-TG vs. WT mice, which was in line with the data obtained for the MyBP-C.mut2-mice (Yang et al., 1999). In the Het (expressing wild-type and E256K protein) and KI (expressing only E256K protein) mice, the level of full-length cMyBP-C protein was reduced by 21% and 90%, respectively, compared to WT. Thus, the estimated ~15% ( $\frac{2}{3}$  of 22%) missense mRNA resulted in 10% full-length mutant protein in total protein extracts of KI mice. In myofilament protein preparations, the level of the E256K protein would be probably even higher. The E256K protein only differs from the WT through one amino acid and therefore this protein is likely near-normal and has not to be degraded by the proteasome.

In conclusion, these data failed to provide direct evidence that the UPS is involved in the degradation of truncated cMyBP-C proteins, but they also did not provide evidence against it. The results could indicate that the UPS only plays a role, when the cell is overwhelmed with mutant cMyBP-C proteins as it was the case for the adenoviral infection. Actually, the UPS remains the most likely involved system and the performed analyses were just not sensitive enough to detect the truncated proteins.

**Hypothesis 2: The degradation of the truncated proteins by the UPS is associated with an impairment of this system.**

Although the data failed to show evidence for an UPS involvement in the degradation of the truncated protein, the UPS function was investigated in M7t-TG and KI mice to analyze whether the UPS was altered by the presence of the truncated protein. In the

M7t-TG mice, the UPS function was neither altered at the ubiquitination nor at the degradation level. Thus, there was a discrepancy between these *in vivo* data and the *ex vivo* data of Sarikas et al. (2005), who showed that the UPS function was impaired by the truncated proteins. The discrepancy is likely again based on the strong difference of the transgene expression at the mRNA level. By adenoviral gene transfer huge amounts of mutant mRNA are reached that are translated in truncated proteins, which in turn have to be degraded by the UPS. It is well conceivable that this finally leads to exhaustion of this system and to accumulation and aggregate formation of the truncated proteins. In contrast, there is a relatively low expression of the mutant mRNA in the M7t-TG mice, and the UPS is apparently able to get completely rid of the nascent truncated proteins. By measuring the chymotrypsin-like activity in 9-month-old M7t-TG mice a slight, but not significant increase was found vs. WT mice. This could be a sign that there are indeed more proteins to be degraded in the M7t-TG mice, namely the truncated ones, and this induces a compensatory increase in the proteasome activity.

In KI mice, the UPS function was investigated from birth to 50 wk of age in myocardial tissue. In the same way, KO mice, which served as a “negative control” for cMyBP-C, were examined to analyze whether a potential UPS alteration is cMyBP-C-dependent. The data provided evidence that the UPS was indeed altered at the level of ubiquitination and degradation in both KI and KO mice. Several aspects have to be pointed out. First, the proteolytic activities of the UPS were not impaired; in contrast, all three activities were significantly increased up to the age of 50 wk. It was originally expected that the truncated protein in the KI and Het mice is rapidly and quantitatively degraded by the UPS, which in turn was expected to be associated with an impairment of this system. But due to the strong regulation already at the transcriptional level, only very low levels of truncated protein are being produced in these mice. These low levels are likely not in a position to impair the proteasome. However, the degradation pathway was activated in both KI and KO mice. Previous studies showed both an increase (Depre et al., 2006) and a decrease (Tsukamoto et al., 2006) in proteasome activity during cardiac hypertrophy in animal models, as well as increases in gene expression of proteins regulating the UPS (Razeghi et al., 2006).

Why, despite increased proteasome activities, the steady-state levels of ubiquitinated proteins were still elevated in both KI and KO mice remains elusive. Using small fluorogenic substrates, which are degraded by the 20S proteasome in a ubiquitination-independent manner, allows to detect alterations in the proteolytic activities, but will fail to detect alterations at any other level of the UPS such as availability of free ubiquitin, polyubiquitination and recognition by the 19S subunit, which is responsible for the deubiquitination, unfolding and channeling of the targeted proteins into the 20S core. For instance, the unfolding and channeling requires ATP. Thus, if an excessive demand on the UPS proceeds with energy depletion, there is not enough ATP for this step. Actually, HCM is known to be associated with myocardial energy depletion: It was proposed that sarcomeric HCM mutations lead to an increased energy demand owing to inefficient sarcomeric ATP utilization. This increased demand compromises the capacity of the cardiomyocyte to maintain free energy levels sufficient for contraction and critical homeostatic functions like the  $\text{Ca}^{2+}$  re-uptake (Ashrafian et al., 2003). In a mouse model of intrasarcoplasmic amyloidosis, which develops concentric cardiac hypertrophy with diastolic malfunction, ubiquitinated proteins were progressively increased, whereby all three proteasomal activities were significantly elevated like in the KI and KO mice (Chen et al., 2005). The cause of proteasomal malfunction was an insufficient delivery of substrate proteins into the 20S proteasome and depletion of key components of the 19S subunit. Furthermore, in explanted hearts from patients with idiopathic dilated cardiomyopathy, a downregulation of the deubiquitinating enzymes isopeptidase-T and ubiquitin-fusion degradation system-1 (UFD-1) has been observed, which in conjunction with unchanged proteasomal subunit levels and proteasomal activity resulted in massive storage of ubiquitinated proteins and in autophagic cell death (Kostin et al., 2003). They conclude that a disturbed balance between a high rate of ubiquitination and inadequate degradation of ubiquitinated proteins may contribute to autophagic cell death. Preliminary determination of the ubiquitin carboxyl-terminal hydrolase L1 (UCHL-1), a deubiquitinating enzyme, revealed a tendency to a decrease at transcriptional level in 9 wk-old KI mice, but further analyses are needed. However, accumulation of ubiquitinated proteins is a very common phenomenon in human hearts with dilated or ischemic cardiomyopathies (Kostin et al., 2003; Weekes et al., 2003) and in other diseases, such as neurodegenerative disorders (Ciechanover and Brundin, 2003), cystic fibrosis or metabolic disorders (Golab et al., 2004). In addition,

increased ubiquitin gene expression was obtained in dilated and ischemic human failing hearts (Yang et al., 2000).

An approach, which allowed to monitor the degradation by the UPS in an ubiquitination-dependent manner, was the crossbreeding between the KI and KO mice and the Ub<sup>G76V</sup>-GFP mice, which express a reporter protein with a tag for efficient degradation by the UPS. As expected from the previous data, the steady-state levels of ubiquitinated proteins were strongly increased in both the old KI (79 wk) and KO (83 wk) mice crossed with Ub<sup>G76V</sup>-GFP mice compared to corresponding WT mice. Only the chymotrypsin-like activity was still significantly elevated in the KO x Ub<sup>G76V</sup>-GFP mice, whereas the two other activities and in the KI x Ub<sup>G76V</sup>-GFP mice all three activities showed just a tendency to be elevated compared to corresponding WT mice. It should be noted that the age of the examined crossed mice was much higher than 50 wk, which represented the last investigated time point from the previous study above. Thus, the fact that the proteolytic activities were not highly elevated anymore could indicate that the 20S proteasome is not anymore able to compensate for increased demand in old age. It was reported that the proteasome activity is declining with age and that the loss in proteasome activity during aging depends at least on three different mechanisms: decreased overall proteasome content, alterations and/or replacement of proteasome subunits and formation of inhibitory cross-linked proteins (Carrard et al., 2002).

Examination of KI and KO mouse lines crossed with the Ub<sup>G76V</sup>-GFP mouse line gave the unique opportunity to determine the function of the UPS in a specific manner. In contrast to the determination of steady-state levels of ubiquitinated proteins, which monitors the balance between ubiquitination on the one hand and deubiquitination and degradation on the other hand, the level of Ub<sup>G76V</sup>-GFP protein indicates specifically the degradation rate (Lindsten et al., 2003). This is because the Ub<sup>G76V</sup>-GFP protein is a direct target of the UPS, i.e. an accumulation of this protein indicates a problem in its degradation. The GFP levels were 3.6-fold higher in the KI x Ub<sup>G76V</sup>-GFP mice and only 1.5-fold higher (n.s.) in the KO x Ub<sup>G76V</sup>-GFP mice compared to corresponding WT mice. This difference in GFP-increase could indicate a specific defect in the KI mice. A likely reason is the presence of low level of mutant cMyBP-C, which in addition to hypertrophic and other damaged proteins keeps the UPS more

busy in these old mice. Interestingly, in a polyglutamine disease model crossed with Ub<sup>G76V</sup>-GFP mice, a significant increase in reporter protein was also observed late in disease (Bowman et al., 2005). But the basis for this increase was explained by a corresponding increase in Ub<sup>G76V</sup>-GFP mRNA. An *in vitro* assay showed normal (slightly increased) 20S activity, which confirmed that the increase in reporter protein did not result from a reduction of proteasome activity. Thus, the expression of Ub<sup>G76V</sup>-GFP at transcriptional level should be determined in the old KI and KO mice crossed with Ub<sup>G76V</sup>-GFP mice.

In conclusion, the increases in 20S proteasome activities and in the steady-state level of ubiquitinated proteins over the entire life span of both KI and KO mice provided clear evidence that the UPS is altered in the hearts of both mouse lines. Most of these alterations appear to be part of the general pathology related to the massive cardiac hypertrophy present in both mouse strains and is in accordance with published data in other animal models of cardiac hypertrophy. Whether the presence of truncated cMyBP-C proteins or their respective transcripts play an own pathogenic role (the initial hypothesis) remains to be further studied. Some evidence, however, supports this notion. First, the chymotrypsin-like activity tended to be increased in 9-mo-old M7t-TG mice (without any hypertrophy). Second, the expected negative correlation between chymotrypsin-like activity and steady-state level of ubiquitinated proteins was present in KO, but absent in KI mice. And finally, the increase in Ub<sup>G76V</sup>-GFP protein was much stronger (formally only present) in old KI crossed with the Ub<sup>G76V</sup>-GFP mice than in respective KO mice. Further analyses are needed to clarify this question.

### **Hypothesis 3: UPS impairment leads or contributes subsequently to cardiac hypertrophy.**

It was originally expected that UPS impairment leads or contributes subsequently to cardiac hypertrophy in the M7t-TG, Het and KI mice. Therefore, the cardiac phenotype was investigated in these mice. By immunofluorescence analysis of M7t-TG AMVM the classical alternation of endogenous cMyBP-C (A-band) and  $\alpha$ -actinin (Z-line) was obtained, which indicated a normal sarcomeric organization. In

comparison, despite normal levels of endogenous cMyBP-C, significant changes in the structure and ultrastructure of the heart were evident in the MyBP-C.mut2 mice lacking the myosin binding site (Yang et al., 1999). These changes were likely caused by the presence of the truncated protein, although it was expressed at a low level.

The M7t-TG mice also did not exhibit significant cardiac abnormalities when analyzed by transthoracic echocardiography. Neither wall-thickening nor dilatation of the left ventricle nor impaired cardiac function (determined by the FS) was found up to the age of two years. A really striking observation was the decreased VW/BW (-14%) in the M7t-TG mice at the age of 9 mo. The significance was caused by the male mice, which exhibited a highly significant decrease of the VW/BW (-18%), whereas the female mice just showed a tendency towards a decrease (-9%). The lower VW/BW did not result from a higher BW in the M7t-TG mice, but indeed from a lower VW. Interestingly, transgenic mice expressing a truncated cardiac troponin T (cTnT) also exhibited a decreased HW/BW (-23%) vs. WT mice (Tardiff et al., 1998). Full dissection of the heart and determination of the individual chamber weight-to-BW-ratios in cTnT mice showed that the decrease in heart mass was restricted to the left ventricle. Surprisingly, a small, but significant increase in atrial size was observed. The decrease in cardiac mass was due to a primary loss of cardiomyocytes and a decrease in cardiomyocyte cell size. These examinations were not performed in the M7t-TG mice, but should be done in the future to identify the reason for the decreased cardiac mass. Actually, nine independent founders were generated with the cTnT-truncation construct, but only three of them expressed the transgene at the protein level, and even then at low levels (<5%). Northern blot analysis showed that the transgene was expressed at high mRNA levels. These findings are suggestive of UPS involvement.

Immunofluorescence analysis of AMVM indicated a normal sarcomeric organization in the KI mice. However, the KI mice exhibited myocyte and eccentric LV hypertrophy with reduced FS and interstitial fibrosis at the age of 3 mo. The HW/BW ratio was already increased at birth (data not shown). Similar results were obtained in the cMyBP-C<sup>t/t</sup> mice, which exhibited neonatal onset of a progressive dilated cardiomyopathy with ventricular dysfunction, which continued throughout life and was accompanied by progressive compensatory LV hypertrophy (McConnell et al.,

1999). At 2-3 mo of age histological abnormalities including myocyte hypertrophy, myofibrillar disarray, interstitial fibrosis and dystrophic calcification were observed in the cMyBP-C<sup>t/t</sup> mice. In contrast, the Het mice did not develop LV hypertrophy up to the age of 18 mo, but exhibited slight myocyte hypertrophy and a higher, not significant level of  $\beta$ -MHC mRNA at the age of 3 mo. In comparison, at the age of 12 mo only 32% of the cMyBP-C<sup>t/+</sup> mice had developed a cardiac hypertrophy (McConnell et al., 2001). In >30-mo-old cMyBP-C<sup>t/+</sup> mice, LVAW and LVPW were significantly greater than in WT mice, and significant increases in hypertrophic markers (ANP and BNP) were found. Histological sections derived from >30-mo-old cMyBP-C<sup>t/+</sup> mice demonstrated myocyte hypertrophy, interstitial fibrosis and myofibrillar disarray in 50% of mutant animals. However, cardiac function in >30-mo-old cMyBP-C<sup>t/+</sup> mice was indistinguishable from that of respective WT mice.

Taken together, the hypothesis that alterations in the UPS contribute to the development of hypertrophy in cMyBP-C transgenic mice could not be substantiated. In case of KI and KO mice, this is likely due to the massive cardiac phenotype due to the complete absence (KO) or large reduction (KI) in cMyBP-C protein. The absence/reduction in cMyBP-C protein by itself is likely a strong trigger for hypertrophy, overriding any further contribution by other factors. It should be mentioned in this respect that it is quite surprising that the KO mice survive the absence of one of the major sarcomeric proteins at all. Moreover, one may argue that the similarly severe phenotype in KI mice, expressing at least 10% of missense cMyBP-C could be related to the affection of the UPS. But this idea needs further studies. On the other hand, the atrophy in M7t-TG mice could argue for just the opposite, namely that the stimulation of the proteasomal degradation machinery in 9-mo-old animals was causally related to atrophy. But this remains speculative at this point.

### **NMD is involved in the regulation of cMyBP-C mutant levels in KI and Het mice.**

Characterization of the cMyBP-C knock-in mouse model revealed that the level of total cMyBP-C mature-mRNA, but not of the pre-mRNA, was markedly reduced in both KI and Het mice compared to WT mice suggesting a specific regulation at the

level of processing pre-mRNAs to mature-mRNAs. A known pathway that specifically eliminates nonsense mRNAs is the NMD. NMD is activated in mRNAs that contain a PTC located >50-55 nt upstream of the last exon-exon junction (Nagy and Maquat, 1998). In the KI and Het mice, the PTC is located in exon 9 in the nonsense mRNA and therefore far upstream of the last junction between exons 34-35 suggesting an involvement of the NMD. Indeed, two differently acting NMD inhibitors, CHX and emetine, markedly increased the level of the nonsense mRNA, but not of the missense mRNA in KI NMCM. This specificity for the nonsense mRNA fits with the rule that NMD only targets aberrant mRNAs containing a PTC. More importantly, CHX treatment *in vivo* resulted as well in increased levels of nonsense mRNA in the KI and Het mice indicating that NMD is operational in the intact whole animal heart. The reduction in missense mRNA points to an additional mechanism, which is not yet known. As already mentioned above, similar expression levels of mutant cMyBP-C transcripts as in the KI and Het mice were obtained in the cMyBP-C<sup>t/t</sup> and cMyBP-C<sup>t/+</sup> mice. The presence of a PTC together with the markedly reduced levels of total cMyBP-C mRNA suggest a NMD involvement in these mice like in the KI and Het mice.

Taken together, an important new result from these studies is that NMD participates in the regulation of pathological cMyBP-C transcripts in the whole animal. On the basis of the results obtained previously (Sarikas et al., 2005) a model can be proposed that involves a two-step quality control. Transcripts are degraded by the NMD if they comply with the NMD rules (PTC >50-55 nt upstream of the last exon-exon junction) and the UPS comes into play if truncated proteins are being produced. The latter is the main degradation system in cases where a cDNA is overexpressed that is devoid of an exon-intron structure.

**The lack of cMyBP-C is probably the main cause of hypertrophy, which in turn activates the 20S proteasome activities.**

As discussed above the present results suggest that the phenotype in Het, KI and also KO mice is mainly attributed to an insufficient amount of normal cMyBP-C. The expression of endogenous cMyBP-C was not altered in the M7t-TG mice compared to



WT mice and probably therefore these mice did not develop cardiac hypertrophy up to the age of two years. The Het mice expressed 79% full-length cMyBP-C (mutant and normal) compared to WT mice and did not develop cardiac hypertrophy up to 18 mo of age. But the reduced level of cMyBP-C protein together with myocyte hypertrophy, the increased (not significant) level of  $\beta$ -MHC mRNA at 3 mo of age and the published data in the >30-mo-old cMyBP-C<sup>t/+</sup> mice suggest that myocyte hypertrophy precedes LV hypertrophy and that the Het mice will develop cardiac hypertrophy later in life. Therefore, examination of >18 mo-old Het mice is absolutely necessary.

In contrast to the M7t-TG and Het mice, KI and KO mice did not express any normal cMyBP-C and exhibited an increased HW/BW already at birth suggesting lack of cMyBP-C as the disease mechanism leading to hypertrophy. The KI mice expressed of course 10% full-length E256K protein, but whether the E256K mutant has a function at all remains at the moment elusive.

If the sarcomere function would be altered or impaired due the insufficient amount of cMyBP-C, the heart may try to compensate the functional deficits by increased myocyte growth resulting in cardiac hypertrophy. When cardiac function remains inadequate despite growth, other pathways are likely activated, as evidenced by an altered gene expression (ANP, BNP,  $\beta$ -MHC), myocyte death (apoptosis) and fibrosis. In general, the UPS is involved in a broad range of cellular pathways, such as apoptosis (Breitschopf et al., 2000; Li and Dou, 2000), cell cycle (King et al., 1996), cell differentiation (Helin, 1998) and immune and stress response (Palombella et al., 1994; Rock et al., 1994). In addition, a number of key regulatory pathways that promote cardiac hypertrophy are either targets or components of the UPS. For instance, it has been reported that several signaling proteins such as  $\beta$ -catenin and calcineurin, which mediate cardiac growth (including pathological hypertrophy), are degraded by the UPS (Glickman and Ciechanover, 2002; Li et al., 2004). Thus, the UPS was likely activated in response to hypertrophy in KI and KO mice and the increase in proteolytic activities was likely a compensatory mechanism against further development of hypertrophy: the 20S proteasome worked more to get rid of the hypertrophic, hypertrophy-promoting and proapoptotic proteins. This was also indicated by the positive correlation between chymotrypsin-like activity and hypertrophy, which was observed in both KI and KO mice.

Thus, these data as well as several recent other studies (Depre et al., 2006; Razeghi et al., 2006) are compatible with the idea that cardiac hypertrophy is generally accompanied by alterations in the UPS, mainly in the sense of increased turnover rate. Our observation that the steady-state level of ubiquitinated proteins did not correlate with the degree of cardiac hypertrophy (in both KI and KO mice) argues for the notion that the system normally reacts to increased protein load by increased activity to keep the steady-state level constant. Accordingly, a negative correlation existed between chymotrypsin activity and the level of ubiquitinated proteins in the KO mice. In other words, the better the proteasome works, the lower the steady-state level of ubiquitinated proteins. Interestingly, this correlation was absent in KI mice, suggesting a specific defect as discussed above. When interpreting these data, it is important to keep in mind that the tests for proteasome activity are performed *in vitro*, i.e. in the absence of any potentially inhibiting truncated protein, whereas the steady-state level of ubiquitinated proteins is determined in the *in vivo* situation.

## Outlook

For the future, some investigations and treatments are yet outstanding for the M7t-TG, KI and Het mice. First, further experiments should be designed to stabilize and detect the truncated protein. In the M7t-TG mice, the UPS is likely involved in the rapid degradation of the truncated protein, although it could not be substantiated under the used conditions. The i.v.-injection of MG132 or epoxomicin in adult (older than 2 mo) M7t-TG mice followed by Western blot analysis of myofilament protein preparations may result in the detection of the truncated protein. In contrast, NMD inhibition is likely useless in the M7t-TG mice: NMD is likely not responsible for the low levels of transgenic mRNA, because it requires at least 1 intron (Zhang et al., 1998) and is therefore inactive towards transgenically expressed cDNAs. A cross between the M7t-TG and KO mice would result in mice, which express only one functional cMyBP-C allele and the NMD-resistant transgene. In contrast to the M7t-TG mice, these crossed mice would mimic the human situation and would be probably better suitable to investigate the UPS involvement *in vivo* for the following reasons: i) NMD cannot act, which leads to a stable expression of the transgene at mRNA level and ii) the endogenous cMyBP-C amount at mRNA and protein level would be reduced (due to

the heterozygous state for cMyBP-C). To detect the truncated protein in the KI and Het mice, the best approach may be to inhibit NMD, e.g. by siRNA-mediated knockdown of SMG-1 or Upf1 (NMD key proteins), followed by blockage of the proteasome by i.v.-injection of MG132 and final analysis of myofilament protein preparations by Western blot. This strategy is only useful to detect the truncated protein, but it will not rescue the phenotype in the KI mice. As already mentioned, the truncated protein is not only lacking the myosin and titin binding site but also the MyBP-C motif with the 3 phosphorylation sites, and is therefore probably not able to play a beneficial structural or functional role. In contrast to NMD inhibition, the treatment with gentamicin, an aminoglycoside, or PTC124 could be useful to rescue the mutant phenotype in the KI mice. Suppression of the PTC in the nonsense mRNA would lead to a mutant almost full-length cMyBP-C protein. Whether this protein would have structural and functional properties at all is difficult to say, because it is at least missing the exon 6, which leads to a frameshift.

A second point, which should be investigated in the future, is the UPS function in the Het mice. The Het mice did not develop cardiac hypertrophy up to 18 mo of age and therefore no altered UPS function is expected. But maybe there is already a tendency towards an increase in both ubiquitination and degradation at this age, which proceeds with age.

Finally, it would be interesting to investigate the stress response in the M7t-TG and Het mice. A striking characteristic of FHC in humans is its preference to cause sudden death, oftentimes during significant cardiac stress brought on by exercise (Maron et al., 1980; Maron et al., 1996). But in general, the laboratory mouse is a sedentary animal in a minimally stressful environment. Controlled regimens have been therefore established to stress mice physically or pharmacologically: mice can be subject to swimming (Kaplan et al., 1994; James et al., 1998) or treadmill exercise (Fewell et al., 1997; James et al., 1998) or to chronic isoproterenol infusion (Kudej et al., 1997). It is expected that phenotypes that may not be present at rest become apparent under these controlled stress regimens. For instance, although the transgenic MyBP-C.mut2 mice appeared overtly healthy, they were significantly compromised in their exercise capacity and exhibited decreased heart rates in response to the treadmill exercise (Yang et al., 1999). Thus, it should be investigated whether under significant

conditions of stress overt cardiovascular abnormalities might become apparent in the M7t-TG and Het mice.

### **Potential therapeutic approaches**

When considering therapeutic interventions, it is important to keep in mind that FHC is, in the vast majority, an autosomal-dominant disease, i.e. it occurs at the heterozygous state. This is different from the mouse models for yet incompletely understood reasons.

Assuming that the (partial) absence is the main cause of hypertrophy in cMyBP-C mutations, putative therapeutic approaches should aim at increasing the amount of full-length cMyBP-C protein. An estimated 70% of the 165 known *MYBPC3* mutations (Richard et al., 2006; Alcalai et al., 2007) should result in a PTC located >50-55 nt upstream of the last exon-exon junction and therefore involve NMD. Up to date, only two papers have analyzed the consequences of frameshift *MYBPC3* mutations in human myocardial tissue (Rottbauer et al., 1997; Moolman et al., 2000). In one patient, an insertion of a single guanine resulted in a newly created splice donor site in exon 25 and a PTC in exon 26 (Moolman et al., 2000). The level of nonsense mRNA was 2-fold lower than the WT mRNA in this patient suggesting the involvement of NMD. In general, NMD is a quality control of the cell and prevents the production of nonfunctional or potentially harmful truncated proteins (Frischmeyer and Dietz, 1999; Maquat, 2004). However, some truncated proteins deleted for the C-terminal domains have been reported to support normal cell functions (Sheppard et al., 1994; Kerr et al., 2001). In the case that a mutant protein retains residual activity that can partially retain normal protein function, NMD might augment the original defects (Cali and Anderson, 1998; Ainsworth, 2005). Thus, the selective inhibition of NMD may provide a novel strategy to rescue the mutant phenotype in PTC-related diseases, in which the mutant protein shows no dominant-negative effect and compensates for the missing cellular functions. For example, wortmannin, an inhibitor of the PI3-kinase-related protein SMG-1 that phosphorylates Upf1 during NMD (Rehwinkel et al., 2006), or siRNA-mediated knockdown of SMG-1 or Upf1 restored the level of PTC-containing collagen VI  $\alpha 2$  mRNA and rescued the

phenotype in fibroblasts of a patient with Ullrich disease (Usuki et al., 2004; Usuki et al., 2006). But in this context it has to be noted that it is not known what kinds of deleterious side effects may arise from a NMD inhibition in humans. For instance, otherwise innocuous, recessive PTC-related mutations carried in heterozygous condition as part of an individual's genetic load could cause unpredictable, adverse side effects. In addition, the accumulation of natural mRNAs could cause adverse side effects.

Other studies have shown that treatment with aminoglycosides can also rescue the mutant phenotype in PTC-related diseases by allowing a PTC read-through, thus permitting the synthesis of a near-normal protein (Howard et al., 1996; Barton-Davis et al., 1999). Aminoglycosides bind to the decoding site of ribosomes and promote the incorporation of an amino acid at the PTC by a near-cognate aminoacylated transfer (t)RNA (Rospert et al., 2005). They have been already used in human patients to suppress PTCs within transcripts associated with cystic fibrosis (Kuzmiak and Maquat, 2006). Unfortunately, long-term use of these antibiotics in humans can cause nephrotoxicity and ototoxicity. The recent development of a new drug, PTC124, which promotes amino acid incorporation at PTCs by an unknown mechanism (Ainsworth, 2005) and which did not evoke kidney failure or deafness in phase I of safety trials, is a promising perspective.

Whether UPS inhibition is a useful strategy to prevent hypertrophy, is depending on the cMyBP-C mutation. If the cMyBP-C mutation results in a nonsense mRNA containing a PTC located <50-55 nt upstream of the last exon-exon junction and leads to the production of a truncated protein, which retains residual activity, UPS inhibition would result in an useful stabilization of this protein. The proteasome inhibitor bortezomib is already in clinical use for the therapy of multiple myeloma (Richardson and Anderson, 2003) and, until now, appears to have a favorable safety profile that does not include cardiac toxicity.

## 5 Summary

Mutations in the *MYBPC3* gene encoding cardiac myosin-binding protein-C (cMyBP-C) are frequent causes of familial hypertrophic cardiomyopathy (FHC). *MYBPC3* mutations mainly result in a frameshift and a premature termination codon (PTC). However, truncated cMyBP-C mutants were undetectable in myocardial tissue of FHC patients with frameshift mutations. Recent data using adenoviral gene transfer in cultured cardiomyocytes showed that truncated cMyBP-C proteins are rapidly and quantitatively degraded by the ubiquitin-proteasome system (UPS). Furthermore, they suggested that the rapid degradation of truncated cMyBP-C mutants saturates the UPS function which, by itself, could play a role in causing hypertrophy. It was the aim of the present thesis to investigate (1) whether the UPS is also responsible for the degradation of truncated cMyBP-C mutants in the whole animal and (2) whether alterations of the UPS that may be secondary to its overuse by truncated cMyBP-C mutants could play an own pathogenetic role in the development of myocardial hypertrophy *in vivo*. As a model system the experiments focused on a cMyBP-C mutant that corresponds to a G>A transition on the last nucleotide of exon 6 and has been found to be associated with poor prognosis in patients. This mutation, when introduced into an exogenous cMyBP-C cDNA, gives rise to a largely truncated mutant and, in the genomic context of the whole animal, is expected to result either in a full-length, missense protein or a truncated protein resulting from exon 6 skipping and a PTC or both.

Two mouse models were developed and characterized. One is a transgenic model expected to overexpress a myc-tagged cMyBP-C cDNA deleted of exon 6 under the control of the  $\alpha$ -myosin heavy chain promoter. No cardiac hypertrophy, but an unexpected cardiac atrophy was observed in the transgenic mice. The level of full-length cMyBP-C protein was similar in transgenic and wild-type (WT) mice, but the truncated protein was undetectable, despite the presence of transgenic mRNA. Whereas this observation is compatible with rapid degradation of the truncated protein by the UPS, inhibition of the proteasome in cultured cardiomyocytes did not result in measurable amounts of truncated protein. Moreover, no evidence was obtained indicating alterations of the UPS, neither in terms of steady-state level of

ubiquitinated proteins nor degradation activity. These data may point to alternative mechanisms such as reduced translational efficiency of mutant mRNAs, but on the basis of the former *in vitro* data involvement of the UPS still appears to be most likely and the apparent absence of the truncated protein may just reflect insufficient sensitivity of the present assay conditions. Further experiments are necessary to solve this issue.

The second mouse model was generated by targeted knock-in of the G>A transition. The homozygous (KI) mice developed myocyte and left ventricular hypertrophy with reduced fractional shortening and interstitial fibrosis, whereas the heterozygous (Het) mice developed only mild myocyte hypertrophy. Both missense and nonsense (exon 6 skipped) mRNAs were present, but the level of total cMyBP-C mRNA was markedly lower in the Het and KI mice vs. WT mice. Inhibition of the nonsense-mediated mRNA decay (NMD) in cardiomyocytes or *in vivo* increased the level of nonsense mRNA several fold. The missense mRNA level was not changed by treatment with NMD inhibitors. The truncated protein was not detected in both the KI and Het mice, even after proteasome inhibition in cardiomyocytes. The amount of the full-length protein was 90% and 21% lower in the KI and Het mice, respectively. These data suggest that, in the whole animal and intact genomic context, the main regulation of the mutant cMyBP-C takes already place at the mRNA level and partially involves NMD.

To investigate the second hypothesis, namely that mutant cMyBP-C cause saturation of the UPS, homozygous KI mice were compared with homozygous cMyBP-C deficient mice (KO). The latter were not expected to have any specific affection of the UPS, because the *MYBPC3* gene was simply inactivated. Both models showed marked cardiac hypertrophy and an increase in the steady-state level of ubiquitinated proteins throughout the life span of the animals. In parallel, the 20S proteasome activities, measured by fluorogenic substrates *ex vivo*, were greater and positively correlated with the degree of hypertrophy. Whereas the steady-state level of ubiquitinated proteins was negatively correlated with the 20S proteasome activity in KO, it was not in KI mice. To specifically monitor the degradation capacity of the UPS *in vivo*, KO and KI mice were crossed with a UPS reporter mouse strain expressing a green fluorescent protein (GFP) linked to a modified ubiquitin. In these

mice, accumulation of GFP indicates compromised UPS function. Indeed, old KI mice showed 4-fold higher GFP levels than WT littermates, but KO mice not or to a lower extent. These data are compatible with the hypothesis that in the KI mice the UPS is specifically affected in addition to a more general effect of cardiac hypertrophy. But this interpretation needs further substantiation.

In conclusion, both the NMD and the UPS result in cMyBP-C haploinsufficiency, and this is likely a major cause of cardiac hypertrophy. The data also suggest that cardiac hypertrophy as such goes along with an increase in UPS activity, which is likely compensatory and triggered by increased protein turnover. The marked increase in GFP in old KI crossed with the UPS reporter mice may, in accordance with the initial hypothesis, point to a specific impairment of the UPS in mice which express truncated cMyBP-C. These data contribute to an improved understanding of the molecular mechanisms of FHC associated with frameshift mutations and maybe also to the development of new therapeutic strategies.



## 5 Zusammenfassung

Mutationen des *MYBPC3* Gens, das kardiales Myosin-bindendes Protein-C (cMyBP-C) kodiert, sind häufig Ursachen der familiären hypertrophen Kardiomyopathie (FHC). Die meisten *MYBPC3* Mutationen resultieren in einer Verschiebung des Leserasters und einem vorzeitigen Terminatorcodon (PTC) und lassen C-terminal trunkierte Proteine erwarten. Trunkierte cMyBP-C Proteine waren jedoch nicht in messbaren Mengen im Myokardgewebe von FHC-Patienten mit einer Frameshift Mutation vorhanden. Eine kürzlich abgeschlossene Versuchsserie, in der verschiedene cMyBP-C Proteine über einen adenoviralen Ansatz in kultivierten Kardiomyozyten überexprimiert wurden, hat gezeigt, dass trunkierte cMyBP-C Proteine rasch und quantitativ durch das Ubiquitin-Proteasom-System (UPS) abgebaut werden. Ebenso ließen die Daten darauf schließen, dass der rasche Abbau der trunkierten cMyBP-C Proteine die proteolytische Leistungsfähigkeit des UPS beeinträchtigt, was an sich Hypertrophie verursachen könnte. Das Ziel dieser Doktorarbeit war es zu untersuchen, ob (1) das UPS auch im ganzen Tier, also *in vivo*, für den Abbau der trunkierten cMyBP-C Proteine verantwortlich ist und (2) Veränderungen des UPS, die zusätzlich zu seinem übermäßigem Gebrauch durch trunkierte cMyBP-C Proteine auftreten könnten, eine eigene pathogene Rolle in der Entwicklung myokardialer Hypertrophie *in vivo* spielen. In dieser Doktorarbeit wurden speziell die molekularen Auswirkungen einer *MYBPC3* Mutation untersucht, die mit einer schlechten Prognose in FHC-Patienten einhergeht. Es handelt sich dabei um eine G>A Mutation an dem letzten Nukleotid des Exon 6. Die Mutation hat ein stark trunkiertes cMyBP-C Protein zur Folge, wenn sie in eine exogene cMyBP-C cDNA eingebracht wird. Wird die Mutation durch homologe Rekombination gezielt in das Genom eingebracht, sollten entweder ein ungekürztes, mutiertes Protein oder ein stark trunkiertes cMyBP-C Protein, welches durch das Überspringen von Exon 6 und dem Auftreten eines PTC in Exon 9 entsteht, oder beide exprimiert werden.

Zwei Mausmodelle wurden entwickelt und charakterisiert. Ein Modell ist ein transgenes Mausmodell, welches eine humane myc-markierte cMyBP-C cDNA, in welcher das Exon 6 entfernt wurde, herzspezifisch unter der Kontrolle des  $\alpha$ -Myosin-Schwere-Kette-Promoter überexprimieren sollte. Es wurde keine kardiale

Hypertrophie, sondern unerwartet eine kardiale Atrophie in diesen transgenen Mäusen festgestellt. Die Expression des endogenen, ungekürzten cMyBP-C Protein war ähnlich in transgenen und Wildtyp (WT)-Mäusen; das trunkierte cMyBP-C Protein war jedoch nicht in nachweisbarer Menge vorhanden, obwohl das Transgen auf mRNA-Ebene exprimiert wurde. Während dieses Ergebnis mit dem raschen Abbau der trunkierten Proteine durch das UPS vereinbar ist, führte eine Hemmung des UPS durch UPS-Inhibitoren nicht zu messbaren Mengen des trunkierten Proteins in kultivierten Kardiomyozyten. Ebenso fand sich kein Hinweis für eine Veränderung des UPS, weder in Bezug auf die Steady-State-Level ubiquitinierten Proteine noch in Bezug auf die 20S-Proteasom-Aktivitäten, welche mit Hilfe von fluorogenen Substraten *ex vivo* gemessen wurden. Diese Ergebnisse könnten auf alternative Mechanismen hinweisen, wie z.B. eine reduzierte Translationseffizienz von mutierten mRNAs. Basierend auf den früheren Daten scheint jedoch eine Beteiligung des UPS am wahrscheinlichsten, und die scheinbare Abwesenheit des trunkierten Proteins ist wahrscheinlich eher auf eine unzureichende Sensitivität zurückzuführen. Weiterführende Experimente sind notwendig, um dies zu klären.

Das zweite Mausmodell wurde durch gezieltes Einbringen der G>A Mutation in das Genom generiert. Die homozygoten (KI) Mäuse entwickelten eine Myozyten- und linksventrikuläre Hypertrophie, eine reduzierte Verkürzungsfraktion des linken Ventrikels und interstitielle Fibrose, während die heterozygoten (Het) Mäuse lediglich eine leichte Myozyten-Hypertrophie zeigten. Es wurde sowohl die Missense (G>A Transition)- als auch die Nonsense (Überspringen von Exon 6)-mRNA in KI- und Het-Mäusen nachgewiesen; die Gesamtmenge an cMyBP-C mRNA war jedoch deutlich geringer in KI- und Het-Mäusen als in WT-Mäusen. Die Hemmung des nonsense-vermittelten mRNA Abbaus (NMD) durch NMD-Inhibitoren erhöhte die Menge an Nonsense-mRNA mehrfach sowohl in kultivierten Kardiomyozyten als auch *in vivo*. Die Menge an Missense-mRNA wurde durch die Behandlung mit NMD-Inhibitoren nicht verändert. Das trunkierte cMyBP-C Protein konnte selbst nach Proteasom-Hemmung weder in den KI- noch in den Het-Mäusen nachgewiesen werden. Die Menge an ungekürztem cMyBP-C Protein war um 90% bzw. 21% geringer in den KI- und Het-Mäusen gegenüber WT-Mäusen. Diese Ergebnisse legen nahe, dass die Regulierung der G>A Transition im ganzen Tier und im intakten

genomischen Kontext hauptsächlich schon auf mRNA-Ebene stattfindet und teilweise NMD mit einschließt.

Um der zweiten Hypothese nachzugehen, nämlich dass trunkierte cMyBP-C Proteine eine Veränderung der UPS-Funktion hervorrufen, wurden die KI-Mäuse mit homozygoten cMyBP-C-defizienten (KO) Mäusen verglichen. Beide Mausmodelle zeigten eine deutliche kardiale Hypertrophie und einen Anstieg der Steady-State-Level ubiquitinerter Proteine über ihre gesamte Lebensdauer. Die 20S-Proteasom-Aktivitäten waren ebenso erhöht und korrelierten positiv mit dem Grad der Hypertrophie. Während die Steady-State-Level ubiquitinerter Proteine in den KO-Mäusen negativ mit den 20S-Proteasom-Aktivitäten korrelierten, taten sie dies in den KI-Mäusen nicht. Um spezifisch die Abbau-Leistung des UPS *in vivo* zu verfolgen, wurden die KI- und KO-Mäuse mit UPS-Reportermäusen gekreuzt. Diese UPS-Reportermäuse exprimieren ein grün fluoreszierendes Protein (GFP), welches wiederum mit einem mutierten Ubiquitinmolekül verbunden ist. Eine GFP-Akkumulation würde daher auf eine beeinträchtigte UPS-Funktion in diesen Mäusen hindeuten. In alten KI-Mäusen (gekreuzt mit den UPS-Reportermäusen) wurde tatsächlich eine 4-fach höhere GFP-Menge detektiert im Vergleich zu WT-Mäusen; in den KO-Mäusen jedoch nicht bzw. in geringerem Ausmaß. Diese Ergebnisse sind vereinbar mit der Annahme, dass das UPS in den KI-Mäusen spezifisch verändert ist, und zwar zusätzlich zu einem generellen Auftreten kardialer Hypertrophie. Diese Interpretation benötigt jedoch weitere Analysen.

Zusammenfassend kann festgestellt werden, dass sowohl der NMD als auch das UPS in einer cMyBP-C Haploinsuffizienz resultieren könnten, die wiederum wahrscheinlich eine Hauptursache für kardiale Hypertrophie darstellt. Die Ergebnisse lassen ebenso vermuten, dass eine kardiale Hypertrophie an sich mit einer gesteigerten UPS-Aktivität einhergeht, welche wahrscheinlich kompensatorisch ist und durch einen gesteigerten Protein-Umsatz ausgelöst wird. Der deutliche Anstieg von GFP-Protein in den alten KI-Mäusen (gekreuzt mit den UPS-Reportermäusen) könnte, im Einklang mit der ursprünglichen Hypothese, auf eine spezifische Beeinträchtigung des UPS in Mäusen, die trunkierte cMyBP-C Proteine exprimieren, hindeuten. Die Ergebnisse tragen zu einem verbesserten Verständnis der molekularen

Mechanismen bei, die über Frameshift Mutationen zu FHC führen, und ermöglichen eventuell neue therapeutische Ansätze.

## 6 References

- Ainsworth C. 2005. Nonsense mutations: running the red light. *Nature*. 438:726-8.
- Alcalai R, Seidman JG, and Seidman CE. 2007. Genetic Basis of Hypertrophic Cardiomyopathy: From Bench to the Clinics. *J Cardiovasc Electrophysiol*. 18:1-7.
- Alyonycheva TN, Mikawa T, Reinach FC, and Fischman DA. 1997. Isoform-specific interaction of the myosin-binding proteins (MyBPs) with skeletal and cardiac myosin is a property of the C-terminal immunoglobulin domain. *J Biol Chem*. 272:20866-20872.
- Andersen PS, Havndrup O, Bundgaard H, Larsen LA, Vuust J, Pedersen AK, Kjeldsen K, and Christiansen M. 2004. Genetic and phenotypic characterization of mutations in myosin-binding protein C (MYBPC3) in 81 families with familial hypertrophic cardiomyopathy: total or partial haploinsufficiency. *Eur J Hum Genet*. 12:673-7.
- Ashrafian H, Redwood C, Blair E, and Watkins H. 2003. Hypertrophic cardiomyopathy: a paradigm for myocardial energy depletion. *Trends Genet*. 19:263-8.
- Barton-Davis ER, Cordier L, Shoturma DI, Leland S, and Sweeney HL. 1999. Aminoglycoside antibiotics restore dystrophin function to skeletal muscles in *mdx* mice. *J. Clin. Invest*. 104:375-381.
- Bonne G, Carrier L, Richard P, Hainque B, and Schwartz K. 1998. Familial hypertrophic cardiomyopathy: from mutations to functional defects. *Circ Res*. 83:579-593.
- Bottinelli R, Coviello DA, Redwood CS, Pellegrino MA, Maron BJ, Spirito P, Watkins H, and Reggiani C. 1998. A mutant tropomyosin that causes hypertrophic cardiomyopathy is expressed in vivo and associated with an increased calcium sensitivity. *Circ. Res*. 82:106-115.
- Bowman AB, Yoo SY, Dantuma NP, and Zoghbi HY. 2005. Neuronal dysfunction in a polyglutamine disease model occurs in the absence of ubiquitin-proteasome system impairment and inversely correlates with the degree of nuclear inclusion formation. *Hum Mol Genet*. 14:679-91.
- Bradford MM. 1976. A rapid and sensitive method for the quantitation of microgram quantities of protein utilizing the principle of protein-dye binding. *Anal Biochem*. 72:248-54.
- Breitschopf K, Zeiher AM, and Dimmeler S. 2000. Ubiquitin-mediated degradation of the proapoptotic active form of bid. A functional consequence on apoptosis induction. *J Biol Chem*. 275:21648-52.

- Buchou T, Vernet M, Blond O, Jensen HH, Pointu H, Olsen BB, Cochet C, Issinger OG, and Boldyreff B. 2003. Disruption of the regulatory beta subunit of protein kinase CK2 in mice leads to a cell-autonomous defect and early embryonic lethality. *Mol Cell Biol.* 23:908-15.
- Cali BM, and Anderson P. 1998. mRNA surveillance mitigates genetic dominance in *Caenorhabditis elegans*. *Mol Gen Genet.* 260:176-84.
- Carrard G, Bulteau AL, Petropoulos I, and Friguet B. 2002. Impairment of proteasome structure and function in aging. *Int J Biochem Cell Biol.* 34:1461-74.
- Carrier L, Bonne G, Bährend E, Yu B, Richard P, Niel F, Hainque B, Cruaud C, Gary F, Labeit S, Bouhour JB, Dubourg O, Desnos M, Hagège AA, Trent RJ, Komajda M, and Schwartz K. 1997. Organization and sequence of human cardiac myosin binding protein C gene (*MYBPC3*) and identification of mutations predicted to produce truncated proteins in familial hypertrophic cardiomyopathy. *Circ Res.* 80:427-434.
- Carrier L, Knoell R, Vignier N, Keller DI, Bausero P, Prudhon B, Isnard R, Ambrosine ML, Fiszman M, Ross J, Jr., Schwartz K, and Chien KR. 2004. Asymmetric septal hypertrophy in heterozygous cMyBP-C null mice. *Cardiovasc Res.* 63:293-304.
- Carter MS, Daskow J, Morris P, Li S, Nhim RP, Sandstedt S, and Wilkinson MF. 1995. A regulatory mechanism that detects premature nonsense codons in T-cell receptor transcripts in vivo is reversed by protein synthesis inhibitors in vitro. *J Biol Chem.* 270:28995-9003.
- Carter MS, Li S, and Wilkinson MF. 1996. A splicing-dependent regulatory mechanism that detects translation signals. *Embo J.* 15:5965-75.
- Charron P, Dubourg O, Desnos M, Bennaceur M, Carrier L, Camproux AC, Isnard R, Hagège A, Langlard JM, Bonne G, Richard P, Hainque B, Bouhour JB, Schwartz K, and Komajda M. 1998. Clinical features and prognostic implications of familial hypertrophic cardiomyopathy related to cardiac myosin binding protein C gene. *Circulation.* 97:2230-2236.
- Chen Q, Liu JB, Horak KM, Zheng H, Kumarapeli AR, Li J, Li F, Gerdes AM, Wawrousek EF, and Wang X. 2005. Intracellular amyloidosis impairs proteolytic function of proteasomes in cardiomyocytes by compromising substrate uptake. *Circ Res.* 97:1018-26.
- Ciechanover A, and Brundin P. 2003. The ubiquitin proteasome system in neurodegenerative diseases: sometimes the chicken, sometimes the egg. *Neuron.* 40:427-46.
- Ciechanover A. 2005. Proteolysis: from the lysosome to ubiquitin and the proteasome. *Nat Rev Mol Cell Biol.* 6:79-87.

- Craig R, and Offer G. 1976. The localization of C-protein in rabbit skeletal muscle. *Proc. Royal. Soc. Lond.* B192:451-454.
- Cuda G, Fananapazir L, Zhu WS, Seller JR, and Epstein NE. 1993. Skeletal muscle expression and abnormal function of  $\beta$ -myosin in hypertrophic cardiomyopathy. *J. Clin. Invest.* 91:2861-2865.
- Culbertson MR. 1999. RNA surveillance. Unforeseen consequences for gene expression, inherited genetic disorders and cancer. *Trends Genet.* 15:74-80.
- Depre C, Wang Q, Yan L, Hedhli N, Peter P, Chen L, Hong C, Hittinger L, Ghaleh B, Sadoshima J, Vatner DE, Vatner SF, and Madura K. 2006. Activation of the cardiac proteasome during pressure overload promotes ventricular hypertrophy. *Circulation.* 114:1821-8.
- El-Armouche A, Boknik P, Eschenhagen T, Carrier L, Knaut M, Ravens U, and Dobrev D. 2006. Molecular determinants of altered  $\text{Ca}^{2+}$  handling in human chronic atrial fibrillation. *Circulation.* 114:670-80.
- El-Armouche A, Pohlmann L, Schlossarek S, Starbatty J, Yeh YH, Nattel S, Dobrev D, Eschenhagen T, and Carrier L. 2007. Decreased phosphorylation levels of cardiac myosin-binding protein-C in human and experimental heart failure. *J Mol Cell Cardiol.* 43:223-9.
- Erdmann J, Raible J, Maki-Abadi J, Hummel M, Hammann J, Wollnik B, Frantz E, Fleck E, Hetzer R, and Regitz-Zagrosek V. 2001. Spectrum of clinical phenotypes and gene variants in cardiac myosin-binding protein C mutation carriers with hypertrophic cardiomyopathy. *J Am Coll Cardiol.* 38:322-30.
- Fewell JG, Osinska H, Klevitsky R, Ng W, Sfyris G, Bahrehmand F, and Robbins J. 1997. A treadmill exercise regimen for identifying cardiovascular phenotypes in transgenic mice. *Am J Physiol.* 273:H1595-605.
- Flavigny J, Souchet M, Sébillon P, Berrebi-Bertrand I, Hainque B, Mallet A, Bril A, Schwartz K, and Carrier L. 1999. COOH-terminal truncated cardiac myosin-binding protein C mutants resulting from familial hypertrophic cardiomyopathy mutations exhibit altered expression and/or incorporation in fetal rat cardiomyocytes. *J Mol Biol.* 294:443-456.
- Flavigny J, Robert P, Camelin J, Schwartz K, Carrier L, and Berrebi-Bertrand I. 2003. Biomolecular interactions between human recombinant  $\beta$ -MyHC and cMyBP-Cs implicated in familial hypertrophic cardiomyopathy. *Cardiovasc Res.* 60:388-396.
- Fougerousse F, Delezoide AL, Fiszman MY, Schwartz K, Beckmann JS, and Carrier L. 1998. Cardiac myosin binding protein C gene is specifically expressed in heart during murine and human development. *Circ Res.* 82:130-133.

- Freiburg A, and Gautel M. 1996. A molecular map of the interactions between titin and myosin-binding protein C. Implications for sarcomeric assembly in familial hypertrophic cardiomyopathy. *Eur J Biochem.* 235:317-326.
- Frischmeyer PA, and Dietz HC. 1999. Nonsense-mediated mRNA decay in health and disease. *Hum Mol Genet.* 8:1893-900.
- Gardin JM, Siri FM, Kitsis RN, Edwards JG, and Leinwand LA. 1995. Echocardiographic assessment of left ventricular mass and systolic function in mice. *Circ Res.* 76:907-14.
- Garneau NL, Wilusz J, and Wilusz CJ. 2007. The highways and byways of mRNA decay. *Nat Rev Mol Cell Biol.* 8:113-26.
- Garvey JL, Kranias EG, and Solaro RJ. 1988. Phosphorylation of C-protein, troponin I and phospholamban in isolated rabbit hearts. *Biochem. J.* 249:709-714.
- Gautel M, Zuffardi O, Freiburg A, and Labeit S. 1995. Phosphorylation switches specific for the cardiac isoform of myosin binding protein C: a modulator of cardiac contraction? *EMBO J.* 14:1952-1960.
- Gautel M, Fürst DO, Cocco A, and Schiaffino S. 1998. Isoform transitions of the myosin-binding protein C family in developing human and mouse muscles. Lack of isoform transcomplementation in cardiac muscle. *Circ. Res.* 82:124-129.
- Geisterfer-Lowrance AA, Kass S, Tanigawa G, Vosberg HP, McKenna W, Seidman CE, and Seidman JG. 1990. A molecular basis for familial hypertrophic cardiomyopathy: a  $\beta$  cardiac myosin heavy chain gene missense mutation. *Cell.* 62:999-1006.
- Glickman MH, and Ciechanover A. 2002. The ubiquitin-proteasome proteolytic pathway: destruction for the sake of construction. *Physiol Rev.* 82:373-428.
- Golab J, Bauer TM, Daniel V, and Naujokat C. 2004. Role of the ubiquitin-proteasome pathway in the diagnosis of human diseases. *Clin Chim Acta.* 340:27-40.
- Gruen M, and Gautel M. 1999. Mutations in beta-myosin S2 that cause familial hypertrophic cardiomyopathy (FHC) abolish the interaction with the regulatory domain of myosin binding protein-C. *J Mol Biol.* 286:933-949.
- Gruen M, Prinz H, and Gautel M. 1999. cAPK-phosphorylation controls the interaction of the regulatory domain of cardiac myosin binding protein C with myosin-S2 in an on-off fashion. *FEBS Lett.* 453:254-259.
- Harris SP, Bartley CR, Hacker TA, McDonald KS, Douglas PS, Greaser ML, Powers PA, and Moss RL. 2002. Hypertrophic cardiomyopathy in cardiac myosin binding protein-C knockout mice. *Circ Res.* 90:594-601.



- Hartzell HC, and Titus L. 1982. Effects of cholinergic and adrenergic agonists on phosphorylation of a 165,000-dalton myofibrillar protein in intact cardiac muscle. *J. Biol. Chem.* 257:2111-2120.
- Helin K. 1998. Regulation of cell proliferation by the E2F transcription factors. *Curr Opin Genet Dev.* 8:28-35.
- Herron TJ, Rostkova E, Kunst G, Chaturvedi R, Gautel M, and Kentish JC. 2006. Activation of myocardial contraction by the N-terminal domains of myosin binding protein-C. *Circ Res.* 98:1290-8.
- Howard M, Frizzell RA, and Bedwell DM. 1996. Aminoglycoside antibiotics restore CFTR function by overcoming premature stop mutations. *Nat Med.* 2:467-9.
- Ingles J, Doolan A, Chiu C, Seidman J, Seidman C, and Semsarian C. 2005. Compound and double mutations in patients with hypertrophic cardiomyopathy: implications for genetic testing and counselling. *J Med Genet.* 42:e59.
- James JF, Hewett TE, and Robbins J. 1998. Cardiac physiology in transgenic mice. *Circ Res.* 82:407-15.
- Kamisago M, Sharma SD, DePalma SR, Solomon S, Sharma P, McDonough B, Smoot L, Mullen MP, Woolf PK, Wigle ED, Seidman JG, Seidman CE, Jarcho J, and Shapiro LR. 2000. Mutations in Sarcomere Protein Genes as a Cause of Dilated Cardiomyopathy. *N. Engl. J. Med.* 343:1688-1696.
- Kaplan ML, Cheslow Y, Vikstrom K, Malhotra A, Geenen DL, Nakouzi A, Leinwand LA, and Buttrick PM. 1994. Cardiac adaptations to chronic exercise in mice. *Am J Physiol.* 267:H1167-73.
- Kerr TP, Sewry CA, Robb SA, and Roberts RG. 2001. Long mutant dystrophins and variable phenotypes: evasion of nonsense-mediated decay? *Hum Genet.* 109:402-7.
- King RW, Deshaies RJ, Peters JM, and Kirschner MW. 1996. How proteolysis drives the cell cycle. *Science.* 274:1652-9.
- Koretz JF. 1979. Effects of C-protein on synthetic myosin filament structure. *Biophys. J.* 27:433-446.
- Kostin S, Pool L, Elsasser A, Hein S, Drexler HC, Arnon E, Hayakawa Y, Zimmermann R, Bauer E, Klovekorn WP, and Schaper J. 2003. Myocytes die by multiple mechanisms in failing human hearts. *Circ Res.* 92:715-24.
- Kudej RK, Iwase M, Uechi M, Vatner DE, Oka N, Ishikawa Y, Shannon RP, Bishop SP, and Vatner SF. 1997. Effects of chronic beta-adrenergic receptor stimulation in mice. *J Mol Cell Cardiol.* 29:2735-46.

- Kulikovskaya I, McClellan G, Flavigny J, Carrier L, and Winegrad S. 2003. Effect of MyBP-C binding to actin on contractility in heart muscle. *J Gen Physiol.* 122:1-15.
- Kumarapeli AR, Horak KM, Glasford JW, Li J, Chen Q, Liu J, Zheng H, and Wang X. 2005. A novel transgenic mouse model reveals deregulation of the ubiquitin-proteasome system in the heart by doxorubicin. *Faseb J.* 19:2051-3.
- Kunst G, Kress KR, Gruen M, Uttenweiler D, Gautel M, and Fink RHA. 2000. Myosin binding protein C, a phosphorylation-dependent force regulator in muscle that controls the attachment of myosin heads by its interaction with myosin S2. *Circ Res.* 86:51-58.
- Kuzmiak HA, and Maquat LE. 2006. Applying nonsense-mediated mRNA decay research to the clinic: progress and challenges. *Trends Mol Med.* 12:306-16.
- Laugwitz KL, Moretti A, Lam J, Gruber P, Chen Y, Woodard S, Lin LZ, Cai CL, Lu MM, Reth M, Platoshyn O, Yuan JX, Evans S, and Chien KR. 2005. Postnatal Isl1+ cardioblasts enter fully differentiated cardiomyocyte lineages. *Nature.* 433:647-53.
- Lejeune F, and Maquat LE. 2005. Mechanistic links between nonsense-mediated mRNA decay and pre-mRNA splicing in mammalian cells. *Curr Opin Cell Biol.* 17:309-15.
- Li B, and Dou QP. 2000. Bax degradation by the ubiquitin/proteasome-dependent pathway: involvement in tumor survival and progression. *Proc Natl Acad Sci U S A.* 97:3850-5.
- Li HH, Kedar V, Zhang C, McDonough H, Arya R, Wang DZ, and Patterson C. 2004. Atrogin-1/muscle atrophy F-box inhibits calcineurin-dependent cardiac hypertrophy by participating in an SCF ubiquitin ligase complex. *J Clin Invest.* 114:1058-71.
- Lindsten K, Menendez-Benito V, Masucci MG, and Dantuma NP. 2003. A transgenic mouse model of the ubiquitin/proteasome system. *Nature Biotechnology.* 21:897-902.
- Ludwig A, Friedel B, Metzko S, Meiners S, Stangl V, Baumann G, and Stangl K. 2005. Effect of statins on the proteasomal activity in mammalian endothelial and vascular smooth muscle cells. *Biochem Pharmacol.* 70:520-6.
- Maquat LE, and Li X. 2001. Mammalian heat shock p70 and histone H4 transcripts, which derive from naturally intronless genes, are immune to nonsense-mediated decay. *Rna.* 7:445-56.
- Maquat LE. 2004. Nonsense-mediated mRNA decay: splicing, translation and mRNP dynamics. *Nat Rev Mol Cell Biol.* 5:89-99.

- Marian AJ, and Roberts R. 2001. The molecular genetic basis for hypertrophic cardiomyopathy. *J Mol Cell Cardiol.* 33:655-670.
- Maron B, Shirani J, Poliac L, Mthenge R, Roberts W, and Mueller F. 1996. Sudden death in young competitive athletes. Clinical, demographic, and pathological profiles. *JAMA.* 276:199-204.
- Maron BJ, Roberts WC, McAllister HA, Rosing DR, and Epstein SE. 1980. Sudden death in young athletes. *Circulation.* 62:218-29.
- Maron BJ, Nichols PF, Pickle LW, Wesley YE, and Mulvihill JJ. 1984. Patterns of inheritance in hypertrophic cardiomyopathy. Assessment by M-mode and two-dimensional echocardiography. *Am. J. Cardiol.* 53:1087-1094.
- Maron BJ, Spirito P, Green KJ, Wesley YE, Bonow RO, and Arce J. 1987. Noninvasive assessment of left ventricular diastolic function by pulsed Doppler echocardiography in patients with hypertrophic cardiomyopathy. *J Am Coll Cardiol.* 10:733-42.
- Maron BJ, Gardin JM, Flack JM, Gidding SS, Kurosaki TT, and Bild DE. 1995. Prevalence of hypertrophic cardiomyopathy in a general population of young adults: echocardiographic analysis of 4111 subjects in the CARDIA study. *Circulation.* 92:785-789.
- Maron BJ. 2002. Hypertrophic cardiomyopathy: a systematic review. *Jama.* 287:1308-20.
- McConnell BK, Jones KA, Fatkin D, Arroyo LH, Lee RT, Aristizabal O, Turnbull DH, Georgakopoulos D, Kass D, Bond M, Niimura H, Schoen FJ, Conner D, Fishman DH, Seidman CE, and Seidman JG. 1999. Dilated cardiomyopathy in homozygous myosin-binding protein-C mutant mice. *J Clin Invest.* 104:1235-1244.
- McConnell BK, Fatkin D, Semsarian C, Jones KA, Georgakopoulos D, Maguire CT, Healey MJ, Mudd JO, Moskowitz IPG, Conner DA, Giewat M, Wakimoto H, Berul CI, Schoen FJ, Kass DA, Seidman CE, and Seidman JG. 2001. Comparison of two murine models of familial hypertrophic cardiomyopathy. *Circ Res.* 88:383-389.
- Moolman JA, Reith S, Uhl K, Bailey S, Gautel M, Jeschke B, Fisher C, Ochs J, McKenna WJ, Klues H, and Vosberg HP. 2000. A newly created splice donor site in exon 25 of the MyBP-C gene is responsible for inherited hypertrophic cardiomyopathy with incomplete disease penetrance. *Circulation.* 101:1396-1402.
- Moolman-Smook J, Flashman E, de Lange W, Li Z, Corfield V, Redwood C, and Watkins H. 2002. Identification of novel interactions between domains of Myosin binding protein-C that are modulated by hypertrophic cardiomyopathy missense mutations. *Circ Res.* 91:704-11.

- Nagy E, and Maquat LE. 1998. A rule for termination-codon position within intron-containing genes: when nonsense affects RNA abundance. *Trends Biochem Sci.* 23:198-9.
- Niimura H, Bachinski LL, Sangwatanaroj S, Watkins H, Chudley AE, McKenna W, Kristinsson A, Roberts R, Sole M, Maron BJ, Seidman JG, and Seidman CE. 1998. Mutations in the gene for cardiac myosin-binding protein C and late-onset familial hypertrophic cardiomyopathy. *N. Engl. J. Med.* 338:1248-1257.
- Okagaki T, Weber FE, Fischman DA, Vaughan KT, Mikawa T, and Reinach FC. 1993. The major myosin-binding domain of skeletal muscle MyBP-C (C protein) resides in the COOH-terminal, immunoglobulin C2 motif. *J. Cell. Biol.* 123:619-626.
- Opie LH. 2004a. Introductory cardiovascular concepts. *In Heart Physiology: From cell to circulation.* Vol. Fourth Edition. L.H. Opie, editor. Lippincott Williams & Wilkins, Philadelphia, PA. 3-15.
- Opie LH. 2004b. Heart cells and organelles. *In Heart Physiology: From cell to circulation.* Vol. Fourth Edition. L.H. Opie, editor. Lippincott Williams & Wilkins, Philadelphia, PA. 42-69.
- Opie LH, and Solaro RJ. 2004. Myocardial contraction and relaxation. *In Heart Physiology: From cell to circulation.* Vol. Fourth Edition. L.H. Opie, editor. Lippincott Williams & Wilkins, Philadelphia, PA. 221-246.
- Palombella VJ, Rando OJ, Goldberg AL, and Maniatis T. 1994. The ubiquitin-proteasome pathway is required for processing the NF-kappa B1 precursor protein and the activation of NF-kappa B. *Cell.* 78:773-85.
- Pohlmann L, Kroger I, Vignier N, Schlossarek S, Kramer E, Coirault C, Sultan KR, El-Armouche A, Winegrad S, Eschenhagen T, and Carrier L. 2007. Cardiac myosin-binding protein C is required for complete relaxation in intact myocytes. *Circ Res.* 101:928-38.
- Razeghi P, Baskin KK, Sharma S, Young ME, Stepkowski S, Essop MF, and Taegtmeier H. 2006. Atrophy, hypertrophy, and hypoxemia induce transcriptional regulators of the ubiquitin proteasome system in the rat heart. *Biochem Biophys Res Commun.* 342:361-4.
- Redwood CS, Moolman-Smook JC, and Watkins H. 1999. Properties of mutant contractile proteins that cause hypertrophic cardiomyopathy. *Cardiovasc. Res.* 44:20-36.
- Rehwinkel J, Raes J, and Izaurralde E. 2006. Nonsense-mediated mRNA decay: Target genes and functional diversification of effectors. *Trends Biochem Sci.* 31:639-46.

- Richard P, Isnard R, Carrier L, Dubourg O, Donatien Y, Mathieu B, Bonne G, Gary F, Charron P, Hagège A, Komajda M, Schwartz K, and Hainque B. 1999. Double heterozygosity for mutations in the beta myosin heavy chain and in the cardiac myosin binding protein C genes in a family with hypertrophic cardiomyopathy. *J. Med. Genet.* 36:542-545.
- Richard P, Charron P, Carrier L, Ledeuil C, Cheav T, Pichereau C, Benaiche A, Isnard R, Dubourg O, Burban M, Gueffet JP, Millaire A, Desnos M, Schwartz K, Hainque B, and Komajda M. 2003. Hypertrophic Cardiomyopathy: Distribution of disease genes, spectrum of mutations and implications for molecular diagnosis strategy. *Circulation.* 107:2227-2232.
- Richard P, Villard E, Charron P, and Isnard R. 2006. The genetic bases of cardiomyopathies. *J Am Coll Cardiol.* 48:A79-89.
- Richardson P, McKenna W, Bristow M, Maish B, Mautner B, O'Connell J, Olsen E, Thiene G, Goodwin J, Gyarfás I, Martin I, and Nordet P. 1996. Report of the 1995 World Health Organisation/International Society and Federation of Cardiology task force on the definition and classification of cardiomyopathies. *Circulation.* 93:841-842.
- Richardson PG, and Anderson KC. 2003. Bortezomib: a novel therapy approved for multiple myeloma. *Clin Adv Hematol Oncol.* 1:596-600.
- Roberts R, and Sigwart U. 2001a. New concepts in hypertrophic cardiomyopathies, part II. *Circulation.* 104:2249-52.
- Roberts R, and Sigwart U. 2001b. New concepts in hypertrophic cardiomyopathies, part I. *Circulation.* 104:2113-6.
- Rock KL, Gramm C, Rothstein L, Clark K, Stein R, Dick L, Hwang D, and Goldberg AL. 1994. Inhibitors of the proteasome block the degradation of most cell proteins and the generation of peptides presented on MHC class I molecules. *Cell.* 78:761-71.
- Rospert S, Rakwalska M, and Dubaquié Y. 2005. Polypeptide chain termination and stop codon readthrough on eukaryotic ribosomes. *Rev Physiol Biochem Pharmacol.* 155:1-30.
- Rottbauer W, Gautel M, Zehelein J, Labeit S, Franz WM, Fischer C, Vollrath B, Mall G, Dietz R, Kübler W, and Katus HA. 1997. Novel splice donor site mutation in the cardiac myosin-binding protein-C gene in familial hypertrophic cardiomyopathy. Characterization of cardiac transcript and protein. *J Clin Invest.* 100:475-482.
- Sadayappan S, Gulick J, Osinska H, Martin LA, Hahn HS, Dorn GW, 2nd, Klevitsky R, Seidman CE, Seidman JG, and Robbins J. 2005. Cardiac myosin-binding protein-C phosphorylation and cardiac function. *Circ Res.* 97:1156-63.

- Sadayappan S, Osinska H, Klevitsky R, Lorenz JN, Sargent M, Molkenstein JD, Seidman CE, Seidman JG, and Robbins J. 2006. Cardiac myosin binding protein c phosphorylation is cardioprotective. *Proc Natl Acad Sci U S A*. 103:16918-23.
- Sano M, Tokudome S, Shimizu N, Yoshikawa N, Ogawa C, Shirakawa K, Endo J, Katayama T, Yuasa S, Ieda M, Makino S, Hattori F, Tanaka H, and Fukuda K. 2007. Intramolecular control of protein stability, subnuclear compartmentalization, and coactivator function of peroxisome proliferator-activated receptor gamma coactivator 1alpha. *J Biol Chem*. 282:25970-80.
- Sarikas A, Carrier L, Schenke C, Doll D, Flavigny J, Lindenberg KS, Eschenhagen T, and Zolk O. 2005. Impairment of the ubiquitin-proteasome system by truncated cardiac myosin binding protein C mutants. *Cardiovasc Res*. 66:33-44.
- Sébillon P, Bonne G, Flavigny J, Venin S, Rouche A, Fiszman M, Vikstrom K, Leinwand L, Carrier L, and Schwartz K. 2001. COOH-terminal truncated human cardiac MyBP-C alters myosin filament organization. *C. R. Acad. Sci*. 324:251-260.
- Seidman JG, and Seidman CE. 2001. The genetic basis for cardiomyopathy: from mutation identification to mechanistic paradigms. *Cell*. 104:557-567.
- Seiler SH, Fischman DA, and Leinwand LA. 1996. Modulation of myosin filament organization by C-protein family members. *Mol. Biol. Cell*. 7:113-127.
- Sheppard DN, Ostedgaard LS, Rich DP, and Welsh MJ. 1994. The amino-terminal portion of CFTR forms a regulated Cl<sup>-</sup> channel. *Cell*. 76:1091-8.
- Starr R, and Offer G. 1978. The interaction of C-protein with heavy meromyosin and subfragment-2. *Biochem. J*. 171:813-816.
- Suzuki M, Carlson KM, Marchuk DA, and Rockman HA. 2002. Genetic modifier loci affecting survival and cardiac function in murine dilated cardiomyopathy. *Circulation*. 105:1824-9.
- Sweeney HL, Straceski AJ, Leinwand LA, Tikunov BA, and Faust L. 1994. Heterologous expression of a cardiomyopathic myosin that is defective in its actin interaction. *J. Biol. Chem*. 269:1603-1605.
- Tardiff JC, Factor SM, Tompkins BD, Hewett TE, Palmer BM, Moore RL, Schwartz S, Robbins J, and Leinwand LA. 1998. A truncated cardiac troponin T molecule in transgenic mice suggests multiple cellular mechanisms for familial hypertrophic cardiomyopathy. *J. Clin. Invest*. 101:2800-2811.

- Tsukamoto O, Minamino T, Okada K, Shintani Y, Takashima S, Kato H, Liao Y, Okazaki H, Asai M, Hirata A, Fujita M, Asano Y, Yamazaki S, Asanuma H, Hori M, and Kitakaze M. 2006. Depression of proteasome activities during the progression of cardiac dysfunction in pressure-overloaded heart of mice. *Biochem Biophys Res Commun.* 340:1125-33.
- Usuki F, Yamashita A, Higuchi I, Ohnishi T, Shiraishi T, Osame M, and Ohno S. 2004. Inhibition of nonsense-mediated mRNA decay rescues the phenotype in Ullrich's disease. *Ann Neurol.* 55:740-4.
- Usuki F, Yamashita A, Kashima I, Higuchi I, Osame M, and Ohno S. 2006. Specific inhibition of nonsense-mediated mRNA decay components, SMG-1 or Upf1, rescues the phenotype of Ullrich disease fibroblasts. *Mol Ther.* 14:351-60.
- Vidal F, Sage J, Cuzin F, and Rassoulzadegan M. 1998. Cre expression in primary spermatocytes: a tool for genetic engineering of the germ line. *Mol Reprod Dev.* 51:274-80.
- Watkins H, Conner D, Thierfelder L, Jarcho JA, MacRae C, McKenna WJ, Maron BJ, Seidman JG, and Seidman CE. 1995. Mutations in the cardiac myosin binding protein-C gene on chromosome 11 cause familial hypertrophic cardiomyopathy. *Nature Genet.* 11:434-437.
- Weber FE, Vaughan KT, Reinach FC, and Fischman DA. 1993. Complete sequence of human fast-type and slow-type muscle myosin-binding-protein C (MyBP-C). Differential expression, conserved domain structure and chromosome assignment. *Eur. J. Biochem.* 216:661-669.
- Weekes J, Morrison K, Mullen A, Wait R, Barton P, and Dunn MJ. 2003. Hyperubiquitination of proteins in dilated cardiomyopathy. *Proteomics.* 3:208-16.
- Witt CC, Gerull B, Davies MJ, Centner T, Linke WA, and Thierfelder L. 2001. Hypercontractile properties of cardiac muscle fibers in a knock-in mouse model of cardiac myosin-binding protein-C. *J Biol Chem.* 276:5353-5359.
- Yang J, Moravec CS, Sussman MA, DiPaola NR, Fu D, Hawthorn L, Mitchell CA, Young JB, Francis GS, McCarthy PM, and Bond M. 2000. Decreased SLIM1 expression and increased gelsolin expression in failing human hearts measured by high-density oligonucleotide arrays. *Circulation.* 102:3046-52.
- Yang Q, Sanbe A, Osinska H, Hewett TE, Klevitsky R, and Robbins J. 1998. A mouse model of myosin binding protein C human familial hypertrophic cardiomyopathy. *J. Clin. Invest.* 102:1292-1300.
- Yang Q, Sanbe A, Osinska H, Hewett TE, Klevitsky R, and Robbins J. 1999. In vivo modeling of myosin binding protein C familial hypertrophic cardiomyopathy. *Circ Res.* 85:841-847.

- Yang Q, Hewett TE, Klevitsky R, Sanbe A, Wang X, and Robbins J. 2001. PKA-dependent phosphorylation of cardiac myosin binding protein C in transgenic mice. *Cardiovasc. Res.* 51:80-88.
- Yu B, French JA, Carrier L, Jeremy RW, McTaggart DR, Nicholson MR, Hambly B, Semsarian C, Richmond DR, Schwartz K, and Trent RJ. 1998. Molecular pathology of familial hypertrophic cardiomyopathy caused by mutations in the cardiac myosin binding protein C gene. *J Med Genet.* 35:205-10.
- Zhang J, Sun X, Qian Y, LaDuca JP, and Maquat LE. 1998. At least one intron is required for the nonsense-mediated decay of triosephosphate isomerase mRNA: a possible link between nuclear splicing and cytoplasmic translation. *Mol Cell Biol.* 18:5272-83.
- Zhang XH, Heller KA, Hefter I, Leslie CS, and Chasin LA. 2003. Sequence information for the splicing of human pre-mRNA identified by support vector machine classification. *Genome Res.* 13:2637-50.
- Zolk O, Schenke C, and Sarikas A. 2006. The ubiquitin-proteasome system: focus on the heart. *Cardiovasc Res.* 70:410-21.



## 7 Appendix

### 7.1 Abbreviations

AA	amino acids
AMC	7-amino-4-methylcoumarin
$\alpha$ -MHC	$\alpha$ -myosin heavy chain
AMVM	adult mouse ventricular myocytes
ANP	atrial natriuretic peptide
APS	ammonium persulfate
AT	annealing temperature
ATP	adenosine 5'-triphosphate
AU	arbitrary unit
$\beta_2$ AR	$\beta_2$ adrenergic receptor
BDM	2,3-butanedione monoxime
$\beta$ -MHC	$\beta$ -myosin heavy chain
$\beta$ NA	$\beta$ -naphtylamide
BNP	brain natriuretic peptide
bp	base pairs
BSA	bovine serum albumin
BW	body weight
$^{\circ}$ C	degree Celsius
cAMP	cyclic adenosine monophosphate
cDNA	complementary deoxyribonucleic acid
CHX	cycloheximide
CMV-IE	cytomegalovirus immediate early
Ct	threshold cycle
cter	COOH-terminus
cTnT	cardiac troponin T
d	diastole
Da	dalton
dCTP	deoxycytidine triphosphate
DMEM	Dulbecco's modified Eagle medium

---

DMSO	dimethyl sulfoxide
DNA	deoxyribonucleic acid
dNTP	deoxynucleoside triphosphate
DTT	dithiothreitol
E1	ubiquitin-activating enzyme
E2	ubiquitin-conjugating enzyme
E3	ubiquitin ligase enzyme
ECG	electrocardiogram
ECL	enhanced chemiluminescence
EDTA	ethylenediaminetetraacetic acid
EF-2	elongation factor 2
e.g.	<i>exempli gratia</i> (for example)
EJC	exon junction complex
Emet	emetine
Epo	epoxomicin
eRF	eukaryotic release factor
ES	embryonic stem
<i>et al.</i>	<i>et alii</i> (and others)
F	founder line
FAM	6-carboxy-fluorescein
FBS	fetal bovine serum
FCS	fetal calf serum
FHC	familial hypertrophic cardiomyopathy
Fig.	figure
FN	fibronectin
FR	fluorescent reporter
FS	fractional shortening
g	gram
GAPDH	glyceraldehyde-3-phosphate dehydrogenase
GD	GFPdgn
GFP	green fluorescent protein
h	hours
HBSS	Hank's balanced salt solution
HCM	hypertrophic cardiomyopathy
HEPES	4-(2-hydroxyethyl)piperazine-1-ethanesulfonic acid

---

Het	heterozygous cMyBP-C knock-in
HR	homologous recombination
HSVtk	herpes simplex virus thymidine kinase
hum	human
HW	heart weight
Hz	hertz
IC <sub>50</sub>	half maximal inhibitory concentration
i.e.	<i>id est</i> (that is)
IgG	immunoglobulin G
Inc.	incorporation
i.p.	intraperitoneal
i.v.	intravenous
IVS	interventricular septum
kb	kilobase
kDa	kilodalton
kg	kilogram
KI	homozygous cMyBP-C knock-in
KO	homozygous cMyBP-C knock-out
LB	Luria-Bertani
LMM	light meromyosin
LSM	laser scanning microscopy
LV	left ventricular
LVH	left ventricular hypertrophy
LVID	left ventricular internal diameter
LVM	left ventricular mass
LVPW	left ventricular posterior wall
M	molar
mA	milliampere
MEM	minimum essential medium
mg	milligram
MGB	minor groove binder
MHz	megahertz
min	minutes
ml	milliliter
mM	millimolar

---

µg	microgram
µl	microliter
µM	micromolar
Miss	missense
mo	months
MW	molecular weight (marker)
mRNA	messenger ribonucleic acid
MyBP-C	myosin-binding protein-C
cMyBP-C	cardiac myosin-binding protein-C
n	number
ng	nanogram
NIH	National Institutes of Health
nm	nanometer
nM	nanomolar
NMCM	neonatal mouse cardiomyocytes
NMD	nonsense-mediated mRNA decay
No.	number
Nons	nonsense
NRCM	neonatal rat cardiomyocytes
nt	nucleotides
Nter	amino-terminus
oligo(dT)	oligodeoxythymidylic acid
P	probability
PA	polyadenylation
PBS	phosphate buffered saline
PCR	polymerase chain reaction
pGK	phosphoglycerate kinase
PKA	protein kinase A (also known as cAMP-dependent protein kinase)
PTC	premature termination codon
r	Spearman value
RFU	relative fluorescence unit
RNA	ribonucleic acid
rpm	rotation per minute
RT	reverse transcription
s	systole

---

S2	subfragment 2
s.c.	subcutaneous
SDS	sodium dodecyl sulfate
sec	seconds
SEM	standard error of the mean
SMG	suppressor with morphogenetic effect on genitalia
Suc	succinyl
SV40	Simian vacuolating virus 40
Sycp-1	synatonemal complex protein 1
TAMRA	6-carboxy-tetramethyl-rhodamine
TBE	Tris borate EDTA
TBS-T	Tris buffered saline with Tween <sup>®</sup> 20
TE	Tris-HCl EDTA
TEMED	tetramethylethylenediamine
TG	transgenic M7t
Tris	Trishydroxymethylaminomethane
TV	targeting vector
U	unit
Ub	ubiquitin
UG	Ub <sup>G76V</sup> -GFP
UPF1-3	up-frameshift protein 1-3
UPS	ubiquitin-proteasome system
V	volt
vs.	versus
VW	ventricular weight
wk	weeks
WT	wild-type

## 7.2 Standard amino acid abbreviations

Alanine	Ala	A
Arginine	Arg	R
Asparagine	Asn	N
Aspartic acid	Asp	D
Cysteine	Cys	C
Glutamic acid	Glu	E
Glutamine	Gln	Q
Glycine	Gly	G
Histidine	His	H
Isoleucine	Ile	I
Leucine	Leu	L
Lysine	Lys	K
Methionine	Met	M
Phenylalanine	Phe	F
Proline	Pro	P
Serine	Ser	S
Threonine	Thr	T
Tryptophan	Trp	W
Tyrosine	Tyr	Y
Valine	Val	V

## 7.3 Risk and safety phrases

Risk (R-) and safety (S-) phrases are an essential guideline for labeling dangerous chemicals to ensure their safe use. R-phrases display a general description of the physio-chemical, environmental and health hazards of a substance. S-phrases provide information on safe storage, handling, disposal, first-aid and employee protection. R- and S-phrases must be given if the preparation contains at least one substance classified as dangerous to man or the environment or if the preparation is otherwise regarded as dangerous.

**R-phrases**

- R1: Explosive when dry
- R2: Risk of explosion by shock, friction fire or other sources of ignition
- R3: Extreme risk of explosion by shock friction, fire or other sources of ignition
- R4: Forms very sensitive explosive metallic compounds
- R5: Heating may cause an explosion
- R6: Explosive with or without contact with air
- R7: May cause fire
- R8: Contact with combustible material may cause fire
- R9: Explosive when mixed with combustible material
- R10: Flammable
- R11: Highly flammable
- R12: Extremely flammable
- R13: Extremely flammable liquefied gas
- R14: Reacts violently with water
- R15: Contact with water liberates highly flammable gases
- R16: Explosive when mixed with oxidizing substances
- R17: Spontaneously flammable in air
- R18: In use, may form flammable/explosive vapor-air mixture
- R19: May form explosive peroxides
- R20: Harmful by inhalation
- R21: Harmful in contact with skin
- R22: Harmful if swallowed
- R23: Toxic by inhalation
- R24: Toxic in contact with skin
- R25: Toxic if swallowed
- R26: Very toxic by inhalation
- R27: Very toxic in contact with skin
- R28: Very toxic if swallowed
- R29: Contact with water liberates toxic gas
- R30: Can become highly flammable in use
- R31: Contact with acids liberates toxic gas
- R32: Contact with acids liberates very toxic gas
- R33: Danger of cumulative effects

- R34: Causes burns
- R35: Causes severe burns
- R36: Irritating to eyes
- R37: Irritating to respiratory system
- R38: Irritating to skin
- R39: Danger of very serious irreversible effects
- R40: Possible risk of irreversible effects
- R41: Risk of serious damage to eyes
- R42: May cause sensitization by inhalation
- R43: May cause sensitization by skin contact
- R44: Risk of explosion if heated under confinement
- R45: May cause cancer
- R46: May cause heritable genetic damage
- R47: May cause birth defect
- R48: Danger of serious damage to health by prolonged exposure
- R49: May cause cancer by inhalation
- R50: Very toxic to aquatic organisms
- R51: Toxic to aquatic organisms
- R52: Harmful to aquatic organisms
- R53: May cause long-term adverse effects in the aquatic environment
- R54: Toxic to flora
- R55: Toxic to fauna
- R56: Toxic to soil organisms
- R57: Toxic to bees
- R58: May cause long-term adverse effects in the environment
- R59: Dangerous to the ozone layer
- R60: May impair fertility
- R61: May cause harm to the unborn child
- R62: Possible risk of impaired fertility
- R63: Possible risk of harm to the unborn child
- R64: May cause harm to breastfed babies
- R65: Harmful: may cause lung damage if swallowed
- R66: Repeated exposure may cause skin dryness or cracking
- R67: Vapors may cause drowsiness and dizziness



R68: Possible risk of irreversible effects

**S-phrases**

S1: Keep locked up

S2: Keep out of reach of children

S3: Keep in a cool place

S4: Keep away from living quarters

S5: Keep contents under ... (appropriate liquid to be specified by the manufacturer)

S6: Keep under ... (inert gas to be specified by the manufacturer)

S7: Keep container tightly closed

S8: Keep container dry

S9: Keep container in a well ventilated place

S12: Do not keep the container sealed

S13: Keep away from food, drink and animal feeding stuffs

S14: Keep away from ... (incompatible materials to be indicated by the manufacturer)

S15: Keep away from heat

S16: Keep away from sources of ignition-No Smoking

S17: Keep away from combustible material

S18: Handle and open container with care

S20: When using do not eat or drink

S21: When using, do not smoke

S22: Do not breathe dust

S23: Do not breathe gas/fumes/vapor/spray (appropriate wording to be specified by manufacturer)

S24: Avoid contact with skin

S25: Avoid contact with eyes

S26: In case of contact with eyes, rinse immediately with plenty of water and see medical advice

S27: Take off immediately all contaminated clothing

S28: After contact with skin, wash immediately with plenty of ... (to be specified by The manufacturer)

S29: Do not empty into drains

S30: Never add water to this product

S33: Take precautionary measures against static discharges

- S34: Avoid shock and friction
- S35: This material and its container must be disposed of in a safe way
- S36: Wear suitable protective clothing
- S37: Wear suitable gloves
- S38: In case of insufficient ventilation, wear suitable respiratory equipment
- S39: Wear eye/face protection
- S40: To clean the floor and all objects contaminated by this material use (to be specified by the manufacturer)
- S41: In case of fire and/or explosion do not breathe fumes
- S42: During fumigation/spraying wear suitable respiratory equipment (appropriate wording to be specified by the manufacturer)
- S43: In case of fire, use ... (indicate in the space the precise type of fire fighting equipment. If water increases the risk, add "never use water")
- S44: If you feel unwell, seek medical advice (show the label where possible)
- S45: In case of accident or if you feel unwell, seek medical advice immediately (show the label where possible)
- S46: If swallowed, seek medical advice immediately and show the container or label
- S47: Keep at temperature not exceeding ... °C (to be specified by the manufacturer)
- S48: Keep wetted with ... (appropriate material to be specified by the manufacturer)
- S49: Keep only in the original container
- S50: Do not mix with ... (to be specified by the manufacturer)
- S51: Use only in well-ventilated areas
- S52: Not recommended for interior use on large surface areas
- S53: Avoid exposure - obtain special instructions before use
- S54: Obtain the consent of pollution control authorities before discharging to waste water treatment plants
- S55: Treat using the best available techniques before discharge into drains or the Aquatic environment
- S56: Do not discharge into drains or the environment; dispose to an authorized waste collection point
- S57: Use appropriate containment to avoid environmental contamination
- S58: To be disposed of as hazardous waste
- S59: Refer to manufacturer/supplier for information on recovery/recycling
- S60: This material and/or its container must be disposed of as hazardous waste

S61: Avoid release to the environment. Refer to special instructions / safety data sheet

S62: If swallowed, do not induce vomiting: seek medical advice immediately and

Show the container label

S63: In case of accident by inhalation: remove casualty to fresh air and keep at rest

S64: If swallowed, rinse mouth with water (only if the person is conscious)

## 7.4 Curriculum Vitae

### **Personal data:**

First name: Saskia  
Last name: Schlossarek  
Date of birth: 21.09.1976  
City of birth: Hamburg

### **Education:**

1987-1996 Wolfgang-Borchert-grammar school Halstenbek  
05.06.1996 Abitur  
04.97-09.01 Study of pharmacy at the University of Hamburg  
27.08.1999 1. state examination  
11.10.2001 2. state examination  
23.01.2003 3. state examination  
11.01-04.02 Internship at the Pfeil-Apotheke in Hamburg  
05.02-10.02 Internship at the Beiersdorf AG in Hamburg  
Since 09.04 PhD student at the Institute of Experimental and  
Clinical Pharmacology and Toxicology,  
University Medical Center Hamburg-Eppendorf

### **Work experience:**

01.97-03.97 Commercial clerk at the comdirect bank  
11.02-05.03 Pharmacist at the Pfeil-Apotheke in Hamburg  
06.03-08.04 Pharmacist at the Humboldt-Apotheke in Hamburg

## 7.5 Publications and congress participations

### 7.5.1 Publications

Pohlmann L, Kröger I, Vignier N, **Schlossarek S**, Krämer E, Coirault C, Sultan KR, El-Armouche A, Winegrad S, Eschenhagen T, and Carrier L. 2007. Cardiac myosin-binding protein C is required for complete relaxation in intact myocytes. *Circ Res.* 101:928-38.

El-Armouche A, Pohlmann L, **Schlossarek S**, Starbatty J, Yeh YH, Nattel S, Dobrev D, Eschenhagen T, and Carrier L. 2007. Decreased phosphorylation levels of cardiac myosin-binding protein-C in human and experimental heart failure. *J Mol Cell Cardiol.* 43:223-9.

Vignier N / **Schlossarek S**, Fraysse B, Mearini G, Krämer E, Juhr D, Pointu H, Mougenot N, Guiard J, Reimer R, Hohenberg H, Schwartz K, Vernet M, Eschenhagen T, and Carrier L. 2007. Nonsense-mediated mRNA decay regulates cMyBP-C mutant levels in cardiomyopathic mice. *In revision.*

### 7.5.2 Congress participations

The presenting person is underlined.

**Schlossarek S**, Vignier N, Mearini G, Krämer E, Pohlmann L, Herrgesell N, Eschenhagen T, and Carrier L. Cardiac myosin-binding protein C and familial hypertrophic cardiomyopathy.

First International CCR Symposium. Cardiovascular Disease: From Basic Mechanisms to Therapeutic Targets, Berlin, October 21-22, 2005, oral communication.

**Schlossarek S**, Vignier N, Mearini G, Pohlmann L, Krämer E, Eschenhagen T, and Carrier L. Instability of cardiac myosin-binding protein C mutant in mouse models of familial hypertrophic cardiomyopathy: involvement of the ubiquitin-proteasome system?

5<sup>th</sup> International Ascona Workshop on Cardiomyocyte Cell Biology: Differentiation, Stability of Cytoarchitecture and Therapeutic Potential of Heart Muscle Cells, Monte Verità, Ascona, April 2-6, 2006, oral communication.

**Schlossarek S**, Vignier N, Krämer E, Mearini G, Eschenhagen T, and Carrier L. Instability of cardiac myosin-binding protein C mutant in two new mouse models of familial hypertrophic cardiomyopathy: implication of the ubiquitin-proteasome system?

72<sup>nd</sup> Annual Meeting of the German Society for Cardiology and Cardiovascular Research, Mannheim, April 20-22, 2006, oral communication.

**Schlossarek S**, Vignier N, Krämer E, Mearini G, Eschenhagen T, and Carrier L. Instability of cardiac myosin-binding protein C mutant in two new mouse models of familial hypertrophic cardiomyopathy: implication of the ubiquitin-proteasome system?

Les Printemps de la Cardiologie, Toulouse, May 10-13, 2006, oral communication.

**Schlossarek S**, Vignier N, Sultan K, Krämer E, Mearini G, Eschenhagen T, and Carrier L. Evidence of alterations of the ubiquitin-proteasome system in mouse models of familial hypertrophic cardiomyopathy. *Circulation*. 114:II\_166.

American Heart Association (Scientific Sessions 2006), Chicago, IL, November 12-15, 2006, oral communication.

Pohlmann L, Kröger I, Vignier N, **Schlossarek S**, Krämer E, Coirault C, El-Armouche A, Winegrad S, Eschenhagen T, and Carrier L. Effects of cardiac myosin-binding protein C knockout (KO) on intact isolated cardiac myocytes.

51<sup>st</sup> Annual Meeting of the Biophysical Society, Baltimore, MD, March 3-7, 2007.

**Schlossarek S**, Vignier N, Mearini G, Eschenhagen T, and Carrier L. Nonsense-mediated mRNA decay and ubiquitin-proteasome system regulate the level of cMyBP-C mutants in cardiomyopathic mice.

73<sup>rd</sup> Annual Meeting of the German Society for Cardiology and Cardiovascular Research, Mannheim, April 12-14, 2007, oral communication.

**Englmann D**, Sultan K, **Schlossarek S**, Vignier N, Eschenhagen T, and Carrier L. Alterations of the ubiquitin-proteasome system in targeted cMyBP-C mice with hypertrophic cardiomyopathy.

73<sup>rd</sup> Annual Meeting of the German Society for Cardiology and Cardiovascular Research, Mannheim, April 12-14, 2007, oral communication.

**Pohlmann L**, Kröger I, Vignier N, **Schlossarek S**, Krämer E, Coirault C, El-Armouche A, Winegrad S, Eschenhagen T, and Carrier L. Cardiac myosin-binding protein C is required for complete sarcomere relaxation in intact myocytes: Evidence from a knock-out mouse model.

73<sup>rd</sup> Annual Meeting of the German Society for Cardiology and Cardiovascular Research., Mannheim, April 12-14, 2007, oral communication.

**Vignier N**, **Schlossarek S**, Pointu H, Mougnot N, Schwartz K, Vernet M, and Carrier L. Nonsense-mediated mRNA decay regulates cMyBP-C mutant levels in cardiomyopathic mice.

24<sup>th</sup> congress of GRRC, Biologie et Pathologie du Coeur et des vaisseaux, Tours, April 25-27, 2007, oral communication.

**Schlossarek S**. Alteration of the ubiquitin-proteasome system in mouse models of familial hypertrophic cardiomyopathy.

Marie Curie Symposium – The ubiquitin-proteasome system in cardiovascular disease, Hamburg, June 8-9, 2007, oral communication.

Decostre V, Arimura T, Muchir A, Khouzami L, Belus A, **Schlossarek S**, Varnous S, Adamy C, Durand M, Guerchet N, Candiani G, Massart C, Pavlidis P, Herron AJ, Fougereousse F, Poggesi C, Carrier L, Worman HJ, Pecker F, and Bonne G. Striated muscle investigation of a KI-Lmna mouse model of Emery-Dreifuss muscular dystrophy and effect of the N-acetyl-L-cysteine treatment.

7<sup>th</sup> Japanese-French Workshop on “Development of molecular therapy toward muscular dystrophy”, Hayama, June 8-9, 2007, oral communication.

**Schlossarek S**, Vignier N, Mearini G, Guiard J, Schwartz K, Vernet M, Eschenhagen T, and Carrier L. Nonsense-mediated mRNA decay degrades cMyBP-C mutants in cardiomyopathic mice. *J Mol Cell Cardiol.* 42:S129-S130.

XIX World Congress of the ISHR, Bologna, June 22-26, 2007.

Sultan K, **Schlossarek S**, Englmann D, Vignier N, Eschenhagen T, and Carrier L. Alterations of the ubiquitin-proteasome system in cardiomyopathic cMyBP-C mice. *J Mol Cell Cardiol.* 42:S167.

XIX World Congress of the ISHR, Bologna, June 22-26, 2007.



## 7.6 Declaration

I declare that the work reported in the dissertation submitted to the University of Hamburg and entitled

Investigation of molecular mechanisms regulating the expression of cMyBP-C  
mutants in familial hypertrophic cardiomyopathy

was realized in person in the Institute of Experimental and Clinical Pharmacology and Toxicology under the supervision of Prof. Dr. Thomas Eschenhagen. All sources of information as well as the results obtained in collaboration with other people are pointed out.

The dissertation has not been submitted in whole or in part for a degree at any other university.

Hamburg, January 2008

---

Saskia Schlossarek

## 7.7 Acknowledgement

I thank Prof. Dr. Thomas Eschenhagen for supervising and supporting me during my thesis.

I thank Prof. Dr. Michael Korth for the supervision of my thesis in the Department of Chemistry of the University of Hamburg.

I would like to express my sincere gratitude to Dr. Lucie Carrier for her committed supervision and constant encouragement during all phases of my thesis. She motivated me a lot and I would not have proceeded so far without her never-ending energy and magnificent support.

Many thanks go to the staff members of the institute for the great working atmosphere. In particular, I would like to thank Lisa Krämer for the assistance with the cloning and many advices concerning the practical work in the lab, Birgit Geertz for the assistance with the echocardiography, Lutz Pohlmann for the assistance with the isolation of the AMVM, Denise Juhr for the assistance with the genotyping, Christina Gedicke for proofreading this thesis, Dr. Karim Sultan, Dr. Felix Friedrich, Daniel Englmann and Nessim Herrgesell. In addition, I thank Lisa, Birgit and Christina for the immense mental support, which they provided to me not only in the lab, but also during congress participations. My most sincere thanks are directed to Dr. Giulia Mearini. When she started working in the institute, many things turned to be much easier for me than before. She was always there for me and supported me in many theoretical and practical issues. I'm very thankful that she proofread this thesis and that she was my hotel room mate during quite all congresses.

I wish to thank all my friends for “remaining” friends throughout these difficult times and for all the mental support outside the lab, especially Katrin Schwerin, Carolin Jahnke and Dr. Vida Zohrabi-Kalantari, who went through the same “misery” as I.

Finally and especially, I wish to thank my parents Manfred and Regina, my brother Simon, my cousin Petra and Rafael Vidal-López, who are the most important persons in my life. They always believe in me and have to “bear” my self-doubts. Without their confidence in me I would not be there where I am now.